Australia's National Science Agency

Australian Government

National Water Grid®

Floodplain inundation mapping and modelling for the Roper catchment

A technical report from the CSIRO Roper River Water Resource Assessment for the National Water Grid

Shaun Kim, Justin Hughes, Cate Ticehurst, Danial Stratford, Linda Merrin, Steve Marvanek, Cuan Petheram

ISBN 978-1-4863-1903-9 (print)

ISBN 978-1-4863-1904-6 (online)

Citation

Kim S, Hughes J, Ticehurst C, Stratford D, Merrin L, Marvanek S and Petheram C (2023) Floodplain inundation mapping and modelling for the Roper catchment. A technical report from the CSIRO Roper River Water Resource Assessment for the National Water Grid. CSIRO, Australia.

Copyright

Important disclaimer

CSIRO Roper River Water Resource Assessment acknowledgements

This report was funded through the National Water Grid's Science Program, which sits within the Australian Government's Department of Climate Change, Energy, the Environment and Water.

Aspects of the Assessment have been undertaken in conjunction with the Northern Territory Government.

The Assessment was guided by two committees:

i. The Assessment's Governance Committee: CRC for Northern Australia/James Cook University; CSIRO; National Water Grid (Department of Climate Change, Energy, the Environment and Water); NT Department of Environment, Parks and Water Security; NT Department of Industry, Tourism and Trade; Office of Northern Australia; Qld Department of Agriculture and Fisheries; Qld Department of Regional Development, Manufacturing and Water

ii. The Assessment's joint Roper and Victoria River catchments Steering Committee: Amateur Fishermen's Association of the NT; Austrade; Centrefarm; CSIRO, National Water Grid (Department of Climate Change, Energy, the Environment and Water); Northern Land Council; NT Cattlemen's Association; NT Department of Environment, Parks Australia; Parks and Water Security; NT Department of Industry, Tourism and Trade; Regional Development Australia; NT Farmers; NT Seafood Council; Office of Northern Australia; Roper Gulf Regional Council Shire

Responsibility for the Assessment's content lies with CSIRO. The Assessment's committees did not have an opportunity to review the Assessment results or outputs prior to its release.

This report was reviewed by Cherry Mateo, CSIRO.

Acknowledgement of Country

CSIRO acknowledges the Traditional Owners of the lands, seas and waters, of the area that we live and work on across Australia. We acknowledge their continuing connection to their culture and pay our respects to their Elders past and present.

Photo

Yellow Waters Billabong near Ngukurr with the Roper River in the background. Source: Nathan Dyer - CSIRO

Director's foreword

Sustainable regional development is a priority for the Australian and Northern Territory governments. Across northern Australia, however, there is a scarcity of scientific information on land and water resources to complement local information held by Indigenous owners and landholders.

Sustainable regional development requires knowledge of the scale, nature, location and distribution of the likely environmental, social and economic opportunities and the risks of any proposed development. Especially where resource use is contested, this knowledge informs the consultation and planning that underpins the resource security required to unlock investment.

In 2019 the Australian Government commissioned CSIRO to complete the Roper River Water Resource Assessment. In response, CSIRO accessed expertise and collaborations from across Australia to provide data and insight to support consideration of the use of land and water resources for development in the Roper catchment. While the Assessment focuses mainly on the potential for agriculture, the detailed information provided on land and water resources, their potential uses and the impacts of those uses are relevant to a wider range of regional-scale planning considerations by Indigenous owners, landholders, citizens, investors, local government, the Northern Territory and federal governments.

Importantly the Assessment will not recommend one development over another, nor assume any particular development pathway. It provides a range of possibilities and the information required to interpret them - including risks that may attend any opportunities - consistent with regional values and aspirations.

All data and reports produced by the Assessment will be publicly available.

Chris Chilcott

Project Director

The Roper River Water Resource Assessment Team

Project Director	Chris Chilcott
Project Leaders	Cuan Petheram, Ian Watson
Project Support	Caroline Bruce
Communications	Chanel Koeleman/Kate Cranney, Siobhan Duffy, Amy Edwards

Activities

Agriculture and socio-economics	Chris Stokes, Caroline Bruce, Shokhrukh Jalilov, Diane Jarvis[1], Adam Liedloff, Yvette Oliver, Alex Peachey[2], Allan Peake, Maxine Piggott, Perry Poulton, Di Prestwidge, Thomas Vanderbyl[7], Tony Webster, Steve Yeates
Climate	David McJannet, Lynn Seo
Ecology	Danial Stratford, Laura Blamey, Rik Buckworth, Pascal Castellazzi, Bayley Costin, Roy Aijun Deng, Ruan Gannon, Sophie Gilbey, Rob Kenyon, Darran King, Keller Kopf[3], Stacey Kopf[3], Simon Linke, Heather McGinness, Linda Merrin, Colton Perna[3], Eva Plaganyi, Rocio Ponce Reyes, Jodie Pritchard, Nathan Waltham[9]
Groundwater hydrology	Andrew R. Taylor, Karen Barry, Russell Crosbie, Phil Davies, Alec Deslandes, Katelyn Dooley, Clement Duvert[8], Geoff Hodgson, Lindsay Hutley[8], Anthony Knapton[4], Sebastien Lamontagne, Steven Tickell[5], Sarah Marshall, Axel Suckow, Chris Turnadge
Indigenous water values, rights, interests and development goals	Pethie Lyons, Marcus Barber, Peta Braedon, Kristina Fisher, Petina Pert
Land suitability	Ian Watson, Jenet Austin, Elisabeth Bui, Bart Edmeades[5], John Gallant, Linda Gregory, Jason Hill[5], Seonaid Philip, Ross Searle, Uta Stockmann, Mark Thomas, Francis Wait[5], Peter L. Wilson, Peter R. Wilson
Surface water hydrology	Justin Hughes, Shaun Kim, Steve Marvanek, Catherine Ticehurst, Biao Wang
Surface water storage	Cuan Petheram, Fred Baynes[6], Kevin Devlin[7], Arthur Read, Lee Rogers, Ang Yang,

Note: Assessment team as at June 15, 2023. All contributors are affiliated with CSIRO unless indicated otherwise. Activity Leaders are underlined.

[1]James Cook University; [2]NT Department of Industry, Tourism and Trade; [3] Research Institute for the Environment and Livelihoods. College of Engineering, IT & Environment. Charles Darwin University; [4]CloudGMS; [5]NT Department of Environment, Parks and Water Security; [6]Baynes Geologic; [7]independent consultant; [8]Charles Darwin University; [9]Centre for Tropical Water and Aquatic Ecosystem Research. James Cook University.

Shortened forms

SHORT FORM	FULL FORM
AEP	annual exceedance probability
AGDC	Australian Geoscience Data Cube
AHD	Australian Height Datum
AWRA-R	Australian Water Resource Assessment – River model
BRDF	Bidirectional Reflectance Distribution Function
CMIP	Coupled Model Intercomparison Project
DEM	digital elevation model
DOI	Digital Object Identifier
ERP	equivalent Riemann problem
ETM	Enhanced Thematic Mapper
ETS	Equitable Threat Score
FAR	False Alarm Ratio
FB	Frequency Bias
GCM	global climate model
GCM-PS	global climate model – pattern scaling
GPU	graphics processing unit
HDF	hierarchical data format
IDL	Interactive Data Language
LiDAR	Light Detection and Ranging
MGA	Map Grid of Australia
MODIS	Moderate-Resolution Imaging Spectroradiometer
NBAR	Nadir BRDF-Adjusted Reflectance
NCI	National Computing Infrastructure
NDWI	Normalized Difference Water Index
OLI	Operational Land Imager
OWL	Open Water Likelihood
POD	Probability Of Detection
PS	pattern scaling
RCP	Representative Concentration Pathway
SILO	scientific information for land owners
SRTM	Shuttle Radar Topography Mission
SSP	Shared Socioeconomic Pathway
TM	Thematic Mapper
URBS	Unified River Basin Simulator

Units

UNIT	DESCRIPTION
cm	centimetre
GL	gigalitre
km	kilometre
m	metre
ML/d	megalitres per day
mm	millimetre
s	second

Preface

Sustainable regional development is a priority for the Australian and Northern Territory governments. For example, in 2023 the Northern Territory Government committed to the implementation of a new Territory Water Plan. One of the priority actions announced by the government was the acceleration of the existing water science program 'to support best practice water resource management and sustainable development'.

The efficient use of Australia's natural resources by food producers and processors requires a good understanding of soil, water and energy resources so they can be managed sustainably. Finely tuned strategic planning will be required to ensure that investment and government expenditure on development are soundly targeted and designed. Northern Australia presents a globally unique opportunity (a greenfield development opportunity in a first-world country) to strategically consider and plan development. Northern Australia also contains ecological and cultural assets of high value and decisions about development will need to be made within that context. Good information is critical to these decisions.

Most of northern Australia's land and water resources, however, have not been mapped in sufficient detail to provide for reliable resource allocation, mitigate investment or environmental risks, or build policy settings that can support decisions. Better data are required to inform decisions on private investment and government expenditure, to account for intersections between existing and potential resource users, and to ensure that net development benefits are maximised.

In consultation with the Northern Territory Government, the Australian Government prioritised the catchment of the Roper River for investigation (Preface Figure 1-1) and establishment of baseline information on soil, water and the environment.

Northern Australia is defined as the part of Australia north of the Tropic of Capricorn. The Murray–Darling Basin and major irrigation areas and major dams (greater than 500 GL capacity) in Australia are shown for context.

The Roper River Water Resource Assessment (the Assessment) provides a comprehensive and integrated evaluation of the feasibility, economic viability and sustainability of water and agricultural development.

While agricultural developments are the primary focus of the Assessment, it also considers opportunities for and intersections between other types of water-dependent development. For example, the Assessment explores the nature, scale, location and impacts of developments relating to industrial and urban development and aquaculture, in relevant locations.

The Assessment was designed to inform consideration of development, not to enable any particular development to occur. As such, the Assessment informs – but does not seek to replace – existing planning, regulatory or approval processes. Importantly, the Assessment does not assume a given policy or regulatory environment. As policy and regulations can change, this enables the results to be applied to the widest range of uses for the longest possible time frame.

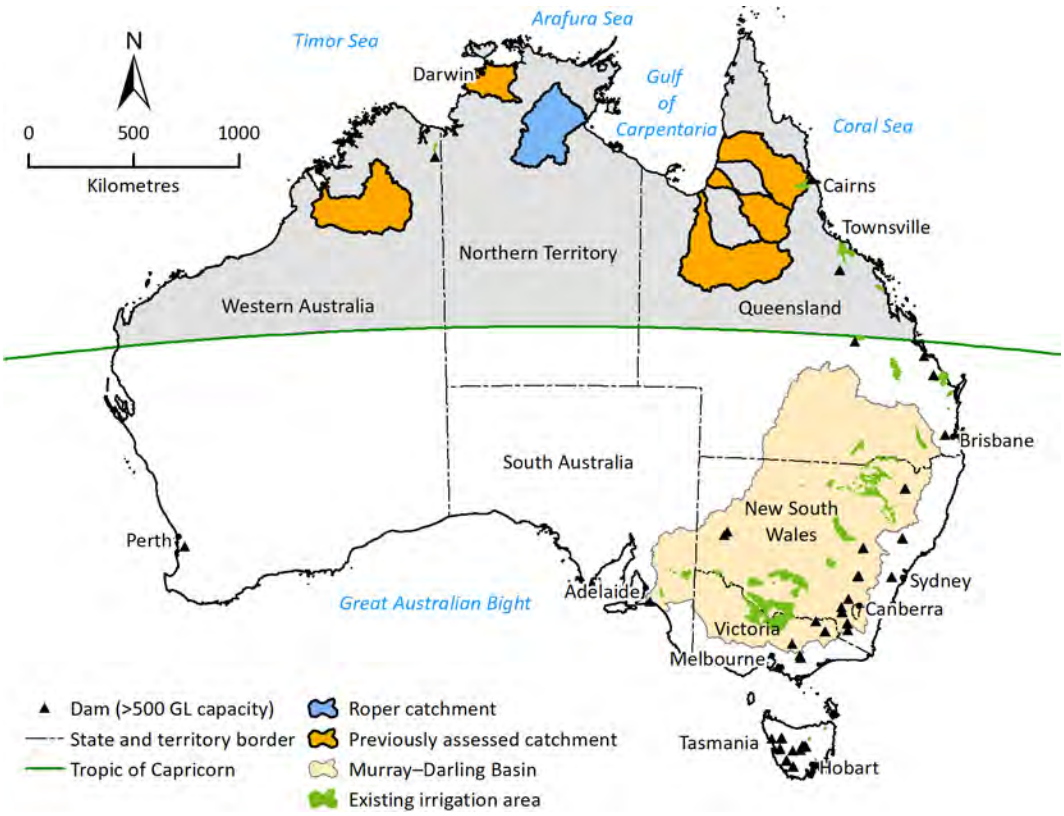

Preface Figure 1-1 Map of Australia showing Assessment area

It was not the intention – and nor was it possible – for the Assessment to generate new information on all topics related to water and irrigation development in northern Australia. Topics not directly examined in the Assessment are discussed with reference to and in the context of the existing literature.

Functionally, the Assessment adopted an activities-based approach (reflected in the content and structure of the outputs and products), comprising eight activity groups; each contributes its part to create a cohesive picture of regional development opportunities, costs and benefits. Preface Figure 1-2 illustrates the high-level links between the eight activities and the general flow of information in the Assessment.

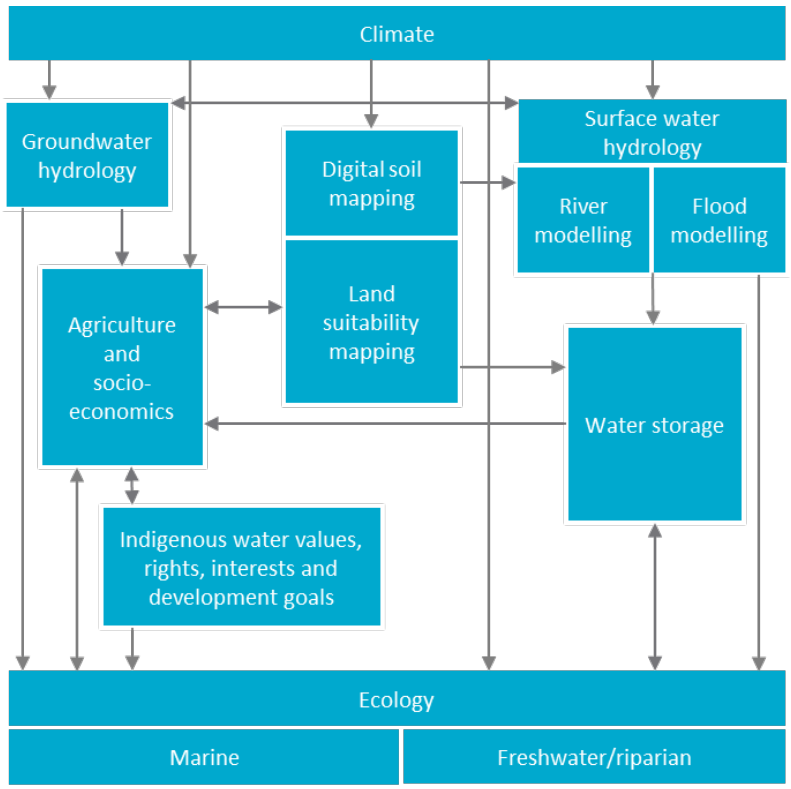

Preface Figure 1-2 Schematic diagram of the high-level linkages between the eight activities and the general flow of information in the Assessment.

Assessment reporting structure

Development opportunities and their impacts are frequently highly interdependent and consequently, so is the research undertaken through this Assessment. While each report may be read as a stand-alone document, the suite of reports most reliably informs discussion and decisions concerning regional development when read as a whole.

The Assessment has produced a series of cascading reports and information products:

- Technical reports; that present scientific work at a level of detail sufficient for technical and scientific experts to reproduce the work. Each of the eight activities has one or more corresponding technical report.
- A Catchment report; that for the Roper catchment synthesises key material from the technical reports, providing well-informed (but not necessarily-scientifically trained) readers with the information required to make decisions about the opportunities, costs and benefits associated with irrigated agriculture and other development options.
- A Summary report; that for the Roper catchment provides a summary and narrative for a general public audience in plain English.
- A Summary factsheet; that for the Roper catchment provides key findings for a general public audience in the shortest possible format.

The Assessment has also developed online information products to enable the reader to better access information that is not readily available in a static form. All of these reports, information tools and data products are available online at https://www.csiro.au/roperriver. The website provides readers with a communications suite including factsheets, multimedia content, FAQs, reports and links to other related sites, particularly about other research in northern Australia.

Executive summary

This report focuses on the flooding characteristics of the catchment of the Roper River. The impact of flooding on agricultural production can be significant, potentially leading to the loss of livestock, fodder, topsoil, and damage to crops and infrastructure. However, it is important to note that flooding plays a vital role in river, wetland and coastal ecosystems. For example flood pulses create opportunities for offstream wetlands to connect with the main river channels allowing the exchange of water, sediments, chemicals, organic matter and biota.

This report provides an overview of the flooding characteristics over the region. It also details the hydrodynamic modelling tools utilised to assess flooding. This includes information on model configuration, data acquisition and the evaluation process, comparing the model results with satellite-based flood inundation maps.

Hydrodynamic models offer several advantages over satellite-based approaches and conceptual node-link river system models when it comes to evaluating flooding. These models enable the assessment of not only the extent of inundation but also water depth and velocity, with the ability to analyse these factors at very fine time intervals, often in the order of seconds. In contrast, satellite-based approaches primarily focus on analysing historical flood events. Hydrodynamic models, on the other hand, can be used to assess how flood characteristics might change under future climate and development scenarios.

The outputs derived from the hydrodynamic modelling play a crucial role in various aspects, which include:

- identifying areas prone to flooding under historical climate conditions and current development levels (baseline)
- estimating changes in inundation across the floodplains under potential future climate and development scenarios
- quantifying the hydrological connectivity of floodplain wetlands, considering the extent, timing and duration of the connection between offstream wetlands and the main river channels
- assessing changes in hydrological connectivity resulting from altered flow regimes.

Model calibration

In the Assessment, a one-dimensional hydrodynamic river model (MIKE 11) was coupled to a two-dimensional hydrodynamic floodplain model (MIKE 21 FM) to simulate floodplain hydraulics and inundation dynamics within two (inland and coastal) zones in the Roper catchment.

Boundary conditions were derived from daily discharge from a calibrated river system model called the Australian Water Resource Assessment – River model (AWRA-R), hourly tide gauge information and Sacramento rainfall-runoff model simulations. Flood inundation maps for individual flood events from 1988 to 2013 were created using high-quality Moderate-Resolution Imaging Spectroradiometer (MODIS) and Landsat imagery. These maps were used to calibrate the hydrodynamic model.

Two separate hydrodynamic models were configured to optimise computation time. Zone 1 extends downstream of Jilkminggan to Red Rock gauge, covering approximately 1500 km^2. Zone 2 is the lower domain extending from the Red Rock gauge to the mouth of the Roper River, covering approximately 2614 km^2.

High-resolution Light Detection and Ranging (LiDAR) data (5 m) was acquired as part of the Assessment over most of the floodplain area. This was a key input to the hydrodynamic model in these areas, while 30-m grid Shuttle Radar Topography Mission (SRTM)-based hydrologically corrected land elevation data (referred to as DEM-H) was used for the remaining model domain.

Each hydrodynamic model was calibrated to four flood events, carefully selected to ensure a range of event sizes and availability of cloud-free MODIS and Landsat images. The hydrodynamic model demonstrated reasonable simulation of spatial floodplain inundation patterns when compared to MODIS and Landsat water maps. Overall, the hydrodynamic models performed better for large floods, followed by medium-sized events, and then small events.

The calibrated hydrodynamic models were utilised to investigate flood characteristics in the two zones and simulate future climate and development scenarios. Due to the extensive computation time required, a limited number of simulation runs were conducted in each zone.

Flood characteristics

Inundation in Zone 1 is primarily driven by high flows down the Roper River, with areas along the Maiwok Creek also displaying significant flooding. The Zone 1 domain consists of a network of complicated braided channels that become activated as water levels rise. In addition to the general anastomosing channel patterns, there are several noteworthy geomorphological features along the Roper River where the main channel suddenly splits into many (more than 10) anabranches that reconnect between 5 and 20 km downstream.

The characteristics of Zone 2 stand in stark contrast to those of Zone 1. Tidal influences reach all the way to Roper Bar, 10 km downstream of the Red Rock gauge. A single Roper River channel is better defined, and less anabranching occurs in the lower zone. Furthermore, Zone 2 contains tidal flats towards the coast along the Roper and Phelp rivers.

Additional observations of flooding under the historical climate in the Roper catchment are as follows:

- Flood peaks typically take about 3 days to travel from Mataranka Homestead to Red Rock, at a mean speed of 3.3 km/hour.
- For flood events of annual exceedance probability (AEP) 1 in 2, 1 in 5 and 1 in 13, the peak discharge (discharge) at Red Rock on the Roper River is 1100, 1500 and 3000 m^3/second, respectively (i.e. 95, 130 and 259 thousand ML/d, respectively).
- Between 1966 and 2019 (53 years), events with a discharge greater than or equal to AEP 1 in 1 occurred during all months between August and April, with about 85% of events occurring between December and March. Of the ten events with the largest flood peak discharge at Red Rock on the Roper River, four events occurred during December, three in January and one event in each of February, March and April.
- The maximum areas inundated for events of AEP 1 in 2 (1988), AEP 1 in 5 (2008), AEP 1 in 13 (1991) were 374, 1476 and 1495 km^2, respectively.

Model scenario analysis

A limited number of simulations were conducted to investigate the hydrological effects of potential climate and development changes in the future.

The model results revealed that the impacts of future projected wet (Scenario Cwet) and dry (Scenario Cdry) climates on floodplain inundation and wetland connectivity were more pronounced than the modelled impacts of water resource development. In both zones, the increase in floodplain inundation and connectivity under Scenario Cwet was larger than the decrease under Scenario Cdry, which is consistent with the changes in modelled streamflow under these climate scenarios.

The inclusion of five hypothetical dams (sites on Flying Fox Creek, Jalboi River, Hodgson River, Waterhouse River and Waterhouse River West Branch) resulted in a 4% decrease in the inundated area downstream for an event with an AEP of 1 in 2 and an 7% decrease for an event with an AEP of 1 in 13. The relatively small impact on inundated area is partly because the potential dams are located in small headwater catchments, and in the Roper catchment, local runoff on the coastal floodplains and surrounding land exceeds that generated in the headwater catchments. That the larger event experienced a larger reduction in maximum inundated area than the smaller event is attributed to antecedent dam storage conditions prior to each event. The 1 in 13 event followed several years of dry conditions and thus the simulated reservoir was largely empty.

The inclusion of only the hypothetical Waterhouse River dam (with a capacity of 219 GL) resulted in a 1% decrease in the maximum inundated area for an event with an AEP of 1 in 2 and an 2% decrease for an event with an AEP of 1 in 13. As with the five hypothetical dams scenario, the larger event experienced a larger reduction in maximum inundated area than the smaller event because the antecedent dam storage conditions were lower for the larger event..

The incorporation of a hypothetical Flying Fox Creek dam, with a capacity of 133 GL, led to a reduction of 1% in the maximum flooded area during both AEP of 1 in 2 and 1 in 13 events.

Water harvesting (660 GL) resulted in a 11% decrease in the flooded area for an event with an AEP of 1 in 2. During an event with an AEP of 1 in 13, there was a very small (0.02%) reduction in the extent of inundation.

Page deliberately left blank

Contents

Director's foreword i

The Roper River Water Resource Assessment Team ii

Shortened forms iii

Units iv

Preface v

Executive summary viii

1 Introduction 1

1.1 Objectives 2

1.2 Previous flood studies in the catchment of the Roper River 2

1.3 Overview of flood modelling frameworks used in the Assessment 2

1.4 Report overview and structure 4

1.5 Key terminology and concepts 4

2 Floodplain inundation mapping 6

2.1 Satellite imagery acquisition and pre-processing 6

2.2 Inundation mapping using MODIS 7

2.3 Inundation mapping using Landsat 8

2.4 Summary 10

3 Floodplain inundation modelling 12

3.1 Hydrodynamic models 12

4 Roper catchment hydrodynamic model calibration 14

4.1 Physical and hydro-meteorological properties 14

4.2 Model configuration 18

4.3 Model input 19

4.4 Selected flood events for model calibration 23

4.5 Hydrodynamic model simulation and outputs 24

4.6 Hydrodynamic model calibration 24

4.7 Results and discussion 27

4.8 Summary 35

5 Flood modelling under future climate and development scenarios 37

5.1 Introduction 37

5.2 Future climate scenarios 38
5.3 Potential development scenarios 41
5.4 Floodplain inundation scenario analyses 41
6 Wetland connectivity assessment 74
6.1 Hydrological connectivity 74
6.2 Method of connectivity assessment 75
6.3 Connectivity assessment for the Roper catchment 76
6.4 Summary 82
7 Summary 83
8 References 85

Figures

Preface Figure 1-1 Map of Australia showing Assessment area vi

Preface Figure 1-2 Schematic diagram of the high-level linkages between the eight activities and the general flow of information in the Assessment. vii

Figure 1-1 Flowchart illustrating the method used to calibrate a hydrodynamic model (MIKE 21) and scenario modelling for future climate and dam impact assessment 3

Figure 2-1 MODIS satellite based flood inundation map of the Roper catchment 8

Figure 2-2 Landsat satellite based flood inundation map of the Roper catchment 10

Figure 4-1 Roper catchment map showing major and minor rivers and stream gauges 15

Figure 4-2 Historical monthly rainfall (range shows the range in values between the 20 and 80% monthly exceedance rainfall) and historical annual rainfall at Ngukurr 16

Figure 4-3 Monthly flow distribution at Red Rock on the Roper River based on observed flow data for the period of 1966 to 2019 17

Figure 4-4 Annual maximum discharge at Red Rock (9030250) on the Roper River since 11966 18

Figure 4-5 Monthly flood frequency in the Roper catchment based on floods of AEP greater or equal to 1 in 1 18

Figure 4-6 Roper hydrodynamic model domain showing the LiDAR data coverage 20

Figure 4-7 Boundary nodes for the flood domains 22

Figure 4-8 Map of soil permeability 23

Figure 4-9 Classification at the grid cell level using a contingency table (Ebert, 2009) 26

Figure 4-10 Comparison of the Zone 1 hydrodynamic model simulated discharge and observed discharge at the Red Rock (9030250) gauge on the Roper River. 28

Figure 4-11 Comparison of the Zone 1 hydrodynamic model simulated stage height and observed stage height at the Red Rock (9030250) gauge on the Roper River. 29

Figure 4-12 Examples of the comparison of the Landsat/MODIS inundation map versus the inundation area simulated by the hydrodynamic modelling for Zone 1 31

Figure 4-13 Examples of the comparison of the Landsat/MODIS inundation map versus the inundation area simulated by the hydrodynamic modelling for Zone 2 32

Figure 4-14 Zone 1 hydrodynamic modelling domain showing wetlands 34

Figure 5-1 Comparison of inflow time series within the hydrodynamic model domain in the Roper catchment from 1988 to 2013 (period over which hydrodynamic model was calibrated) for Zone 1 (a) and Zone 2 (b) 39

Figure 5-2 Simulated aggregated streamflow used as inflows in the hydrodynamic model for two different flood events (1988 and 1991) under scenarios A (baseline), Cwet and Cdry 40

Figure 5-3 Percentage inundation frequency in the Zone 1 model domain under Scenario A (Baseline) and B (all dams) 43

Figure 5-4 Percentage inundation frequency in the Zone 2 model domain under Scenario A (Baseline) and B (all dams) 43

Figure 5-5 Maximum inundation extent in the Zone 1 model domain under scenarios A (Baseline) and B (all dams) 44

Figure 5-6 Maximum inundation extent in the Zone 2 model domain under scenarios A (Baseline) and B (all dams) 44

Figure 5-7 Depth at maximum inundation extent in the Zone 1 model domain under scenarios A (Baseline) and B (all dams) 45

Figure 5-8 Depth at maximum inundation extent in the Zone 2 model domain under scenarios A (Baseline) and B (all dams) 45

Figure 5-9 Comparison of inundated area in square kilometres over Zone 1 (left) and 2 (right) under scenarios A (Baseline) and B (all dams) 46

Figure 5-10 Percentage inundation frequency in the Zone 1 model domain under Scenario A (Baseline) and B (Waterhouse River dam) 47

Figure 5-11 Percentage inundation frequency in the Zone 2 model domain under Scenario A (Baseline) and B (Waterhouse River dam) 47

Figure 5-12 Maximum inundation extent in the Zone 1 model domain under scenarios A (Baseline) and B (Waterhouse River dam) 48

Figure 5-13 Maximum inundation extent in the Zone 2 model domain under scenarios A (Baseline) and B (Waterhouse River dam) 49

Figure 5-14 Depth at maximum inundation extent in the Zone 1 model domain under scenarios A (Baseline) and B (Waterhouse River dam) 49

Figure 5-15 Depth at maximum inundation extent in the Zone 2 model domain under scenarios A (Baseline) and B (Waterhouse River dam) 50

Figure 5-16 Comparison of inundated area in square kilometres over Zone 1 (left) and 2 (right) under scenarios A (Baseline) and B (Waterhouse River dam) 51

Figure 5-17 Percentage inundation frequency in the Zone 1 model domain under Scenario A (Baseline) and B (Flying Fox Creek dam) 52

Figure 5-18 Percentage inundation frequency in the Zone 2 model domain under Scenario A (Baseline) and B (Flying Fox Creek dam) 52

Figure 5-19 Maximum inundation extent in the Zone 1 model domain under scenarios A (Baseline) and B (Flying Fox Creek dam) 53

Figure 5-20 Maximum inundation extent in the Zone 2 model domain under scenarios A (Baseline) and B (Flying Fox Creek dam) 53

Figure 5-21 Depth at maximum inundation extent in the Zone 1 model domain under scenarios A (Baseline) and B (Flying Fox Creek dam) 54

Figure 5-22 Depth at maximum inundation extent in the Zone 2 model domain under scenarios A (Baseline) and B (Flying Fox Creek dam) 54

Figure 5-23 Comparison of inundated area in square kilometres over Zone 1 (left) and 2 (right) under scenarios A (Baseline) and B (Flying Fox Creek dam) 55

Figure 5-24 Percentage inundation frequency in the Zone 1 model domain under Scenario A (Baseline) and B (Water Harvesting) 56

Figure 5-25 Percentage inundation frequency in the Zone 2 model domain under Scenario A (Baseline) and B (Water Harvesting) 56

Figure 5-26 Maximum inundation extent in the Zone 1 model domain under scenarios A (Baseline) and B (Water Harvesting) 57

Figure 5-27 Maximum inundation extent in the Zone 2 model domain under scenarios A (Baseline) and B (Water Harvesting) 57

Figure 5-28 Depth at maximum inundation extent in the Zone 1 model domain under scenarios A (Baseline) and B (Water Harvesting) 58

Figure 5-29 Depth at maximum inundation extent in the Zone 2 model domain under scenarios A (Baseline) and B (Water Harvesting) 58

Figure 5-30 Comparison of inundated area in square kilometres over Zone 1 (left) and 2 (right) under scenarios A (Baseline) and B (Water Harvesting) 59

Figure 5-31 Percentage inundated frequency in the Zone 1 model domain under scenarios A and C 60

Figure 5-32 Percentage inundated frequency in the Zone 2 model domain under scenarios A and C 61

Figure 5-33 Maximum inundation extent in the Zone 1 model domain under scenarios A and C 61

Figure 5-34 Maximum inundation extent in the Zone 2 model domain under scenarios A and C 62

Figure 5-35 Depth at maximum inundation extent in the Zone 1 model domain under scenarios A and C 62

Figure 5-36 Depth at maximum inundation extent in the Zone 2 model domain under scenarios A and C 63

Figure 5-37 Comparison of inundated area in square kilometres (left) and mean depth in metres (right) over the Zone 1 and 2 domains under Scenario C 64

Figure 5-38 Percentage inundation frequency in the Zone 1 model domain under Scenario A (Baseline) and Ddry (all dams) 65

Figure 5-39 Percentage inundation frequency in the Zone 2 model domain under Scenario A (Baseline) and Ddry (all dams) 66

Figure 5-40 Maximum inundation extent in the Zone 1 model domain under scenarios A (Baseline) and Ddry (all dams) 66

Figure 5-41 Maximum inundation extent in the Zone 2 model domain under scenarios A (Baseline) and Ddry (all dams) 67

Figure 5-42 Depth at maximum inundation extent in the Zone 1 model domain under scenarios A (Baseline) and Ddry (all dams) 67

Figure 5-43 Depth at maximum inundation extent in the Zone 2 model domain under scenarios A (Baseline) and Ddry (all dams) 68

Figure 5-44 Comparison of inundated area in square kilometres over Zone 1 (left) and 2 (right) under scenarios A (Baseline) and Ddry (all dams) 69

Figure 5-45 Percentage inundation frequency in the Zone 1 model domain under Scenario A (Baseline) and Ddry (water harvesting) 70

Figure 5-46 Percentage inundation frequency in the Zone 2 model domain under Scenario A (Baseline) and Ddry (water harvesting) 70

Figure 5-47 Maximum inundation extent in the Zone 1 model domain under scenarios A (Baseline) and Ddry (water harvesting) 71

Figure 5-48 Maximum inundation extent in the Zone 2 model domain under scenarios A (Baseline) and Ddry (water harvesting) 71

Figure 5-49 Depth at maximum inundation extent in the Zone 1 model domain under scenarios A (Baseline) and Ddry (water harvesting) 72

Figure 5-50 Depth at maximum inundation extent in the Zone 2 model domain under scenarios A (Baseline) and Ddry (water harvesting) 72

Figure 5-51 Comparison of inundated area in square kilometres over Zone 1 (left) and 2 (right) under scenarios A (Baseline) and Ddry (water harvesting) 73

Figure 6-1 A schematic representation of wetland connectivity assessment 75

Figure 6-2 Wetlands and river network used for hydrological connectivity analysis in the Roper catchment 76

Figure 6-3 Typical example of spatial variation in inundation duration across floodplains of the Roper River for 1991 flood (AEP of 1 in 13) 78

Figure 6-4 Timing and duration of connectivity of selected wetlands in the Roper catchment under Scenario A for the (a) 1988 flood (AEP of 1 in 2) (b) 1991 flood (AEP of 1 in 13) (c) 2008 flood (AEP of 1 in 5) and (d) 2013 flood (AEP 1 in 3) events 80

Tables

Table 4-1 Manning's roughness coefficient (*n*) for the Roper catchment 21

Table 4-2 River model boundary gauge nodes used for the flood model domains 21

Table 4-3 Flood events used for calibration 24

Table 4-4 Flood event dates, and number of Landsat/MODIS images for the Roper River hydrodynamic model domains 30

Table 4-5 Detection statistics for the Landsat/MODIS images considered in the analysis for Zone 1 33

Table 4-6 Detection statistics for the Landsat/MODIS images considered in the analysis for Zone 2 33

Table 4-7 Average detection statistics for wetland sites in Zone 1 35

Table 5-1 Summary of selected future climate and development scenarios 37

Table 5-2 Summary of inundated area under Scenario C and associated changes compared to Scenario A 64

Table 6-1 List of selected wetlands in the Roper catchment 77

Table 6-2 Summary of mean changes in wetland connectivity for 171 wetlands under Scenario D for the flood events of 2001 (AEP of 1 in 16), 2006 (AEP of 1 in 2) and 2009 (AEP of 1 in 5) 81

1 Introduction

While floods are generally perceived as natural disasters, they can provide many environmental and ecological benefits (Tockner et al., 2008; Opperman et al., 2010). Floodplain inundation contributes to species diversity and relative abundance, aquatic biota growth (Phelps et al., 2015), groundwater recharge (Doble et al., 2012) and soil fertility (Ogden and Thoms, 2002). During floods there is an exchange of water, sediments, chemicals, organic matter and biota between the main river channels and floodplains (Thoms, 2003; Bunn et al., 2006; Tockner et al., 2010). Since publication of the Flood Pulse Concept (Junk et al., 1989), the importance of floodplain inundation for these exchanges and the productivity of diverse aquatic biota in river–floodplain systems has been emphasised in many studies (e.g. Bayley, 1991; Heiler et al., 1995; Middleton, 2002; Welcomme et al., 2006; Gallardo et al., 2009). Yet, our knowledge of the frequency and duration of floodplain inundation and subsequent connectivity between water bodies and ecological functioning of many of the world's largest floodplain systems is very limited and insufficient to inform water management and biodiversity protection, or adaptation to future climate (Beighley et al., 2009; Arthington et al., 2014).

Despite centuries of human activities that alter river floodplains, remnant permanent water bodies still exist on the floodplains, but they are diminishing at increasing rates (Bayley, 1995; Sparks, 1995; Tockner et al., 2008). An important issue for the management of floodplain water bodies, including wetlands of historical, cultural and economic values, is to know the extent, frequency and duration of floodplain inundation and hydrological connectivity between them to derive ways to maintain or even enhance an optimal level of biophysical exchanges between rivers and floodplains. The study area in the Assessment has large floodplains in its middle and lower reaches and they support a larger number of offstream wetlands with high ecological, cultural and biodiversity values. Therefore, it is important to quantify the inundation dynamics in terms of extent, frequency and duration, and hydrological connectivity between offstream wetlands and a main channel or several channels under historical climate, and to assess how the inundation and connectivity could be impacted under future climate and development.

However, quantification of floodplain inundation dynamics and hydrological connectivity between water bodies is still a great challenge. Several studies have used a combination of remotely sensed inundated area and concurrent river flow to predict how flooded area changes with river flow (e.g. Townsend and Walsh, 1998; Hess et al., 2003; Overton, 2005; Frazier et al., 2003; Peake et al., 2011). The same approach has also been used to quantify how the number of inundated wetlands changes with river flow (Shaikh et al., 2001; Frazier et al., 2003; Ganf et al., 2010). However, this approach is not dynamic and cannot produce a continuous time series of inundation extent and it is not possible to quantify the duration of wetland connectivity, which can have an important influence on wetland ecology. With the development of computational methods and computer technology, hydrodynamic modelling has become popular for the study of floodplain hydraulics and for quantifying the time course of flood inundation with high spatial and temporal resolution (Nicholas and Mitchell, 2003; Stelling and Verwey, 2005; Schumann et al., 2009). By combing these modelling techniques with high-resolution topography, the duration, frequency and timing of wetland connectivity can be quantified (Karim et al., 2012; Karim et al., 2015). Previous studies of

this type have used a combination of hydrological and hydrodynamic models of simplified one-dimensional (e.g. Beighley et al., 2009; Chormanski et al., 2009; Ganf et al., 2010) to more complex two-dimensional (Tuteja and Shaikh, 2009) modelling. In the Assessment, a coupled one- and two-dimensional hydrodynamic model (MIKE FLOOD) has been used with advanced model configuring tools to simulate floodplain inundation and hydrological connectivity between offstream wetlands and rivers.

1.1 Objectives

The Roper River Water Resource Assessment flood modelling activity seeks to answer the following questions:

- What areas on the floodplains are susceptible to flooding under the historical climate?
- What were the extent, duration and frequency of flooding under the historical climate?
- What could be the changes in inundation dynamics under future projected climate and hypothetical development scenarios?
- How offstream wetlands are hydrologically connected with the main rivers?
- What could be the changes in hydrological connectivity between floodplain water bodies due to flow regime change under future projected climate and hypothetical development scenarios?

This report describes the configuration and calibration of the coupled one- and two-dimensional river and floodplain hydrodynamic model (MIKE FLOOD) and scenario modelling using the calibrated model for the study area to address the above questions.

1.2 Previous flood studies in the catchment of the Roper River

Past flood modelling in the Roper catchment is very limited. A flood study of the upper Roper River was undertaken by Connell Wagner Pty Ltd in 2001 and aimed to achieve two primary objectives: (i) to conduct a flood risk analysis for the Beswick Community situated on the Waterhouse River, and (ii) to develop a flood warning model for the communities of Beswick, Mataranka Resort, Djilkminggan and Elsey Station. The study employed the MIKE 11 surface water modelling package in tandem with boundary condition discharge hydrographs derived from the Unified River Basin Simulator (URBS) rainfall-runoff model (Connell Wagner Pty Ltd, 2001).

1.3 Overview of flood modelling frameworks used in the Assessment

Hydrodynamic models have been in common use for several decades worldwide and are used for a wide variety of purposes including simulating flood events for engineering design, land-use planning and risk assessment studies (Nicholas and Mitchell, 2003). Because these models have a strong underlying physical basis (e.g. the use of water equilibrium equations, such as Saint–Venant equations) they can be used to model water movement in river channels and over floodplains and used to estimate inundation extent, duration, depth and frequency of wetting and velocity of travel. Depending on the modelling objectives of the study and the availability of data and resources, a variety of hydrodynamic models can be selected including one-dimensional models, two-dimensional models or coupled one- and two-dimensional models. The hydrodynamic models

need to be calibrated against historical streamflow and inundation data before they can be applied with a degree of confidence. Traditionally flood models are calibrated by comparing instream water heights (commonly gauge records) and floodplain inundation (commonly water marks on trees, buildings and electric poles). However, for relatively remote and sparsely populated catchments, it is often not possible to collect the field data that are necessary to robustly calibrate the model. This serves as a major constraint to the use of hydrodynamic models in remote and data-sparse areas. In recent years there have been major advances in flood inundation mapping using satellite and airborne remote sensing. While the satellite imagery based approaches have some limitations, including spatial and temporal resolutions, these techniques provide very useful data for hydrodynamic model calibration. In the Assessment, a combination of field-based observed stage heights and satellite-based inundation maps were used to calibrate the hydrodynamic model. Figure 1-1 shows the general steps in configuring and calibrating the one- and two-dimensional coupled hydrodynamic model (MIKE FLOOD), and scenario modelling for future climate and resource development impact assessment.

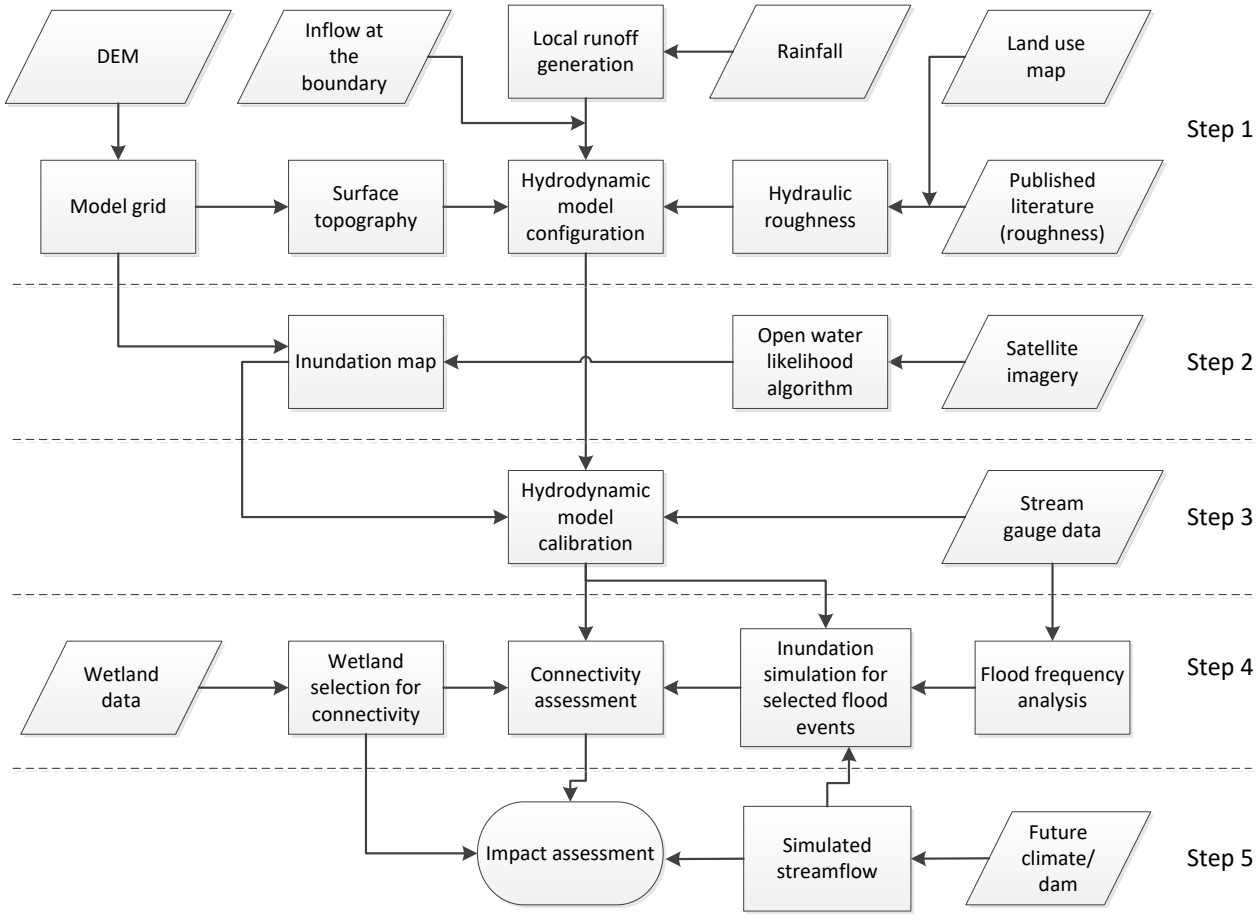

Figure 1-1 Flowchart illustrating the method used to calibrate a hydrodynamic model (MIKE 21) and scenario modelling for future climate and dam impact assessment

DEM = digital elevation model.

1.4 Report overview and structure

This report has been prepared to:

- document the methods that were used to calibrate the MIKE FLOOD hydrodynamic models for the study area
- assess and report on hydrodynamic model performance relative to satellite-based flood inundation mapping
- report on potential flood inundation extent under historical climate and current level of development
- report on potential changes to flood inundation and wetland connectivity under future climate and development.

This report is structured as follows. Chapter 2 describes the inundation mapping approach using satellite data and provides a summary of long-term inundation extent for the study area. Chapter 3 describes the hydrodynamic modelling approach, including the rationale for the selection of the MIKE FLOOD models, their input/output data requirements and model calibration algorithm. Chapters 4, 5 and 6 describe the hydrodynamic model configuration and calibration results against satellite-based flood inundation for the Roper catchment. Chapter 7 provides results and discussion on impacts of future climate and infrastructure on floodplain inundation and Chapter 8 summarises the impacts on wetland connectivity.

1.5 Key terminology and concepts

1.5.1 WATER YEAR AND WET AND DRY SEASONS

Northern Australia has a highly seasonal climate, with most rain falling from December to March. Unless specified otherwise, the Assessment defines the wet season as the 6-month period from 1 November to 30 April, and the dry season as the 6-month period from 1 May to 31 October.

All results in the Assessment are reported over the water year, defined as the period 1 September to 31 August, unless specified otherwise. This allows each individual wet season to be counted in a single 12-month period, rather than being split over two calendar years (i.e. counted as two separate seasons). This is more realistic for reporting climate statistics from a hydrological and agricultural assessment viewpoint.

1.5.2 SCENARIO DEFINITIONS

The Assessment considered four scenarios, reflecting a combination of different levels of development and historical and future climates, much like those used in the Northern Australia Sustainable Yields project (CSIRO, 2009a, 2009b, 2009c) and the Flinders and Gilbert Agriculture Resource Assessment (Petheram et al., 2013a, 2013b):

- Scenario A – historical climate and current development
- Scenario B – historical climate and hypothetical future water resource development
- Scenario C – future climate and current development

- Scenario D – future climate and hypothetical future water resource development.

Scenario A

Scenario A is historical climate and current development. The historical climate series is defined as the observed climate (rainfall, temperature and potential evaporation for water years from 1 September 1910 to 31 August 2019). All results presented in this report are calculated over this period unless specified otherwise. The current level of surface water, groundwater and economic development were assumed (as of 31 August 2019). Scenario A was used as the baseline against which assessments of relative change were made. Historical tidal data were used to specify downstream boundary conditions for the hydrodynamic modelling.

Scenario B

Scenario B is historical climate and future development, as generated in the Assessment. Scenario B used the same historical climate series as Scenario A. River inflow, groundwater recharge and flow, and agricultural productivity were modified to reflect future development. The impacts of changes in flow due to this future development were assessed, including impacts on:

- instream, riparian and near-shore ecology
- Indigenous water values
- economic costs and benefits
- opportunity costs of expanding irrigation
- institutional, economic and social considerations that may impede or enable adoption of irrigated agriculture.

Scenario C

Scenario C is future climate and current development. Future climate impacts on water resources were explored within a sensitivity analysis framework by applying percentage changes in rainfall and potential evaporation to modify the 109-year historical climate series (as in Scenario A). The percentage change values adopted were informed by projected changes in rainfall and potential evapotranspiration under Shared Socioeconomic Pathways SSP2-4.5 and SSP5-8.5, which are used in the United Nations Intergovernmental Panel on Climate Change Sixth Assessment Report. SSP2-4.5 is broadly considered representative of a likely projection given current global commitments to reducing emissions and SSP5-8.5 is representative of an (unlikely) upper bound. The current level of surface water, groundwater and economic development were assumed.

Scenario D

Scenario D is future climate and future development. It used the same future climate series as Scenario C. River inflow was modified to reflect future development, as in Scenario B. Therefore, in this report, the climate data for scenarios A and B were the same (historical observations from 1 September 1910 to 31 August 2019) and the climate data for scenarios C and D are the same (the above historical data scaled to reflect a plausible range of future climates).

2 Floodplain inundation mapping

Spatial maps of water in the landscape derived from satellite imagery for dates coinciding with flood events are useful to help calibrate and post-audit the hydrodynamic models used to simulate flood events for the floodplain of the Roper catchment. These maps were produced using satellite imagery from the Moderate-Resolution Imaging Spectroradiometer (MODIS) and Landsat sensors. However, frequent cloud occurrence during the wet season across northern Australia limits optical remote sensing opportunities for capturing inundation extents over the different rivers and floodplains in the hydrodynamic model domain, particularly during the flood peak. Refer to the technical report on Earth observation methods, Sims et al. (2016), for further details on the satellite data, processing methods and calibration of these products.

2.1 Satellite imagery acquisition and pre-processing

MODIS satellite data were used for producing daily maps of surface water. The MODIS sensor is an optical/infrared sensor from the National Aeronautics and Space Administration. There are two MODIS sensors currently orbiting the Earth (TERRA since 2000 and AQUA since 2002). They acquire daytime images of Australia around 10 am (TERRA) and 2 pm (AQUA). MODIS surface reflectance data are available from early 2000 until the present https://dap.nci.org.au/thredds/catalog.htmlfrom the United States Geological Survey (USGS) Land Processed Distributed Active Archive Center (LP-DAAC) (https://lpdaac.usgs.gov/) as grided tiles, which are also stored at CSIRO for the whole of Australia. These data are available in hierarchical data format (HDF), in a sinusoidal projection, with a pixel size of 0.004697 degrees (approximately 500 m). Daily images of surface reflectance from both the TERRA and AQUA MODIS sensors (MOD09GA and MYD09GA respectively), as well as an 8-day composite product (based on cloud-free, good quality images; from TERRA – MOD09A1) were used.

Landsat data, when available, are also useful for mapping surface water. These data are at a much finer spatial resolution (30-m pixels) than MODIS, which is better suited to identify narrow or small water features. However, Landsat images are only available every 16 days at best. This is usually less frequent due to cloud cover and missing data. Landsat 5 data (also called Thematic Mapper or TM), Landsat 7 data (also called Enhanced Thematic Mapper or ETM), and Landsat 8 data (also called Operational Land Imager or OLI) are available from Digital Earth Australia (DEA) from 1987 until the present. The DEA provides consistent pre-processing, organisation and analytics of Landsat data for the Australian continent (Dhu et al., 2017). This processing involves corrections for illumination and observation angles, the Bidirectional Reflectance Distribution Function (BRDF, which influences relative pixel brightness across large scene areas) and atmospheric conditions. Refer to the companion technical report on Earth observation methods, Sims et al. (2016), for further details on Landsat data processing.

2.2 Inundation mapping using MODIS

The Open Water Likelihood (OWL) algorithm (Guerschman et al., 2011) was used for mapping open surface water with MODIS imagery at a 500-m pixel resolution. The OWL was developed using empirical statistical modelling and calculates the fraction of water within a MODIS pixel. A cloud mask was applied using the MODIS state band associated with each product, which contains information on cloud and cloud-shadow location. Refer to the companion technical report on Earth observation methods, Sims et al. (2016), for further details on the MODIS OWL algorithm. The daily MODIS OWL water maps (one from TERRA – MOD, and AQUA – MYD), as well as 8-day MODIS OWL water maps (from TERRA – MOD) were extracted from the Australia-wide products for the study area using python code.

A limitation of MODIS maps of surface water is that they are not of sufficient detail to map narrow water features of less than 1 pixel in width (~500 m). This problem is even more exaggerated when the narrow river channel is covered by vegetation along the banks, or floating vegetation, which obscures the water from the sensor.

2.2.1 Event maps

The daily MODIS maps were subset for the Roper hydrodynamic model domains for flood events used for inundation modelling. The years 1988, 1991, 2008 and 2013 were considered. The MODIS OWL water maps were converted into a map of water and non-water pixels. A threshold was used to stratify the MODIS OWL water fraction into water/non-water. Ticehurst et al. (2015) showed that in the Flinders catchment a 10% threshold resulted in the best match when comparing MODIS and Landsat inundation maps. Thus, all pixels above the OWL threshold of 10% were mapped as water, and the images reprojected to the geographic latitude/longitude (coordinate system code EPSG:4326) coordinate system, before conversion to a GeoTIFF format for use with the hydrodynamic models.

2.2.2 Summary maps

Summary maps were also produced for the flood events used in the hydrodynamic modelling (Figure 2-1). These used composites of the MOD09A1 MODIS OWL water maps to show maximum inundation extent, and the percentage of clear observations (i.e. without clouds and/or nulls).

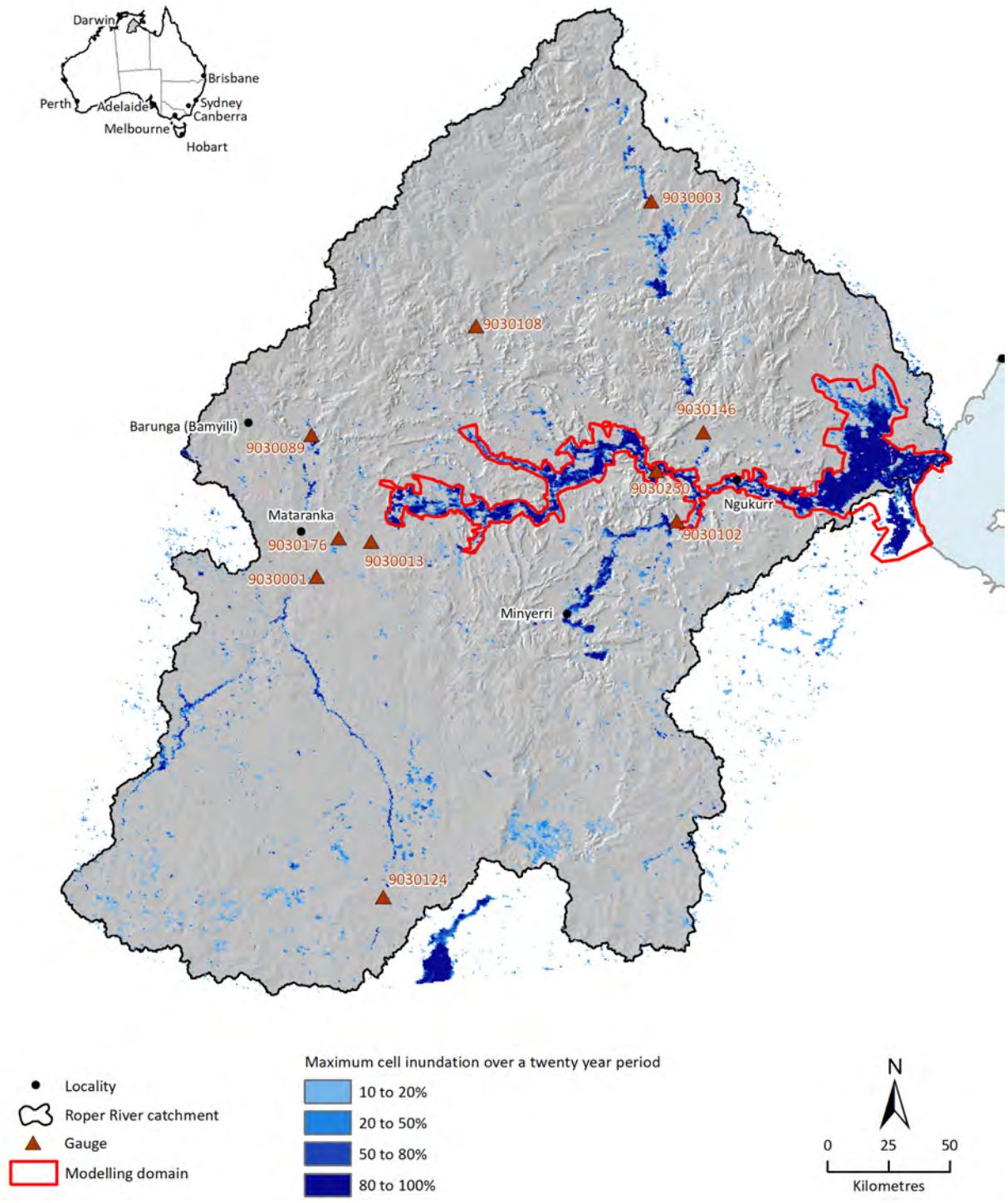

Figure 2-1 MODIS satellite based flood inundation map of the Roper catchment

Data captured using MODIS satellite imagery. This figure illustrates the maximum percentage of MODIS pixel inundation between 2000 and 2020.

2.3 Inundation mapping using Landsat

2.3.1 Algorithm used

Landsat 5 Thematic Mapper (TM), 7 Enhanced Thematic Mapper (ETM) and 8 Operational Land Imager (OLI) data were extracted from the DEA. For mapping flood inundation, the Normalized

Difference Water Index $(NDWI)_{Xu}$ (Xu, 2006) – an index based on the green and mid infrared wavelengths – was used. Water was separated from other features using a threshold of $NDWI_{Xu} \geq -0.3$, which is consistent with Sims et al. (2014) and balances errors of omission and commission in most landscapes. Masking of cloud cover was undertaken by extracting the pixel quality band available with each Nadir BRDF-Adjusted Reflectance (NBAR) product.

2.3.2 Event maps

Landsat water maps were selected for the same hydrodynamic model domains and flood events as the MODIS data. These were examined to find those images least affected by cloud cover, which greatly limited the number of available images, given that deep clouds and sustained rain prevail during the wet season across northern Australia and the infrequent satellite overpass. These were then converted to the geographic latitude/longitude (EPSG:4326) coordinate system and GeoTIFF format for use with the hydrodynamic models.

2.3.3 Summary maps

Summary maps were produced for the flood events used in the hydrodynamic modelling by combining all images to delineate maximum flooding extent (Figure 2-2). These used the Landsat composite water maps, which used all available images to show maximum inundation extent for the selected periods, and the percentage of clear observations (i.e. without clouds and/or nulls).

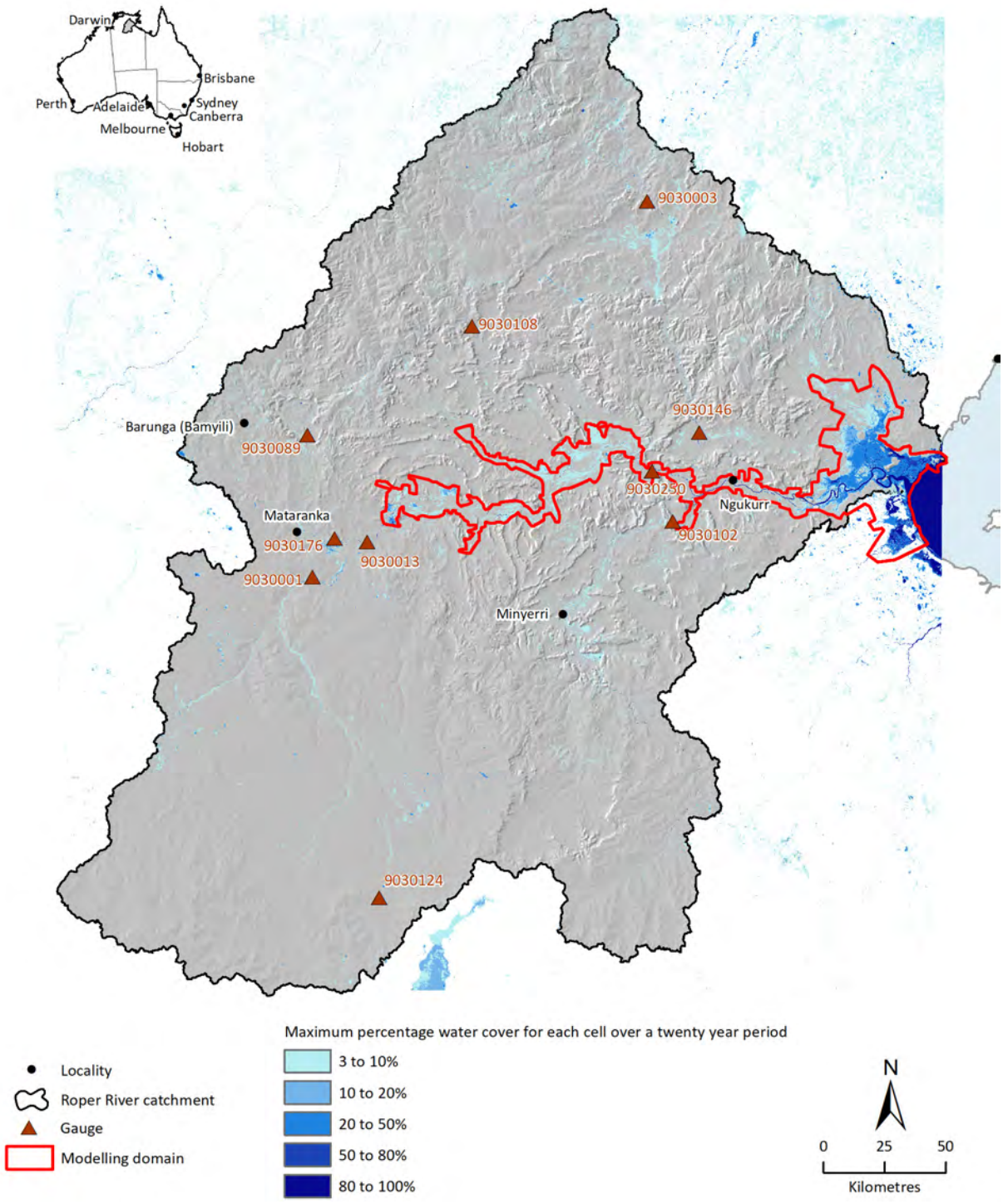

Figure 2-2 Landsat satellite based flood inundation map of the Roper catchment

Data captured using Landsat satellite imagery. This figure illustrates the maximum percentage of Landsat pixel inundation between 2000 and 2020.

2.4 Summary

Flood inundation maps were produced using MODIS and Landsat imagery for the Roper catchment. MODIS surface reflectance data are available since 2000 for the whole of Australia. Daily images of surface reflectance from both the TERRA and AQUA MODIS sensors (MOD09GA and MYD09GA, respectively), and 8-day composite images of surface reflectance from the TERRA

MODIS sensor (MOD09A1) were used in the analysis. Landsat data are available from DEA from 1987 until the present in a consistent analysis-ready format.

The OWL algorithm was used for mapping open surface water with MODIS imagery at a 500-m pixel resolution. The OWL was developed using empirical statistical modelling and calculates the fraction of water within a MODIS pixel. The daily MODIS OWL water maps (one each from TERRA – MOD and AQUA – MYD) were extracted and subset for the Roper catchment hydrodynamic model domains and a series of flood maps were produced for selected flood days for hydrodynamic model calibration.

The NDWI algorithm was used for mapping flood inundation based on Landsat imagery. Water was separated from other features using a threshold of NDWI ≥ –0.3, which balances errors of omission and commission in most landscapes. Similarly, for MODIS, a set of event-based and summary maps were produced using Landsat data.

Water maps generated from satellite imagery are particularly useful for covering large areas at a reasonable temporal frequency. While MODIS can provide daily water maps, it is of a poorer spatial resolution (~500 m) compared to Landsat (30 m pixel), and surface water of less than 1 pixel in width (~500 m) cannot be mapped, particularly if there is vegetation along the river banks. In general, it was found that in northern Australia's wet–dry tropical/monsoonal climate, MODIS produces better flood maps for the large floodplains and/or big flood events. Care must be taken when interpreting the MODIS water maps due to artefacts in the imagery and confusion with dark soils and dark rocks as well as residual cloud and topographic shadow. Unusual water features appearing in only one image need to be treated with caution, and a flood-likelihood mask would greatly benefit interpretation of the data.

The Landsat water maps are very useful for detecting fine water features, however, the temporal frequency of the imagery made it difficult to analyse flood events as the flood peak was often missed due to the timing of satellite overpass and cloud. However, like MODIS, the Landsat water maps will also be affected by the same difficulties in detecting water under flooded vegetation, as well as confusion with dark features (e.g. residual cloud and topographic shadow).

The maximum percentage water cover for MODIS imagery is higher compared to Landsat imagery. The reason for this is that MODIS OWL water maps can identify wet soil as water (Sims et al., 2016). Another reason for the difference could be due to MODIS having a much higher temporal frequency (daily) than Landsat (every 16 days), which means Landsat will fail to coincide with more flood events than MODIS.

3 Floodplain inundation modelling

3.1 Hydrodynamic models

Two-dimensional hydrodynamic models (e.g. MIKE 21, TUFLOW, LISFLOOD-FP) are commonly used to simulate flood levels and inundation extent in a river–floodplain system (Neal et al., 2012; Neelz and Pender, 2013; Kvocka et al., 2015). The main strengths of the hydrodynamic models are that they produce floodplain hydraulics to estimate inundation extent, duration, depth and frequency of wetting and drying at desired spatial (e.g. 5 to 10 m grid) and temporal (e.g. hourly) scales (Horritt and Bates, 2002). Based on the modelling objectives and availability of input data, either a two-dimensional regular grid model (DHI, 2012) or a two-dimensional flexible grid model (DHI, 2016) can be selected. Technical considerations include the size of the hydrodynamic model domain, irregularity in land topography, availability of topography data and complexity of the hydraulic regime. These two-dimensional models have the option to be coupled with one-dimensional river models, which allows a finer representation of the highly dynamic river processes with river cross-sections.

For the Assessment, a two-dimensional flexible mesh model (MIKE 21 FM) coupled with a one-dimensional river model (MIKE 11) was selected for the Roper catchment primarily based on availability of fine-scale laser altimetry (LiDAR) data and the one-dimensional MIKE 11 model provided by Northern Territory Government (Knapton, 2009). A brief description of the models is presented in the following sections.

3.1.1 ONE-DIMENSIONAL HYDRODYNAMIC MODEL – MIKE 11

The MIKE 11 hydrodynamic module uses an implicit, finite difference scheme for the computation of unsteady flows in rivers and estuaries (DHI, 2021). The model simulates user-defined networks composed of channel cross-sections. MIKE 11 routes water while accounting for bed roughness and both point and diffuse fluxes. The model is appropriate for efficient simulation of channelised flow but is not suitable for large overbank events.

Model input data includes river cross-sections, inflow and outflow conditions, and bed resistance. Rainfall and evaporation data can be incorporated in MIKE 11. Model output includes time series of water depth, velocity and discharge.

The one-dimensional Roper River model was provided by the Northern Territory Government (Knapton, 2009), which was adapted for use in the flood study by updating boundary conditions and river bed roughness coefficients. The MIKE 11 model was coupled to the MIKE 21 FM model.

3.1.2 TWO-DIMENSIONAL HYDRODYNAMIC MODEL – MIKE 21 FM

The hydrodynamic module of the MIKE 21 Flow Model FM (hereafter referred to as MIKE 21 FM) is based on the numerical solution of the two-dimensional incompressible Reynolds-averaged Navier–Stokes equations, assuming hydrostatic pressure. Primitive variable equations are discretised using an element-centred finite volume method. The spatial domain is discretised into

non-overlapping elements, which can be either triangular or quadrilateral (DHI, 2016). The finite volume method sets up an equivalent Riemann problem (ERP) across each element interface, and solves it to determine the variable fluxes between elements. The technique used in MIKE 21 FM determines an exact solution to an approximate Riemann problem. The approach treats the problem as one-dimensional in the direction perpendicular to each element interface (Guinot, 2003).

MIKE 21 FM has two options for time integration accuracy, with these being a first order explicit Euler method (referred to as the lower temporal order scheme), and a second order Runge–Kutta method (referred to as the higher temporal order scheme). There are also two options for spatial integration, with the second order (higher order) accuracy being achieved through a variable gradient reconstruction technique prior to the ERP formulation (DHI, 2016). In the Assessment, a triangular flexible mesh model was coupled to a MIKE 11 model for the Roper catchment floodplain inundation modelling.

The flexible mesh model is preferable over the classic MIKE 21 regular grid model when highly detailed elevation data (e.g. LiDAR) are available because the model allows selection of a very small grid at the area of interest and the alignment of model grids to the river banks.

3.1.3 ONE- AND TWO-DIMENSIONAL HYDRODYNAMIC MODEL COUPLING – MIKE FLOOD

As mentioned in the previous sections, the Roper catchment floodplain inundation modelling was performed by coupling the one-dimensional MIKE 11 model with the two-dimensional MIKE 21 FM model. This is to utilise the precise and efficient representation of the within river bank processes of MIKE 11, while using the MIKE 21 FM model to simulate floodplain processes. The combination of the two models is nominally called MIKE FLOOD. The two models are linked via overbank flow connections (or lateral links). That is, water is exchanged between the MIKE 11 and MIKE 21 FM model when the water levels in the river exceed the height of the river bank markers. Water can be exchanged from the river to the floodplain and also from the floodplain to the river (to represent return flows and overland flooding).

4 Roper catchment hydrodynamic model calibration

4.1 Physical and hydro-meteorological properties

The Roper catchment is 77,432 km^2 in area and features flat, tidally affected coastal plains that extend 20 to 60 km inland. These plains typically lie at less than 10 mAHD and are prone to seasonal flooding (Figure 4-1). The Roper River extends approximately 300 km from the east of the Roper mouth with major tributaries, the Wilton River and the Hodgson River, entering the Roper mid-river from the north and south respectively. In headwater catchments situated in the north-western part of the catchment, altitudes reach up to 420 mAHD. Tidal influence on streamflow is detectable as far upstream as Roper Bar, around 130 km from the mouth of the Roper River.

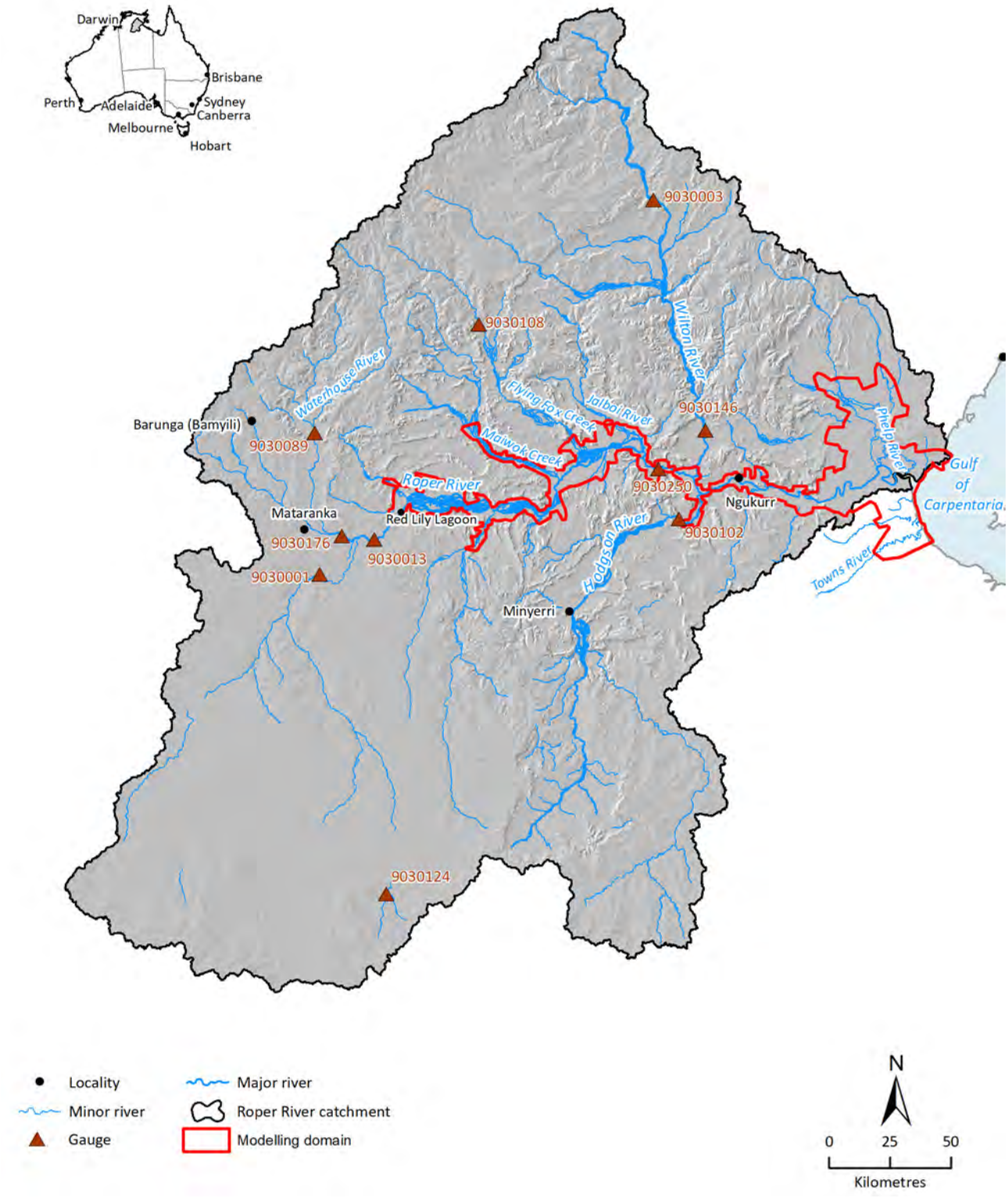

Figure 4-1 Roper catchment map showing major and minor rivers and stream gauges

4.1.1 CLIMATE

The Roper catchment has a highly seasonal climate with an extended dry season (Figure 4-2). It receives, on average, 792 mm of rain per year, 96% of which falls during the wet season. Mean daily temperatures and potential evaporation are high relative to other parts of Australia. On average, potential evaporation is approximately 1900 mm/year; however, the annual net

evaporative loss (annual evaporation minus rainfall) ranges from about 350 to 1770 mm. Since 1969–1970, the Roper catchment experienced one tropical cyclone in 40% of cyclone seasons and two tropical cyclones in 8% of seasons.

Approximately a third of global climate models (GCMs) project an increase in mean annual rainfall by more than 5%, a fifth project a decrease in mean annual rainfall by more than 5% and about half indicate 'little change'.

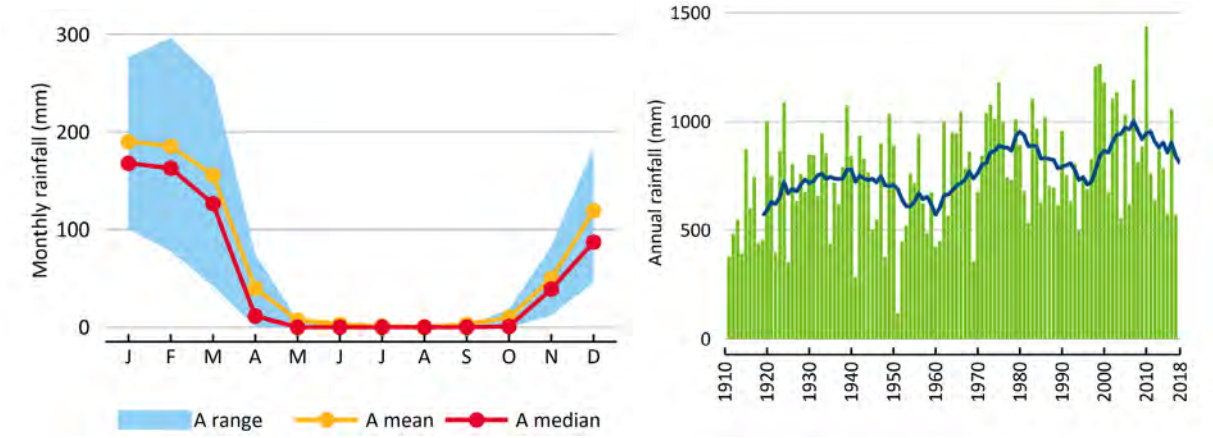

Figure 4-2 Historical monthly rainfall (range shows the range in values between the 20 and 80% monthly exceedance rainfall) and historical annual rainfall at Ngukurr

Blue line represents 10-year moving mean.

4.1.2 STREAMFLOW

Driven by the highly seasonal climate, streamflow in the Roper River displays very strong seasonal patterns (e.g. Figure 4-3). The reaches of the Roper catchment exhibit a wide range of flow regimes. While the Roper and Wilton rivers are perennial, streams in upper parts of the catchment are intermittent/ephemeral. Streamflow gauges in southern portions of the catchment exhibit, in general, fewer days of observed flow per year than streams in the northern areas of the catchment, sometimes in combination with very low runoff coefficients associated with the Sturt Plateau (Watson et al., 2023). The end-of-system discharge volume is relatively large compared to the other catchments, draining into the Gulf of Carpentaria with a mean annual streamflow of 5560 GL (estimated for the reporting period 1910–2019) (see companion technical report on river modelling in the Roper catchment, Hughes et al., 2023).

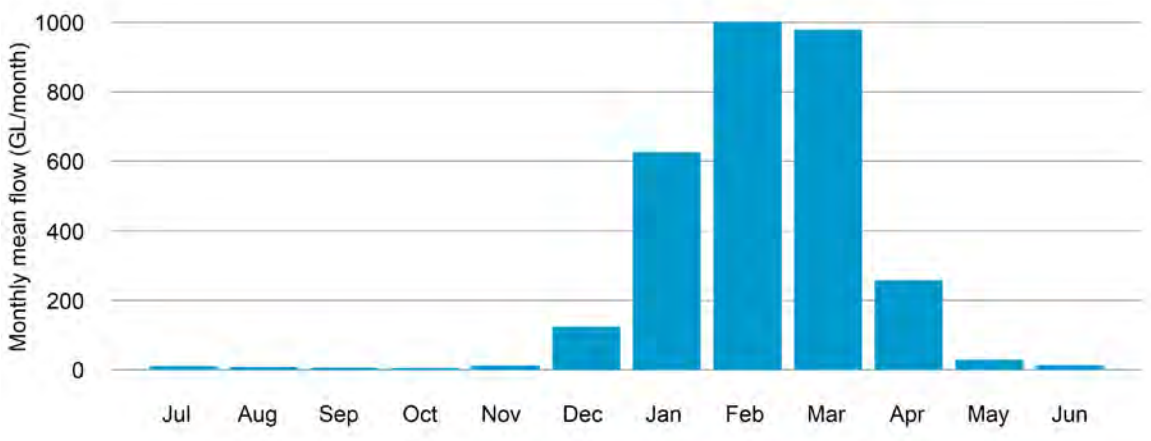

Figure 4-3 Monthly flow distribution at Red Rock on the Roper River based on observed flow data for the period of 1966 to 2019

4.1.3 FLOODING

The Roper catchment experiences intense seasonal rains from December to March causing significant flooding. Coastal flooding is common downstream of Ngukurr (around 100 km from the mouth of the Roper River), particularly in the intertidal flats along the coastline and Phelp River. Flooding is also pronounced in inland areas between Mataranka and Ngukurr where the Roper River splits into large anabranching features and along tributaries such as the Hodgson and Wilton rivers and Maiwok Creek. There are several interesting geomorphological features along the Roper River where the main channel suddenly splits into more than ten anabranches, which reconnect between 5 and 20 km downstream.

There have been 54 floods (ranging from small to large) since 1966. This was based on an overbank threshold of 40 m^3/second, which was estimated by obtaining daily streamflow at the Red Rock (9030250) gauge that corresponded to floodplain inundation from available satellite imagery. Figure 4-4 Annual maximum discharge at Red Rock (9030250) on the Roper River since 11966

shows the annual maximum mean daily discharge (m^3/second) over the past 53 years (1966 to 2019) at Red Rock. While floods can occur in any month between November to June, about 88% of historical floods have occurred between January and March (Figure 4-5). Flood peaks typically take about 3 days to travel from Mataranka Homestead to Red Rock, at a mean speed of 3.3 km/hour.

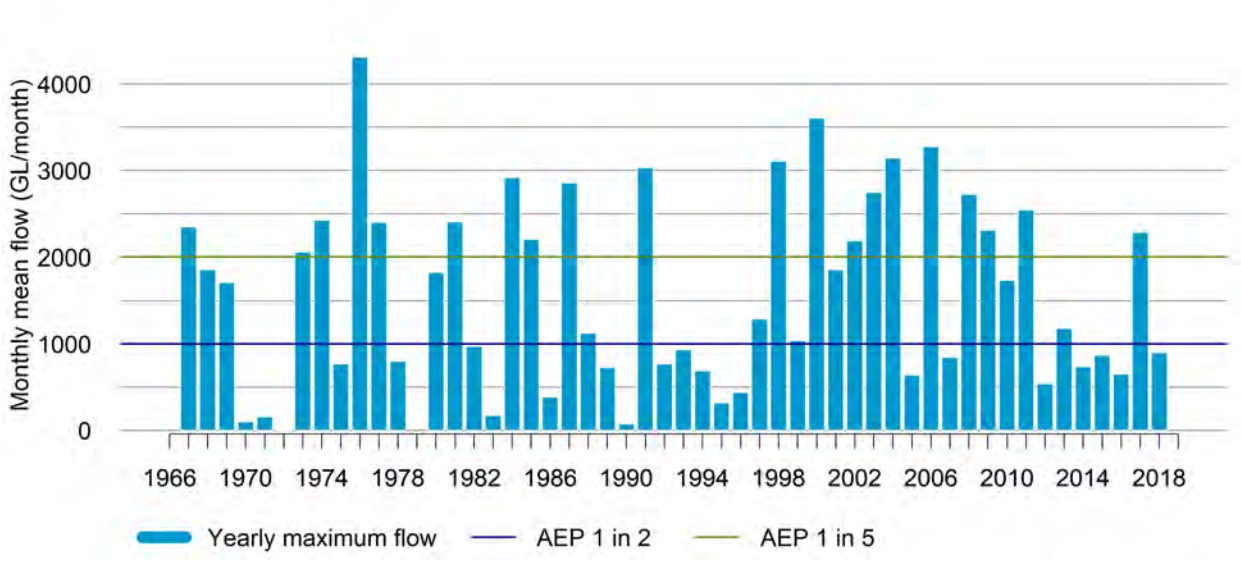

Figure 4-4 Annual maximum discharge at Red Rock (9030250) on the Roper River since 11966

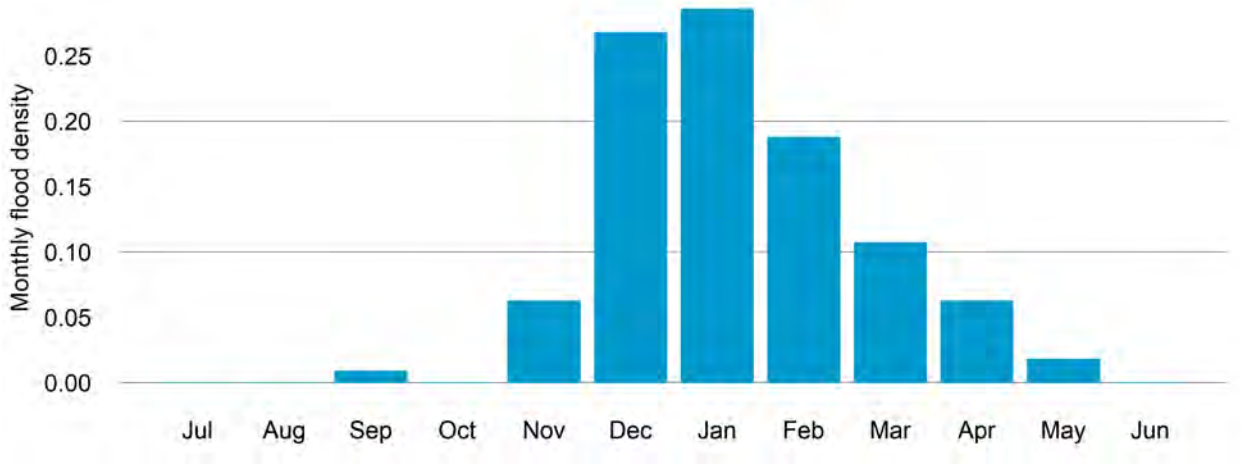

Figure 4-5 Monthly flood frequency in the Roper catchment based on floods of AEP greater or equal to 1 in 1

4.2 Model configuration

The floodplain inundation area was broken into two model domains (Figure 4-6) to make the modelling more manageable. The two hydrodynamic model domains include:

- Roper Zone 1: Upper domain, which extends downstream of Jilkminggan to Red Rock gauge (1500 km^2)
- Roper Zone 2: Lower domain, which extends from the Red Rock gauge to the mouth of the Roper River (2614 km^2)

The two zones were run independently for several reasons. First and foremost, this was to improve run time efficiency. Running the zones independently allows for corrections at the model boundaries of discharge errors that might be introduced by the upstream Roper Zone 1 model. In

addition, the flood scenario simulations are dependent on the simulations generated by the river system model proposed by Hughes et al. (2023), and therefore, it is imperative to maintain a high degree of consistency between them.

4.3 Model input

4.3.1 TOPOGRAPHY

A digital elevation model (DEM) was produced for the Roper MIKE 21 FM model domain by using LiDAR 5-m DEM and patching with the 30-m DEM-H. The highest resolution topographic information across the entire Roper catchment is the 1-second (i.e. approximately 30 m) DEM-H (Gallant et al., 2011), which was used to represent the north-eastern area surrounding upper Phelp River in Zone 1. Laser altimetry (LiDAR) derived fine resolution (5 m grid) topography data (±0.3 m horizontal and ±0.1 m vertical accuracy) collected for the Assessment was acquired by Fugro.

The LiDAR covers the Roper River from Jilkminggan to the river mouth and includes the tributary Maiwok Creek, which regularly floods (Figure 4-6). While there was LiDAR coverage for all of Zone 1, Zone 2 required patching by the coast mainly outside the northern and southern LiDAR extents. The lower two-dimensional model domain covered an area of approximately 2614 km^2. The area covered by LiDAR is 1716 km^2, which is about 66% of the Zone 2 domain.

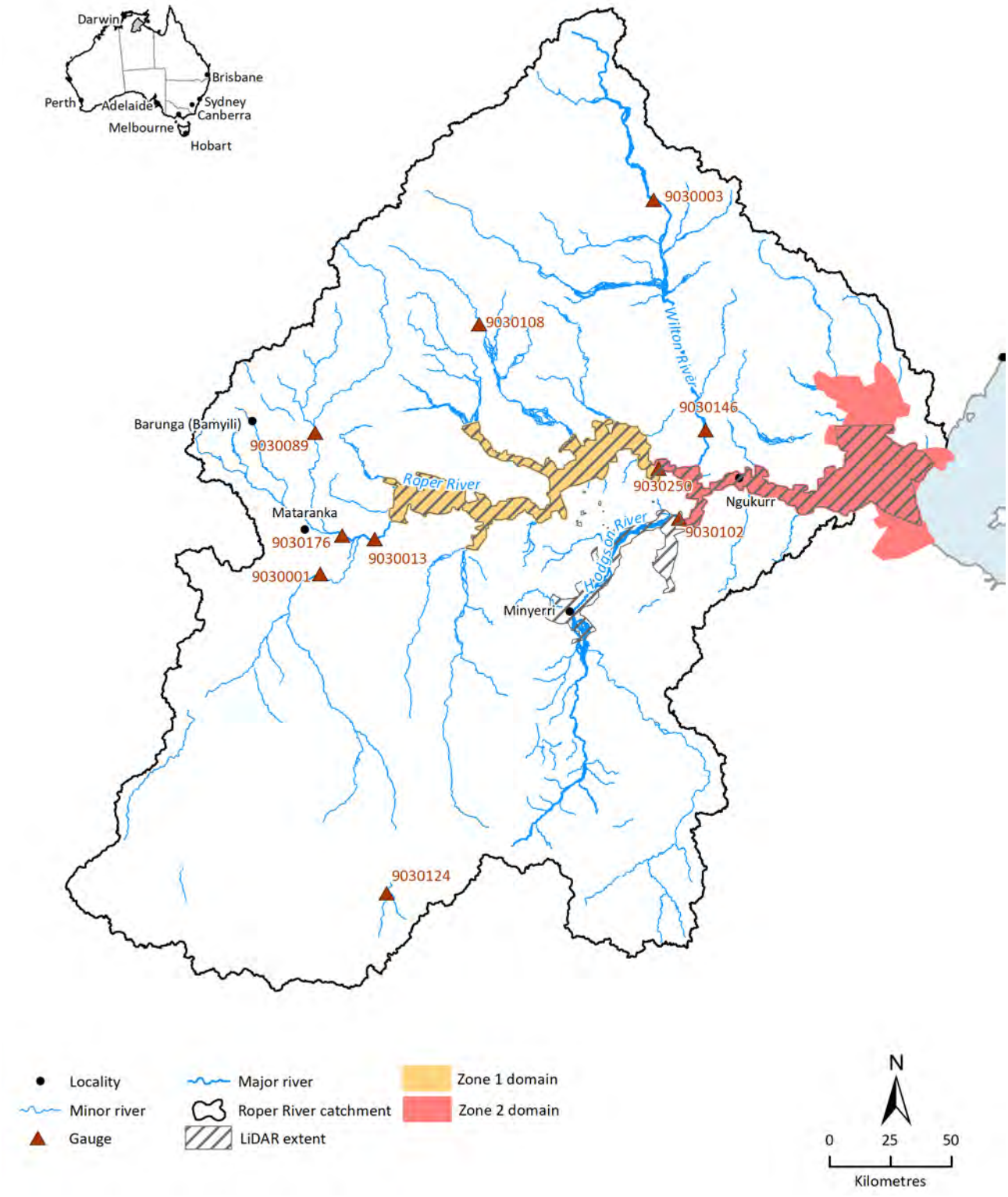

Figure 4-6 Roper hydrodynamic model domain showing the LiDAR data coverage

4.3.2 SURFACE ROUGHNESS

Hydraulic roughness coefficients of the land surface were derived from a remotely sensed land cover map (Geoscience Australia, 2011) and were represented in the model using Manning's roughness coefficient (*n*). A roughness map was then produced by replacing land-cover categories with roughness coefficients. Roughness coefficients were estimated based on published literature (e.g. Chow, 1959; Arcement and Schneider, 1989; LWA, 2009) (Table 4-1).

Table 4-1 Manning's roughness coefficient (*n*) for the Roper catchment

LAND COVER TYPE	MANNING'S *n* ($s/m^{1/3}$)
Open water	0.02
Natural aquatic vegetation	0.04
Natural terrestrial vegetation	0.05
Cultivated terrestrial vegetation	0.03
Natural bare surface	0.04
Artificial surface	0.02

4.3.3 STREAMFLOW AND SEA LEVEL BOUNDARY CONDITIONS

The upstream river boundary conditions of the hydrodynamic models were generated from Australian Water Resource Assessment – River model (AWRA-R) simulations (see companion technical report on river modelling in the Roper catchment, Hughes et al., 2023). The river model discharge gauge nodes used in the hydrodynamic models are shown in Table 4-2. In addition to these, the tidal sea level data was used for the downstream coastal boundary. For this the Milner Bay – Groot Eylandt tidal station was used, which is the closest long-term tide gauge station to the mouth of the Roper River. Remaining inflows to the boundary of the hydrodynamic model domain which were not captured by the river model were simulated using the Sacramento rainfall-runoff model based on the residual reach parameters from the AWRA-R calibrations (Hughes et al., 2023). The boundary rainfall-runoff model nodes are shown in Figure 4-7.

Table 4-2 River model boundary gauge nodes used for the flood model domains

STATION ID	STATION NAME	CATCHMENT AREA (km^2)	PERIOD OF RECORD
9030001	Elsey Crk – Warlock Ponds	16,945	1966–2022
9030102	Hodgson River – Wulli Pulli	12,417	1965–1985
9030176	Roper River – D/S Mataranka Homestead	5,819	1961–2023
9030250	Roper River – Red Rock	43,161	1966–2023
9035283	Wilton River Xng, Ngukurr Road	12,482	2006–2023

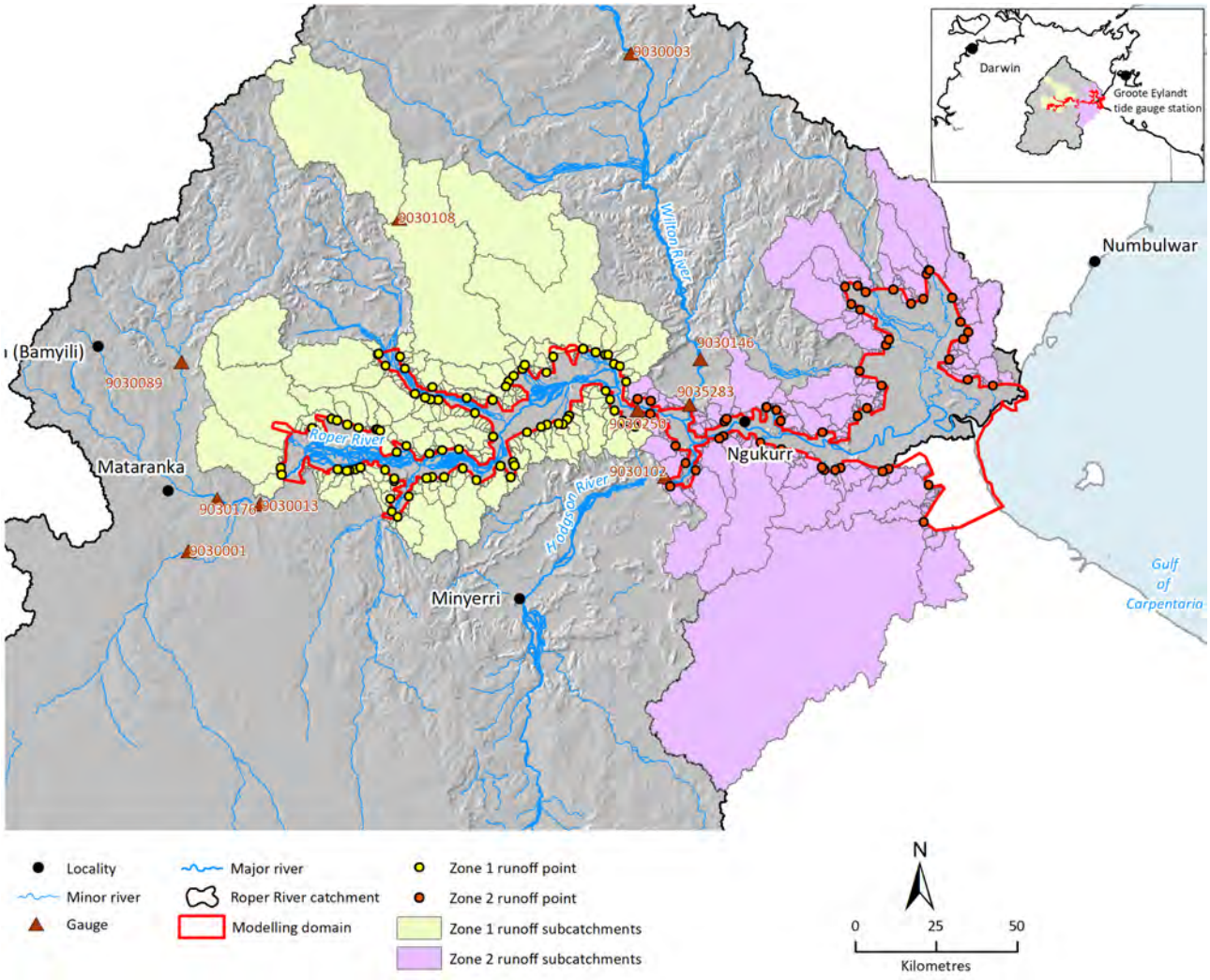

Figure 4-7 Boundary nodes for the flood domains

4.3.4 RAINFALL AND EVAPORATION

Gridded scientific information for land owners (SILO) climate data (Jeffrey et al. 2001) were used for the rainfall and evaporation fluxes over the floodplain. The SILO daily data are available at 0.05 × 0.05 degree resolution across Australia from 1889 to present.

4.3.5 INFILTRATION

The infiltration rates for the floodplain were based on soil permeability maps (see companion technical report on soil and land suitability for the Roper catchment, Thomas et al., 2022), which show that most of the two-dimensional model domain is made up of low permeability (5–50 mm/day) with some moderate permeability (50–500 mm/day) soils (Figure 4-8). During initial simulations, the durations of modelled floodplain inundation were found to be longer than what was observed in the satellite imagery, particularly for large events. Thus, the saturated conductivity of 100 mm/day was later chosen for the whole study area. This assumes that the infiltration is dominated by faster draining soils, which would be the case when flood waters are connected.

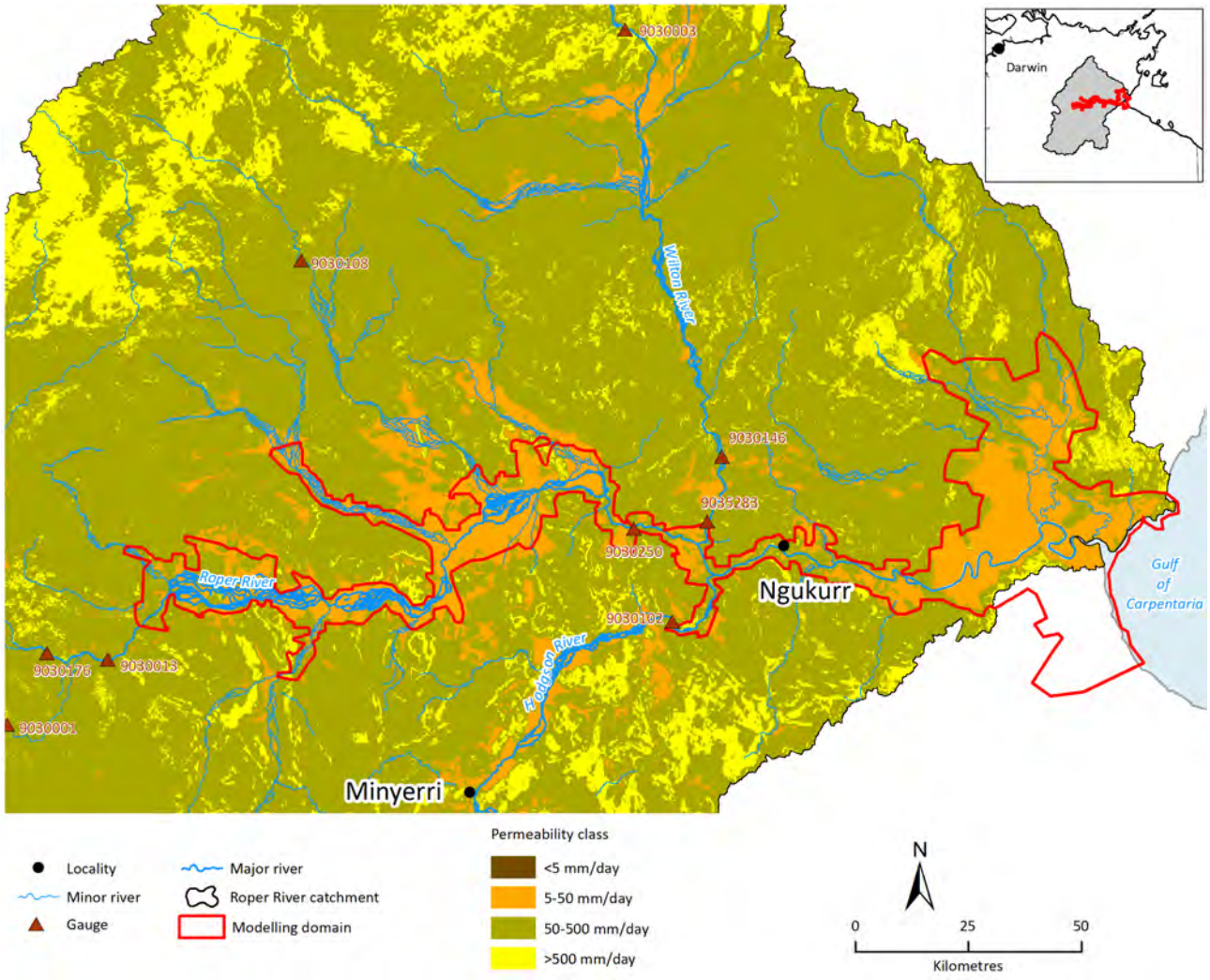

Figure 4-8 Map of soil permeability

See companion technical report on soil and land suitability for the Roper catchment, Thomas et al. (2022), for details on digital soil mapping.

4.4 Selected flood events for model calibration

The magnitude of flood events were calculated using a flood frequency analysis that used the Red Rock (9030250) gauge on the Roper River as the reference station. A flood event was defined as the occurrence of overbank flows that could be identified through satellite imagery. Based on these observations, a threshold flow rate of 40 m^3/second was established as the starting point for flood events. If the flow rate dropped below this threshold for three consecutive days, the event was considered to have ended. To determine the number of times each event was exceeded, the occurrences of events with higher peak discharge and larger total event volume were counted. Due to the extensive cloud cover during the flooding periods, the availability of Landsat satellite imagery to assist the calibration of the hydrodynamic model was severely restricted.

Flood events were selected for model calibration based on the availability of cloud free Landsat satellite imagery, and to ensure the magnitude of flood events spanned the annual exceedance probabilities of interest to ecologists and the land suitability analysis. Four events were selected and these are presented in Table 4-3. The requirement for a large number of simulations involving

all combinations of scenarios and calibration events necessitated the use of only the 1988 and 1991 events for scenario simulations.

Table 4-3 Flood events used for calibration

EVENT PERIOD	FREQUENCY	DURATION (DAYS)	NUMBER OF MODIS/LANDSAT IMAGES	PURPOSE
13/2/1988 – 29/2/1988	1 in 2	17	1	Calibration, scenario modelling
9/1/1991 – 23/3/1991	1 in 13	74	3	Calibration, scenario modelling
11/2/2008 – 14/4/2008	1 in 5	64	23	Calibration
30/3/2013 – 21/4/2013	1 in 3	23	7	Calibration

4.5 Hydrodynamic model simulation and outputs

The simulations for the hydrodynamic models in calibration were undertaken at a 1- to 5-second time step to satisfy numerical stability criteria for the biggest flood event in the analysis. The MIKE FLOOD models were run on graphics processing unit (GPU) machines consisting of 4 P100 Nvidia GPUs.

It took about 4 weeks of computer time to simulate the 1 in 13 event (74 days) for Roper Zone 2. At inflow boundaries, daily discharge was specified and at the seaside boundaries, hourly tide level was specified. The model used its inbuilt interpolation technique to derive sub-daily flow variables at each computational time step.

Total water depths and water velocities were obtained from the one-dimensional and two-dimensional models. For ease of postprocessing, the two-dimensional triangular flexible mesh output for the floodplain was converted to 5 × 5 m gridded data via an inverse distance weight interpolation algorithm. Using the same method, the river chainage output was converted to 5 × 5 m gridded data to cover the area within the river banks. Finally, the one-dimensional and two-dimensional gridded outputs were merged for each zone so that analyses could be performed on the river and floodplain simultaneously.

4.6 Hydrodynamic model calibration

The calibration process was constrained by the excessive hydrodynamic model simulation times, which limited the number of iterations for tuning. However, simulations were checked to ensure correct activation of anabranches and connectivity to waterholes such as Red Lily Lagoon. The duration of floodplain inundation was tuned by adjusting the floodplain infiltration rates to ensure wetland connectivity was consistent with observations of the satellite/remotely sensed imagery. In addition to evaluations against satellite imagery, the hydrodynamic model discharge and stage height outputs were compared to observed data at the Red Rock (9030250) gauge on the Roper River, which is located on the downstream boundary of Zone 1.

The evaluation of hydrodynamic modelled inundation extent was performed using all available and suitable Landsat and MODIS inundation maps for the selected flood events (including at least one image for each flood event). To evaluate the performance of the hydrodynamic model using the remotely sensed flood extent observations, two evaluation methods were employed:

- A visual comparison of spatial inundation area between satellite image and model simulation was performed to assess how the main inundation patterns are represented by the hydrodynamic model.
- Quantitative assessment of spatial inundation metrics (whether the model correctly simulates inundated pixels or not) were computed to assess how well the hydrodynamic model captures overall inundation extent.

Both evaluation methods were performed by resampling the remotely sensed inundation maps (Landsat 30 m and MODIS 500 m) to 5 m grid pixel horizontal resolution to be consistent with the hydrodynamic model gridded output. The satellite inundation maps were masked to only include the modelled area within the hydrodynamic model domains.

In many cases, satellite-derived inundation maps (even for a sensor like MODIS, with a twice-daily satellite overpass frequency) will only capture portions of the hydrodynamic model domain due to persistent cloud cover during flood events. Thus, only pixels in the satellite images showing inundated or non-inundated were considered; this means all cloudy or no data pixels were removed from the analysis.

4.6.1 Categorical statistics

Detection metrics were computed for each adjusted hydrodynamic model domain and per grid cell. Every available satellite inundation map and modelled inundation extent was classified with a contingency table following Ebert et al. (2007) as a hit (H, observed inundation correctly detected), miss (M, observed inundation not detected by product), or false alarm (F, inundation detected but none observed) (Figure 4-9).

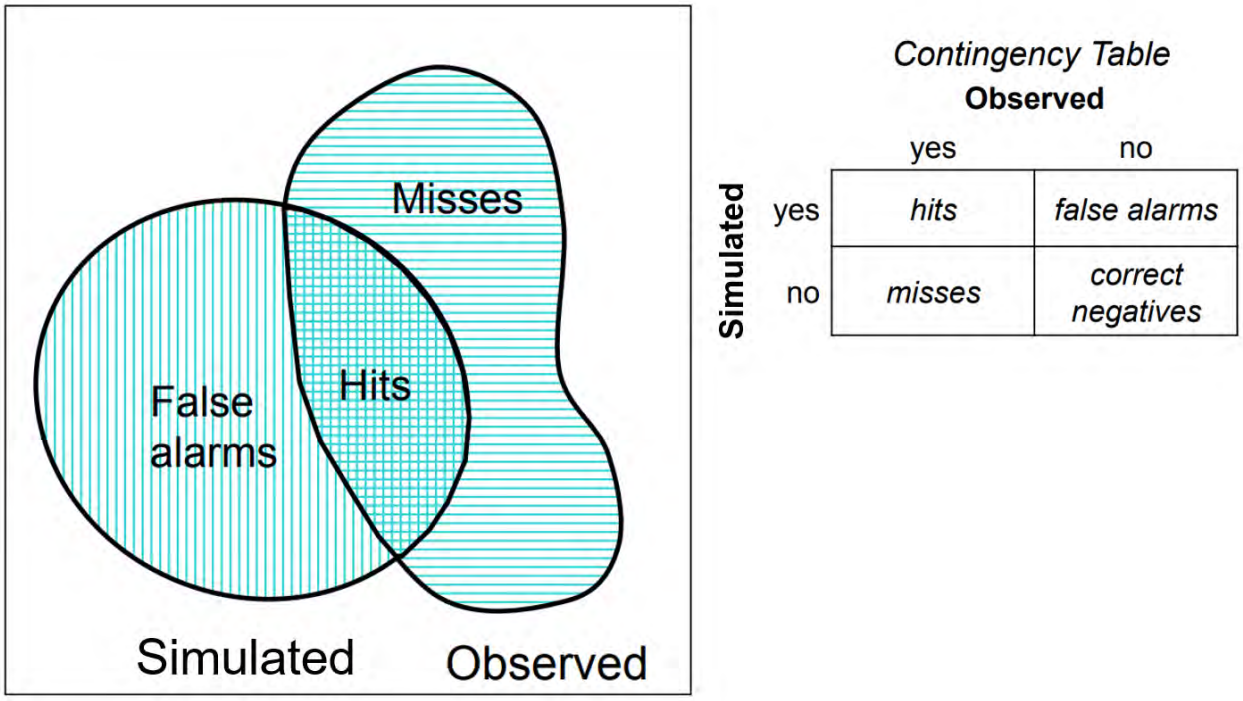

Figure 4-9 Classification at the grid cell level using a contingency table (Ebert, 2009)

The following statistics were computed from the contingency table (description from http://www.cawcr.gov.au/):

- The probability of detection, POD = H/(H + M), gives the fraction of inundated pixels correctly detected (range 0 to 1 and perfect score of 1). Sensitive to hits, but ignores false alarms. Should be used in conjunction with the false alarm ratio (below).
- The false alarm ratio, FAR = F/(H + F), gives the fraction of wrongly detected inundated pixels (range 0 to 1 and perfect score of 0). Sensitive to false alarms, but ignores misses.
- The frequency bias, FB = (H + F)/(H + M), gives the ratio of the simulated to observed inundated pixels frequency (range 0 to ∞ and perfect score of 1). Measures the ratio of the frequency of modelled inundated pixels to the frequency of satellite inundated pixels. Indicates whether the hydrodynamic model tends to underestimate (FB < 1) or overestimate (FB > 1) events. It does not measure how well the modelled inundation extent corresponds to the satellite inundation extents, only measures relative frequencies.
- The equitable threat score (ETS), used as an overall performance metric, gives the fraction of inundated pixels that was correctly detected, adjusted for correct detections (He) that would be expected due to random chance: ETS = (H – He)/(H + M + F – He), where He = (H + M)(H + F)/N and N the total number of estimates (range –1/3 to 1, perfect score of 1 and 0 indicating no skill). It is sensitive to hits. Because it penalises both misses and false alarms in the same way, it does not distinguish the source of error.

Although the detection statistics described above are well constrained, there are issues to consider in the interpretation of the results such as:

- Satellite inundation images may show areas inundated that remain in the landscape as ponded areas in between flood events, partly because of the gentle topography and low infiltration rates.

- Results of grid-to-grid comparison between hydrodynamic model and satellite will be inherently poor where satellite images (MODIS in particular) are of a lower spatial resolution than river channel widths, river morphology and resulting inundation dynamics.

The two approaches mentioned above (visual comparison and detection statistics) complement each other – visual comparisons, although labour intensive and subjective, highlight the sources or nature of the errors and provide diagnostic information on possible changes in the inputs or hydrodynamic model set up. On the other hand, statistical metrics provide an objective and comparable metric to assess overall model performance. The calibration is considered successful if both comparisons provide a reasonable assessment in the form of overall inundation patterns captured and reasonable detection statistics.

4.7 Results and discussion

4.7.1 DISCHARGE AND STAGE HEIGHT

Due to the lack of observed stage and discharge data within the model domains, evaluations of these variables were only possible for Zone 1 using information from the Red Rock (9030250) gauge site, which lies on the downstream boundary of Zone 1. Discharge comparisons for each of the calibration events are presented in Figure 4-10. The simulated peaks from the hydrodynamic model occurred 1 to 4 days earlier than what was observed and the magnitude of the peaks were underestimated. However, discharges at the start and end of the events were well matched. The stage height results (Figure 4-11) show similar behaviour except that water heights are generally overestimated at the start and end of the events by 1 to 2m.

There are multiple possible reasons for the performance issues concerning the discharge and stage height simulations of the Zone 1 hydrodynamic model. Firstly, surface roughness values were not tuned during the calibration; instead they were estimated based on land-cover mapping (see Section 4.3.2 for further details). It is likely that improvements in timing and magnitude of the peaks could be obtained through reduction of surface roughness. Secondly, the infiltration rates used for the floodplain assumed moderate permeability (see Section 4.3.5 for further details), which would have intercepted some volume entering or re-entering the main river channel. Finally, the river-floodplain connections require adjustment so that more floodplain waters are able to return to the river. Future development of the Zone 1 hydrodynamic model should include more connectivity between the river and floodplains. If this is combined with a reduction of infiltration rates, peak magnitudes should be better matched to observed while preventing excessive duration of water on the floodplain.

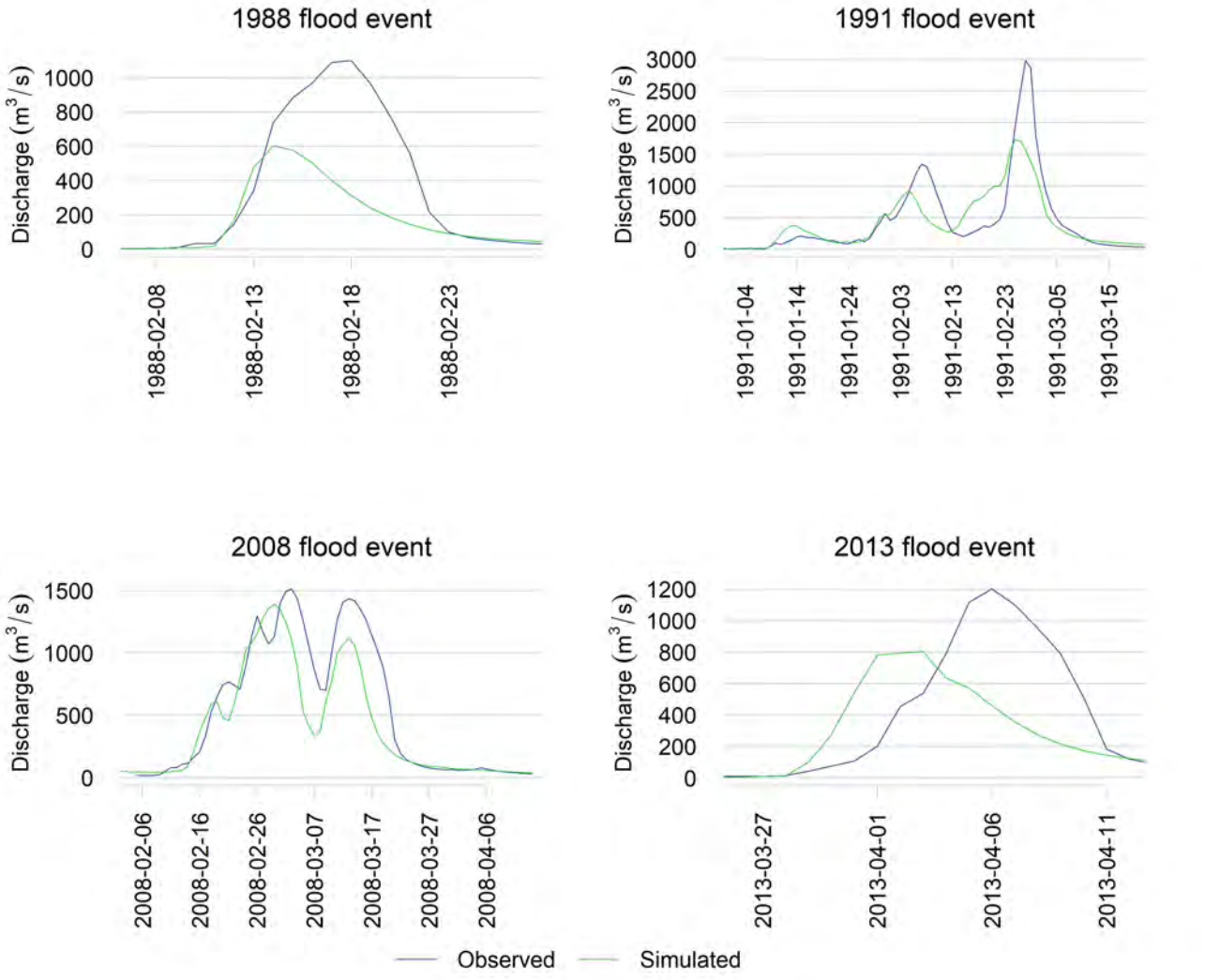

Figure 4-10 Comparison of the Zone 1 hydrodynamic model simulated discharge and observed discharge at the Red Rock (9030250) gauge on the Roper River.

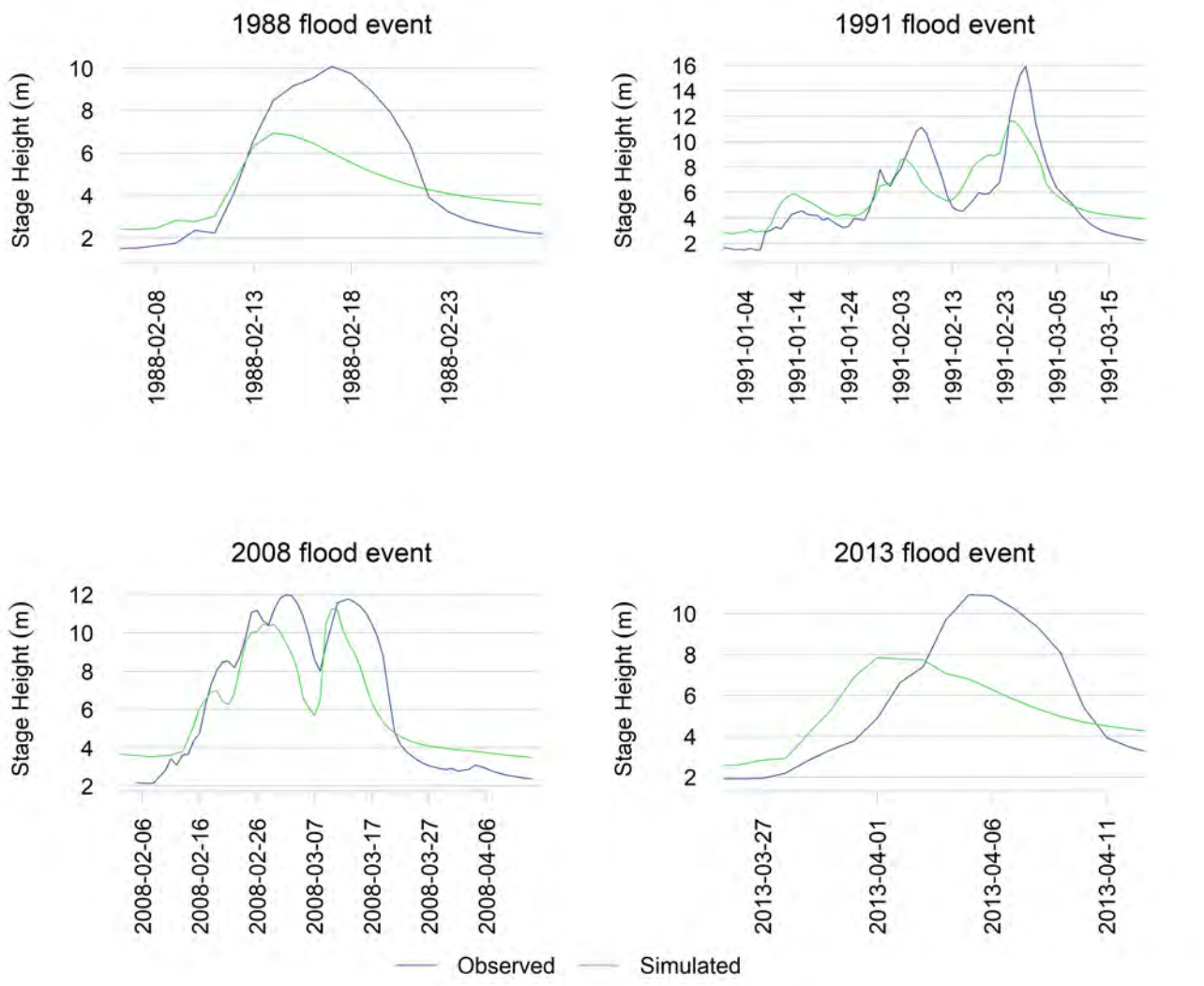

Figure 4-11 Comparison of the Zone 1 hydrodynamic model simulated stage height and observed stage height at the Red Rock (9030250) gauge on the Roper River.

4.7.2 SATELLITE-BASED FLOOD MAPS

The MODIS and Landsat inundation maps were processed for the Roper River hydrodynamic model domains for the calibration periods (Table 4-4). The availability of images and the proportion of cloud/null effects were reported. Due to the large number of MODIS images, only those images containing 80% or less clouds/nulls were processed to obtain inundation maps. Also, to exclude images with no to little flooding, only images with 1% or more observed inundated area were used for Zone 1 and 5% or more for Zone 2.

Table 4-4 Flood event dates, and number of Landsat/MODIS images for the Roper River hydrodynamic model domains

ZONE	START DATE	END DATE	NUMBER OF LANDSAT IMAGES	NUMBER OF MODIS IMAGES
1	13/2/1988	29/2/1988	0	0
1	9/1/1991	23/3/1991	1	0
1	11/2/2008	14/4/2008	1	6
1	30/3/2013	21/4/2013	0	3
2	13/2/1988	29/2/1988	1	0
2	9/1/1991	23/3/1991	2	0
2	11/2/2008	14/4/2008	4	12
2	30/3/2013	21/4/2013	1	3

4.7.3 INUNDATION EXTENT

Results of the hydrodynamic modelling in the Roper catchment were compared to satellite inundation maps through a direct visual comparison and detection metrics. In the first instance, images that passed the first cloud cover filtering were further scrutinised to coincide with flood patterns that could be used to inform the calibration of the hydrodynamic modelling. The images within the modelling simulation period (Table 4-4) that showed limited inundation, or images with large cloud cover over the inundated areas, were omitted from further analysis. Generally, at least one image was retained for each flood event to assist in the calibration. As examples, Figure 4-12 and Figure 4-13 show Landsat/MODIS inundation maps with corresponding hydrodynamic model inundation maps for one date in each flood event, where available.

Table 4-5 and
Table 4-6 present the detection statistics for all images considered in the analysis (see Table 4-3 for the flood events). For Zone 1, POD values were generally low (POD mean 0.24, POD range 0.06–0.52). In addition, FAR was generally high with an average of 0.69 (range 0.15–0.94) indicating a misalignment of inundation patterns. ETS values (mean 0.11, range 0.02–0.3) imply some but limited model skill. Reasonable FB values (close to 1) coincided with high FAR and low POD, which suggests that on occasion total inundation area might be reproducible while inundated patterns may be unreliable. There is an apparent underestimation during peak flows demonstrated by low FB values. Conversely, there is also overestimation during lower flows demonstrated by high corresponding FB values.

Compared to Zone 1, inundation patterns generated by the hydrodynamic model in Zone 2 were better matched to the Landsat/MODIS inundation maps. This resulted in reasonable detection statistics for most images analysed. Detection statistics showed that on average, ETS was 0.32 (range 0.06–0.52), POD was 0.52 (range 0.08–0.89), FAR was 0.37 (range 0.08–0.71) and FB was 0.85 (range 0.13–1.67).

Locations of poor fit in Zone 1 generally coincided with complex anabranching networks. Closer inspection of satellite imagery in these locations revealed that they often do not display flooding of these anabranches. The inability of MODIS to capture inundation in narrow floodplains has been reported in the Fitzroy (Karim et al., 2011) and other catchments in Australia (Ticehurst et al.,

2013). This explains much of the poor fit performance in Zone 1. Furthermore, MODIS regularly falsely identifies cloud shadow as inundation, which is particularly an issue when using imagery with high (up to 80%) cloud cover.

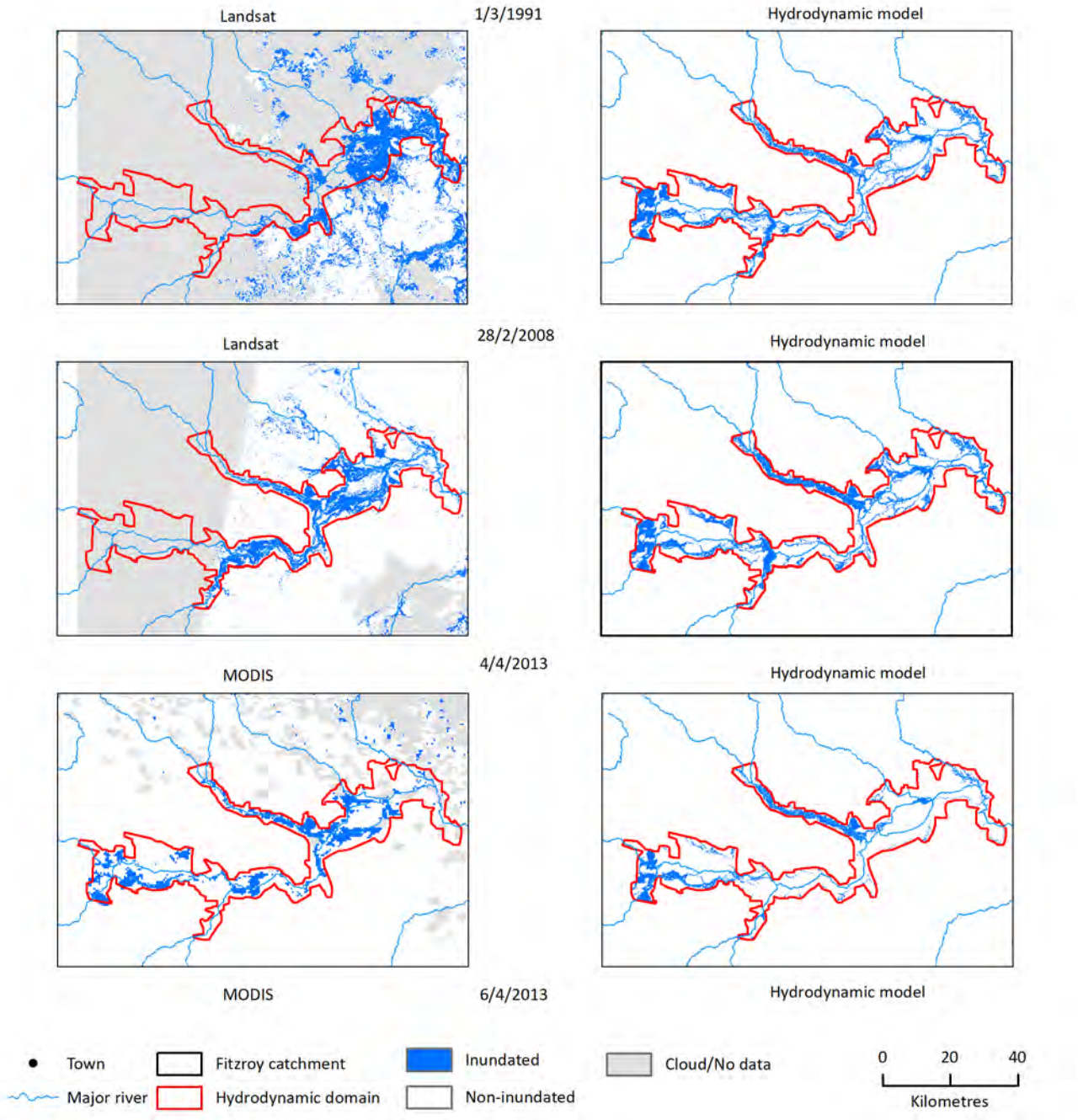

Figure 4-12 Examples of the comparison of the Landsat/MODIS inundation map versus the inundation area simulated by the hydrodynamic modelling for Zone 1

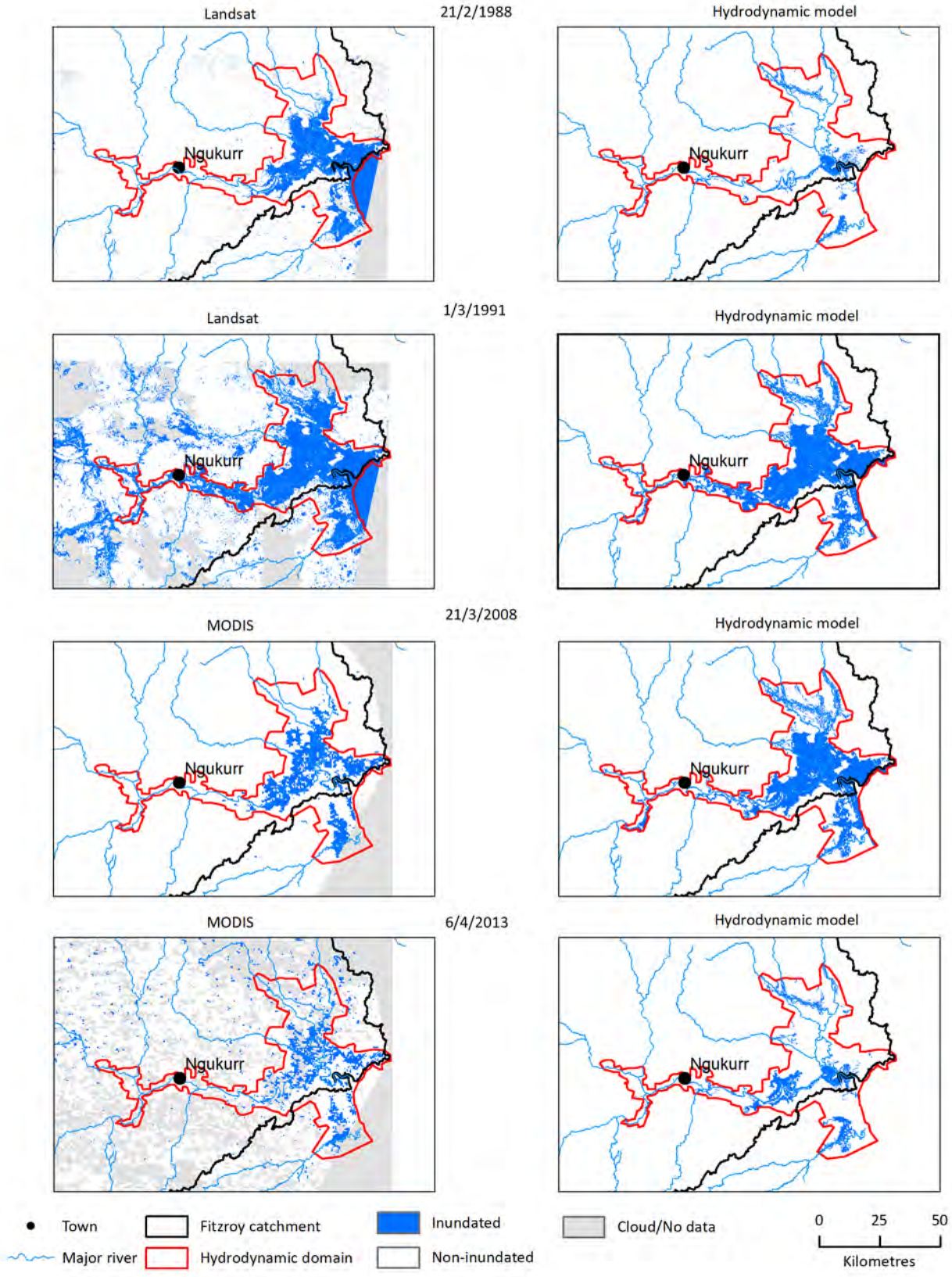

Figure 4-13 Examples of the comparison of the Landsat/MODIS inundation map versus the inundation area simulated by the hydrodynamic modelling for Zone 2

Table 4-5 Detection statistics for the Landsat/MODIS images considered in the analysis for Zone 1

Percentage available refers to pixels other than cloud/null (including inundated and non-inundated pixels) within the hydrodynamic model domain. Percentage wet refers to observed inundated pixels within the hydrodynamic model domain. ETS stands for equivalent threat score (a measure of overall performance), POD for the probability of detection, FAR for the false alarm ratio and FB for frequency bias.

SATELLITE	DATE	% AVAILABLE	% WET	ETS	POD	FAR	FB
Landsat	1/3/1991	36	12	0.07	0.12	0.15	0.14
MODIS	27/2/2008	34	3	0.13	0.25	0.65	0.72
Landsat	28/2/2008	55	7	0.3	0.4	0.27	0.54
MODIS	29/2/2008	62	3	0.13	0.37	0.79	1.76
MODIS	3/3/2008	97	2	0.06	0.31	0.91	3.45
MODIS	5/3/2008	39	2	0.03	0.12	0.89	1.02
MODIS	12/3/2008	71	2	0.18	0.52	0.77	2.22
MODIS	17/3/2008	44	4	0.03	0.1	0.83	0.58
MODIS	4/4/2013	94	5	0.21	0.31	0.52	0.66
MODIS	6/4/2013	58	1	0.04	0.11	0.9	1.09
MODIS	7/4/2013	60	2	0.02	0.06	0.94	1.13

Table 4-6 Detection statistics for the Landsat/MODIS images considered in the analysis for Zone 2

Percentage available refers to pixels other than cloud/null (including inundated and non-inundated pixels) within the hydrodynamic model domain. Percentage wet refers to observed inundated pixels within the hydrodynamic model domain. ETS stands for equivalent threat score (a measure of overall performance), POD for the probability of detection, FAR for the false alarm ratio and FB for frequency bias.

SATELLITE	DATE	% AVAILABLE	% WET	ETS	POD	FAR	FB
Landsat	21/2/1988	93	11	0.13	0.17	0.35	0.25
Landsat	1/3/1991	81	24	0.37	0.48	0.08	0.52
Landsat	17/3/1991	93	10	0.17	0.21	0.34	0.32
Landsat	28/2/2008	60	11	0.32	0.42	0.21	0.54
MODIS	1/3/2008	21	6	0.37	0.78	0.4	1.3
MODIS	9/3/2008	25	5	0.45	0.67	0.28	0.93
MODIS	10/3/2008	67	8	0.48	0.74	0.34	1.12
MODIS	11/3/2008	78	8	0.5	0.84	0.39	1.38
MODIS	12/3/2008	59	7	0.52	0.81	0.34	1.23
MODIS	13/3/2008	79	7	0.47	0.89	0.45	1.61
MODIS	16/3/2008	42	5	0.46	0.75	0.37	1.19
MODIS	17/3/2008	35	8	0.31	0.47	0.25	0.63
MODIS	18/3/2008	46	5	0.44	0.76	0.41	1.27
MODIS	19/3/2008	74	7	0.4	0.72	0.46	1.34
MODIS	21/3/2008	93	7	0.43	0.85	0.49	1.67
MODIS	23/3/2008	85	6	0.45	0.83	0.47	1.58

SATELLITE	DATE	% AVAILABLE	% WET	ETS	POD	FAR	FB
Landsat	23/3/2008	76	10	0.43	0.55	0.22	0.71
Landsat	31/3/2008	97	13	0.22	0.28	0.28	0.39
Landsat	8/4/2008	78	8	0.13	0.16	0.29	0.23
MODIS	4/4/2013	49	6	0.14	0.19	0.44	0.35
MODIS	6/4/2013	59	6	0.12	0.19	0.59	0.47
MODIS	11/4/2013	89	6	0.06	0.09	0.71	0.32
Landsat	14/4/2013	88	11	0.06	0.08	0.39	0.13

Although overall fit performance was poor in Zone 1, satisfactory detection statistics were found in localised areas. Masks were determined by creating two kilometre buffers around Zone 1's points of interest (Figure 4-14). These points represent the ecologically important wetlands in Zone 1 (See Section 6.3 for the methods for establishing the water assets). The detection statistics were then computed for each masked area. Eleven sites had satisfactory performance based on their average detection statistics results (Table 4-7).

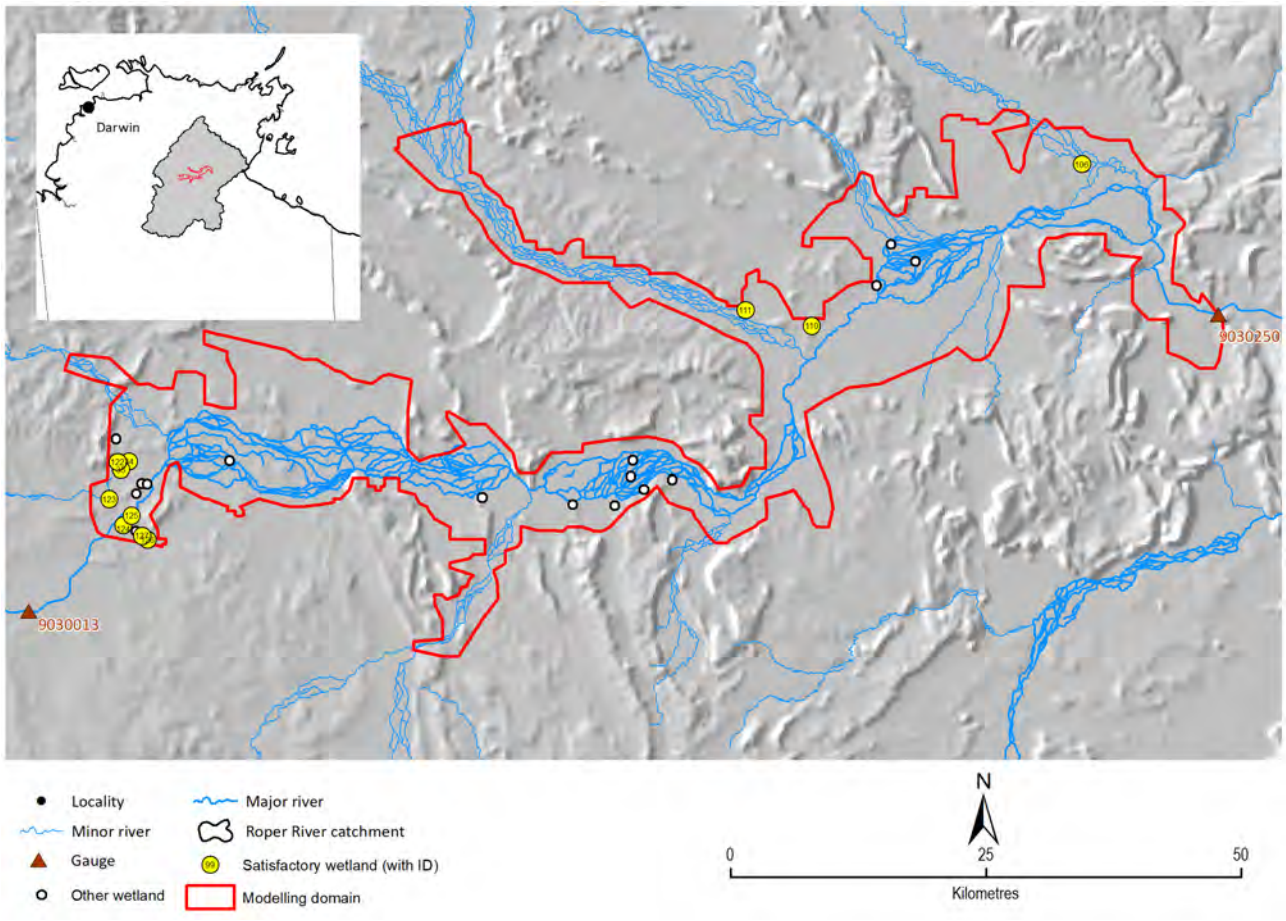

Figure 4-14 Zone 1 hydrodynamic modelling domain showing wetlands

Table 4-7 Average detection statistics for wetland sites in Zone 1

*indicates the site had satisfactory performance. ETS stands for equivalent threat score (a measure of overall performance), POD for the probability of detection, FAR for the false alarm ratio and FB for frequency bias.

WETLAND	MEAN ETS	MEAN POD	MEAN FAR	MEAN FB
33	0	0.07	0.82	0.29
34*	0.15	0.61	0.35	1
35*	0.11	0.52	0.5	1.32
36	-0.01	0.01	0.92	0.11
106*	0.11	0.32	0.32	0.5
107	0.04	0.08	0.31	0.1
108	0.04	0.19	0.55	0.41
109	0.03	0.11	0.46	0.16
110*	0.13	0.29	0.24	0.39
111*	0.15	0.64	0.36	1.1
112	-0.01	0.06	0.34	0.11
113	0.09	0.19	0.41	0.28
114	0	0.05	0.18	0.06
115	0.01	0.07	0.48	0.17
116	0.01	0.04	0.44	0.07
117	0.03	0.14	0.46	0.32
118	0.02	0.1	0.82	0.35
119	0.07	0.39	0.62	1.04
120	0.08	0.53	0.27	0.87
121	0.02	0.19	0.47	0.8
122*	0.17	0.62	0.48	1.25
123*	0.11	0.38	0.4	0.75
124*	0.13	0.55	0.25	0.82
125*	0.14	0.64	0.36	1.12
126*	0.13	0.46	0.31	0.74
127*	0.1	0.5	0.34	0.86

4.8 Summary

The Roper catchment has large floodplain areas in its upper and lower reaches and it supports several offstream and instream wetlands with high ecological and cultural value. Floodplains, including the offstream wetlands, are inundated during seasonal flooding between the months of December to March.

Flood inundation maps were produced using MODIS and Landsat imagery. MODIS imagery of 500-m resolution at a daily interval were acquired from November 2000 to March 2013 and processed using the OWL algorithm. Landsat imagery of 30-m resolution at 16-day intervals were acquired

from 1990 to 2018 and processed using the NDWI algorithm. A total of 10 Landsat images and 24 MODIS images were processed based on data quality and relevance to selected flooding events for the hydrodynamic model calibration. Event-based inundation maps were produced for individual floods and composite flood maps were produced by combining all images. Cloud cover was a challenge when producing event-based inundation maps. The Landsat shows inconsistencies in the spatial flood extent due to limited cloud-free observations. The inability of MODIS to capture inundation in narrow floodplains has been reported in the Fitzroy (Karim et al., 2011) and other catchments in Australia (Ticehurst et al., 2013).

The Roper River floodplain inundation area was modelled using two domains. Zone 1 extends downstream of Jilkminggan to the Red Rock gauge covering an area of 1500 km^2. Inundation in Zone 1 is primarily driven by high flows down the Roper River, with areas along the Maiwok Creek also displaying significant flooding. The Zone 1 domain consists of a network of complicated braided channels that become activated as water levels rise. In addition to the general anastomosing channel patterns, there are several noteworthy geomorphological features along the Roper River where the main channel suddenly splits into many (more than 10) anabranches, which reconnect between 5 and 20 km downstream.

The characteristics of Zone 2 stand in stark contrast to those of Zone 1. The Zone 2 domain extends from the Red Rock gauge to the mouth of the Roper River and covers a much larger area of 2614 km^2. Tidal influences reportedly reach all the way to Roper Bar (Faulks, 2001), which is 10 km downstream of the Red Rock gauge. A single Roper River channel is better defined, and less anabranching occurs in the lower zone. Furthermore, Zone 2 contains tidal flats towards the coast along the Roper and Phelp rivers.

One-dimensional hydrodynamic river models (MIKE 11) were coupled with two-dimensional hydrodynamic floodplain models (MIKE 21 FM) to produce MIKE FLOOD models for Zone 1 and 2. The hydrodynamic model was calibrated for the 1988, 1991, 2008 and 2013 flood events using inundation maps derived from MODIS and Landsat imagery. The models were calibrated primarily by adjusting the infiltration rate.

Compared to the Landsat and MODIS inundation maps, the hydrodynamic model captured overall inundation patterns for Zone 2, including the inundation of coastal flat areas and ephemeral waterways that become active during flood events. However, the detection statistics show that the cell-to-cell matching of Zone 1 against observed satellite data was overall poor, largely due to the inability of MODIS to detect inundation of narrow floodplains. For Zone 1, the detection metrics suggest that there is underestimation during peak flows, and conversely, overestimation during lower flows, as well as a general misalignment of inundation patterns. Although overall fit performance was poor in Zone 1, satisfactory detection statistics were found for eleven ecologically important wetland sites.

5 Flood modelling under future climate and development scenarios

5.1 Introduction

Rising global air temperatures are likely to be accompanied by changes in the intensity and patterns of rainfall. AR5 GCM projections were used to produce climate data reflecting a future where the global mean surface air temperatures are 2.2 °C higher relative to approximate 1990 global temperatures under an RCP8.5 emissions scenario for approximately 2060. McJannet et al. (2023) found that pattern-scaled GCMs (GCM-PS) results indicated changes in rainfall in the Roper catchment. These changes in rainfall are usually amplified in runoff. Consequently, increases in global temperatures may be accompanied by changes to the extent and patterns of flood inundation.

In addition, the development of the surface water resources for irrigated agriculture in the highly seasonal streamflow regime prevailing in the Roper River is likely to require some degree of storage and river regulation. Surface water storage options were evaluated at five hypothetical dam locations (refer to the companion technical report on surface water storage, Petheram et al. (2022)). Flood waters stored during the wet season and their gradual release during the dry season will modify the timing and magnitude of floods and subsequent inundation of floodplains. The impacts of water harvesting during high-flow events were also evaluated during the flood study.

To explore how flood characteristics may change under projected future climate and hypothetical development scenarios, a series of simulation experiments or scenarios were devised. Due to the long run times of the hydrodynamic model it was only possible to explore a limited number of scenarios. Hence scenarios were selected to enable generalised conclusions to be drawn. A summary of the future climate and development scenarios undertaken in each study area is presented in Table 5-1

Table 5-1 Summary of selected future climate and development scenarios

ASSESSMENT AREA	SCENARIO NAME	FLOOD START DATE (DURATION OF SIMULATION IN DAYS)	EXCEEDANCE PROBABILITY (YEARS)
Roper catchment (Zone 1 and 2)	Scenario B Historic climate and hypothetical future development (soil-limited water harvest, Waterhouse River dam site, Flying Fox Creek dam site, all dams)	13/2/1988 (17)	1 in 2
		9/1/1991 (74)	1 in 13
	Scenario C Projected future climate (dry and wet) and current levels of development	13/2/1988 (17)	1 in 2
		9/1/1991 (74)	1 in 13
	Scenario D Projected future climate (dry and wet) and hypothetical future development (soil-limited water harvest, all dams)	13/2/1988 (17)	1 in 2
		9/1/1991 (74)	1 in 13

5.2 Future climate scenarios

To simulate and assess the uncertainty in the range of future runoff predictions, future climate projections from a large range of archived GCM simulations were downloaded from the Coupled Model Intercomparison Project (CMIP5) website (https://pcmdi.llnl.gov/mips/cmip5/). There were 42 GCMs available for the Representative Concentration Pathways RCP8.5 emissions scenario with rainfall and temperature data; however, ten of these GCMs did not have solar radiation and/or humidity data, which were required for other parts of the Assessment such as hydrological modelling, groundwater recharge modelling, agricultural production systems simulator crop modelling and pasture modelling. From the 32 GCMs that have data available for rainfall, temperature, solar radiation and humidity, a subset of 21 GCMs were selected after taking into account the results of a comprehensive assessment of the skill of GCMs for: (i) mean climate over Australia, (ii) variability, (iii) teleconnections, and (iv) important climate features such as Madden–Julian Oscillation, Southern Annular Mode, blocking and cut-off lows (Moise et al., 2015). Refer to Charles et al. (2016) and McJannet (2023), from where these methods were adopted.

For hydrological modelling analyses, which provide runoff inputs into the hydrodynamic modelling, three pattern-scaled GCMs (GCM-PS) – a 'wet', a 'mid' and a 'dry' – were selected for further analysis and reporting for the Assessment. The GCMs were selected based on ranked mean annual rainfall (September 1910 to August 2019) averaged across each Assessment study area, with the wet, mid and dry GCMs corresponding to those GCMs with the 10th, 50th and 90th percentile, respectively. The seasonal pattern scaling (PS) method employed used output from the 21 GCMs to scale the 109 years of historical daily rainfall, temperature, radiation and humidity sequences (i.e. SILO climate data), to construct the 21 by 109-year sequences of future daily rainfall, temperature, radiation and humidity. The method comprised two broad steps. The first step involved estimating the seasonal scaling factors for four 3-month blocks – December to February, March to May, June to August, and September to November – for the changes between two time slices centred around 1990 (1975 to 2005) and 2060 (2046 to 2075). This is representative of a 2.2 °C temperature rise under an RCP8.5 emissions scenario. The total rainfall was calculated for each season and over each time slice.

Seasonal scaling factors were then calculated as the ratio of the total season's rainfall over the 2060 time slice divided by the total rainfall over the 1990 time slice. The historical climate sequence was then scaled using these seasonal scaling factors. The second step involved rescaling the entire series so that it matched the annual scaling factors, to maintain consistency with annual projected changes in the GCMs (Chiew et al., 2009; Petheram et al., 2012). Refer to the companion technical report on climate, McJannet et al. (2023), for further details on future climate selection and scaling. The catchment average runoff for the Roper catchment under 'mid' scaled projections was similar to the mean runoff under Scenario A, hence all comparisons of 'wet' and 'dry' climates were performed against this scenario. The calibrated river system models of the Assessment catchments were used to simulate streamflow under future climate scenarios (Cwet and Cdry) for the upstream boundary and climate conditions to the hydrodynamic models for the future climate scenarios. The future climate was also to re-simulate the Sacramento rainfall-runoff model to update the ungauged boundary inflows.

The Roper catchment rainfall under scenarios Cwet and Dwet (corresponding to the 90th percentile ranked mean annual rainfall) were represented by climate projections of the FIO-ESM

model, whereas the Cdry and Ddry (corresponding to the 10th percentile ranked mean annual rainfall) were represented by climate projections of the ACCESS1-0 model.

Figure 5-1 shows projected monthly streamflow (catchment mean runoff used as inflow input in the hydrodynamic model plus upstream inflows into the main river) in the Roper catchment under scenarios A, Cwet and Cdry from 1988 to 2013 (the hydrodynamic model was calibrated for flood events within this period). Under Scenario Cwet the mean annual catchment streamflow increased by 51%, and the mean wet-season (December to March) streamflow increased by 49%. Under Scenario Cdry, mean annual catchment streamflow decreased by 29% and mean wet-season streamflow by 28%. The maximum annual flow in the water year 1990–1991 increased by 37% under Scenario Cwet whereas it decreased by 21% under Scenario Cdry.

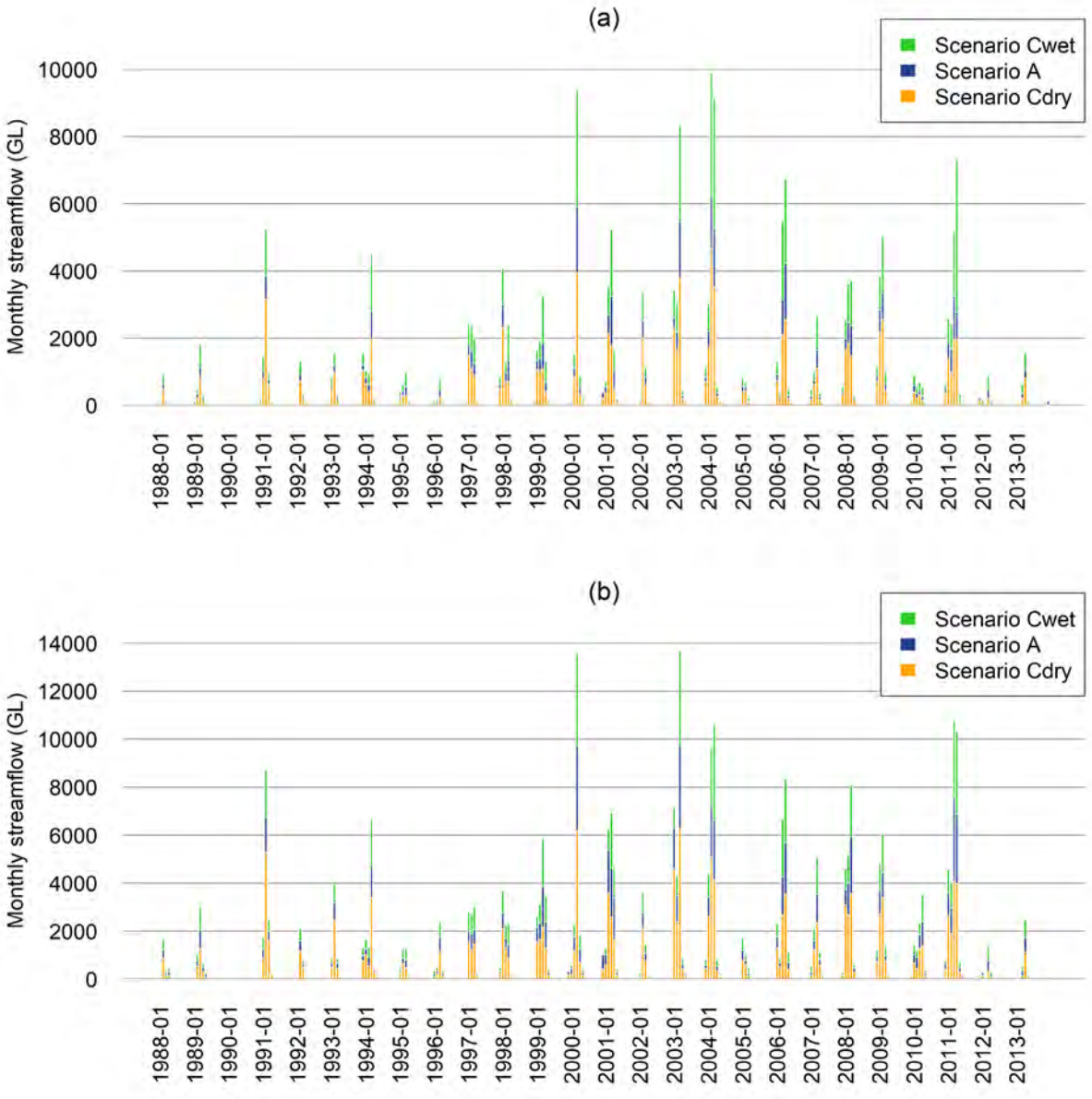

Figure 5-1 Comparison of inflow time series within the hydrodynamic model domain in the Roper catchment from 1988 to 2013 (period over which hydrodynamic model was calibrated) for Zone 1 (a) and Zone 2 (b)

Figure 5-2 compares the simulated discharge under the current and future climate for the Roper River system and rainfall-runoff models used as inflows to the hydrodynamic model for the 1988, and 1991 flood events (Section 4.4). It shows relatively large changes in peak and total discharge under scenarios Cwet and Cdry compared to Scenario A for each event. Under Scenario Cdry, peak streamflow decreased by 22 and 21% for the 1988 and 1991 flood events, respectively, for Zone 1. Zone 2 showed similar changes with peak streamflow decreasing by 24 and 19% for the 1988 and 1991 flood events, respectively. For Zone 1, total discharge decreased by 25 and 18% for the 1988 and 1991 flood events, respectively; and a 27 and 22% decrease for 1988 and 1991 flood events, respectively, for Zone 2.

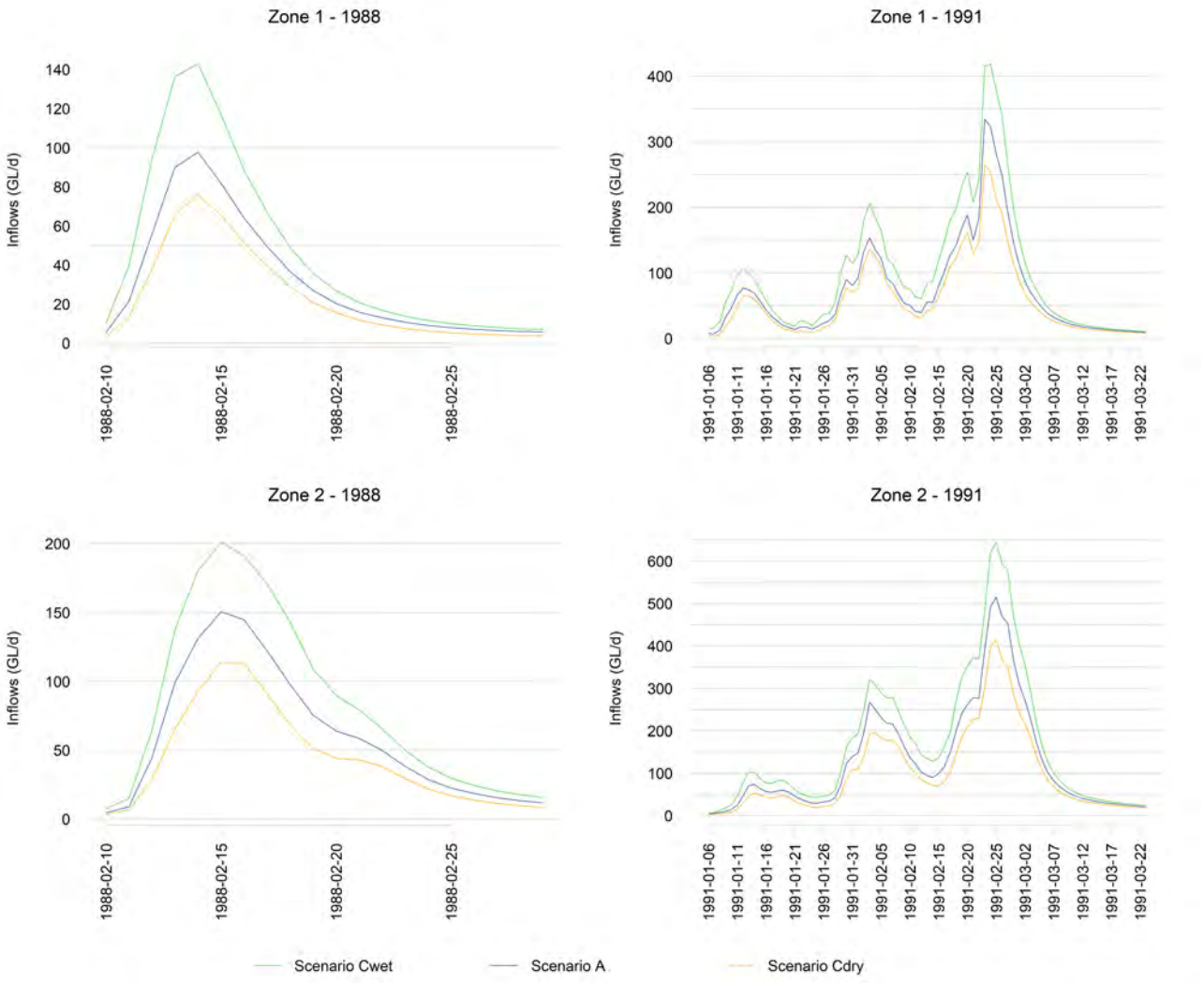

Figure 5-2 Simulated aggregated streamflow used as inflows in the hydrodynamic model for two different flood events (1988 and 1991) under scenarios A (baseline), Cwet and Cdry

Under Scenario Cwet for Zone 1, peak streamflow is increased by 46 and 25% for the 1988 and 1991 flood events, respectively; and total discharge is increased by 44 and 36% for the 1988 and 1991 and 2008 flood events, respectively. For Zone 2, peak streamflow is increased by 33 and 25% for the 1988 and 1991 flood events, respectively; and total discharge is increased by 38 and 30% for the 1988 and 1991 and 2008 flood events, respectively.

5.3 Potential development scenarios

Potential dams identified in the companion technical report on surface water storage, Petheram et al. (2022), were located outside of each of the hydrodynamic model domains. Hence to explore the impact of in-stream dams and water harvesting on flood inundation downstream, river system models were configured with various scenarios (refer to the companion technical report on river model calibration and scenario analysis, Hughes et al. (2023)) and the resulting river system model output provided for the upstream boundary of the hydrodynamic model domains. Only streamflow at the upstream boundaries of the hydrodynamic model domains were updated, whereas the remaining input datasets and boundary conditions in the calibrated hydrodynamic models remained unchanged.

Three dam scenarios were considered:

1. "all dams" – five potential dam sites with no transparent flows including sites on Flying Fox Creek (FSL: 177m EMG96, maximum capacity: 174 GL), Jalboi River (FSL: 70m EMG96, maximum capacity: 189 GL), Hodgson River (FSL: 106 m EMG96, maximum capacity: 394 GL), Waterhouse River (FSL: 200 m EMG96, maximum capacity: 391 GL) and Waterhouse River West Branch (FSL: 188 m EMG96, maximum capacity: 223 GL)
2. Waterhouse River potential dam site only with no transparent flows (FSL: 200 m EMG96, maximum capacity: 391 GL)
3. Flying Fox Creek potential dam site only with no transparent flows (FSL: 177m EMG96, maximum capacity: 174 GL).

Within the Roper catchment, the availability of soils suitable for irrigation with a reasonable distance of surface water is relatively limited. For this reason, soil-limited water harvesting scenarios were investigated using the flood inundation models. The soil-limited water harvesting scenario represented an annual diversion of 660 GL at 75% annual reliability with no end-of-system requirement (Hughes et al., 2023). Where water harvesting occurred within the hydrodynamic model domains, distributed extractions were introduced along the relevant river sections within the MIKE 11 model set-up. Refer to the companion technical report on river model calibration and scenario analysis, Hughes et al. (2023), for further details about instream dam and water harvesting scenarios.

5.4 Floodplain inundation scenario analyses

The evaluation of hydrodynamic modelled scenarios was performed by comparing future development (Scenario B), future climate (Scenario C), and future climate and development (Scenario D) to the baseline simulation (Scenario A). Two types of evaluations were performed across the hydrodynamic model domains (note that connectivity of selected floodplains is discussed in Chapter 6) for each scenario in the two model domains (Table 5-1):

- a spatial comparison using maps of percentage inundation frequency (the ratio of the times a pixel is inundated to the entire duration of the simulation), maximum inundation extent and inundated depth at maximum inundation extent
- a time-series comparison of inundated area and mean depth.

5.4.1 SCENARIO B CURRENT CLIMATE AND ALL DAMS

Maps of percentage inundated frequency (Figure 5-3 and Figure 5-4), maximum inundation extent (Figure 5-5 and Figure 5-6) and depth at maximum inundation (Figure 5-7 and Figure 5-8) show that for both the 1988 (AEP of 1 in 2) and 1991 (AEP of 1 in 13) flood events, the dams decrease inundation (frequency, extent and depth) downstream of the potential dam sites however the effects are relatively small.

The impacts of the dams on flood characteristics over the hydrodynamic model domain are small (Figure 5-9). The maximum inundated area under Scenario A for the 1988 event is 545 km^2, and 523 km^2 under Scenario B (all dams). This represents a decrease in inundated area of about 4%. The maximum inundated area under Scenario A for the 1991 event (1 in 13 AEP) is 1697 km^2, and 1583 km^2 under Scenario B (all dams), representing a decrease of about 7%. The larger relative impact found for the 1 in 13 AEP event during 1991 was due to the different antecedent storage levels at the beginning of each event. Dam storage was 56% of total capacity at the beginning of the 1988 event opposed to only 10% at the beginning of the 1991 event. The Roper River had experienced several years of only small flow events prior to 1991, where relatively high flows were seen the year before the 1988 event (Figure 4-4). Also, higher impact is expected to events earlier in the wet season (as in the 1991 event) since dams will generally be emptier then, thus capturing more flood waters.

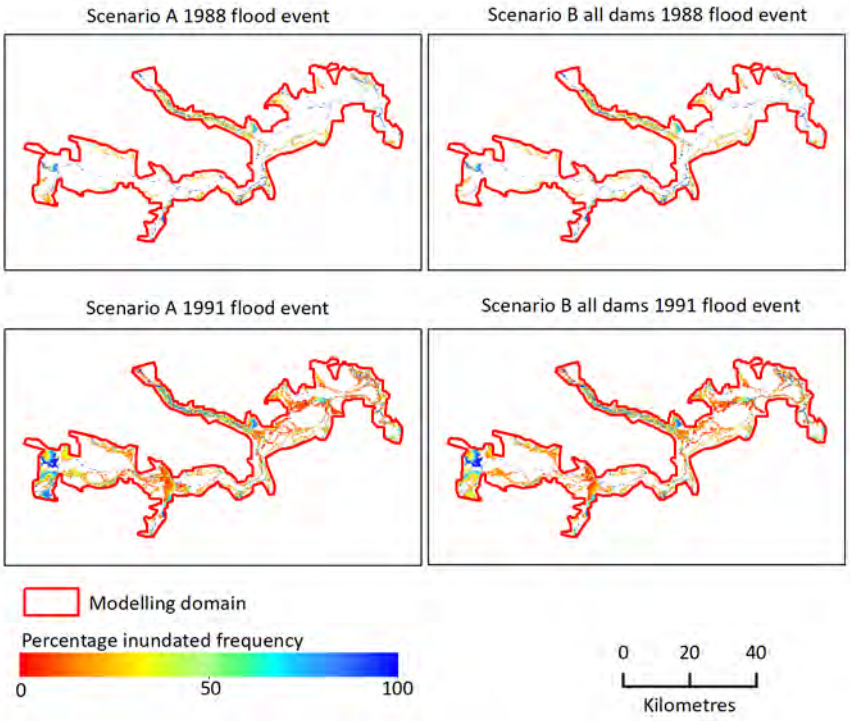

Figure 5-3 Percentage inundation frequency in the Zone 1 model domain under Scenario A (Baseline) and B (all dams)

The 1988 flood event had an AEP of 1 in 2 and the 1991 flood event had an AEP of 1 in 13.

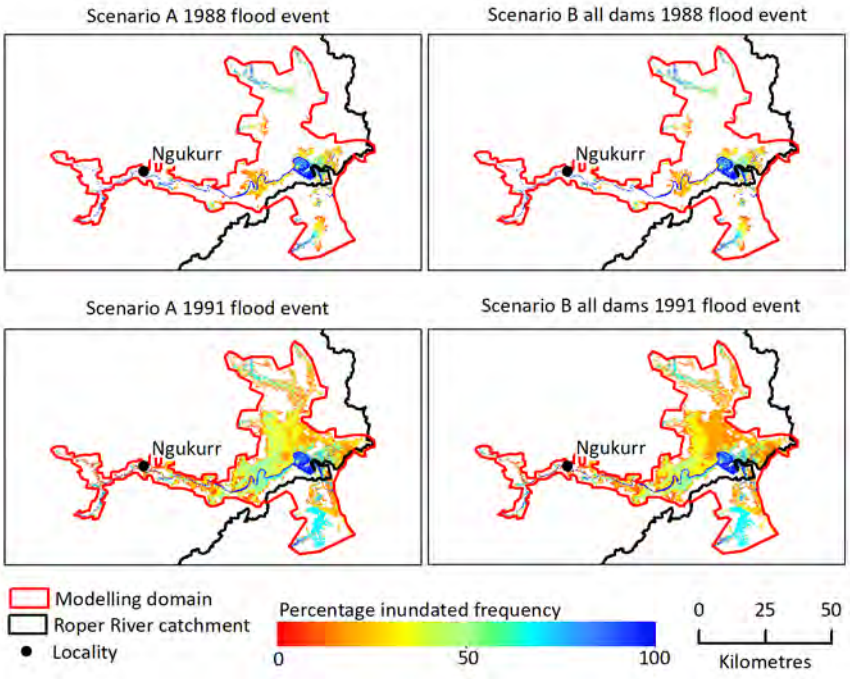

Figure 5-4 Percentage inundation frequency in the Zone 2 model domain under Scenario A (Baseline) and B (all dams)

The 1988 flood event had an AEP of 1 in 2 and the 1991 flood event had an AEP of 1 in 13.

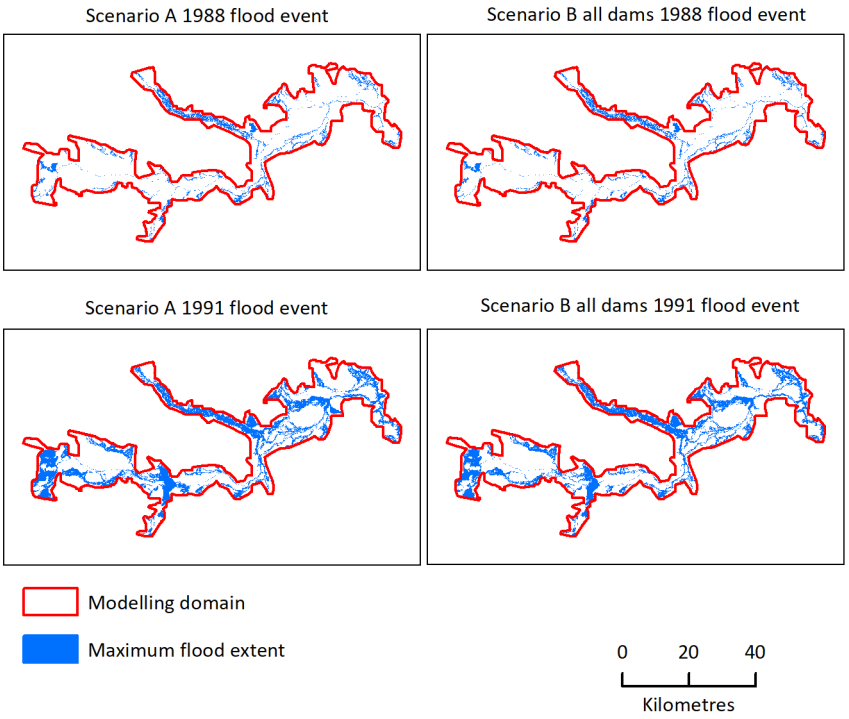

Figure 5-5 Maximum inundation extent in the Zone 1 model domain under scenarios A (Baseline) and B (all dams)

The 1988 flood event had an AEP of 1 in 2 and the 1991 flood event had an AEP of 1 in 13.

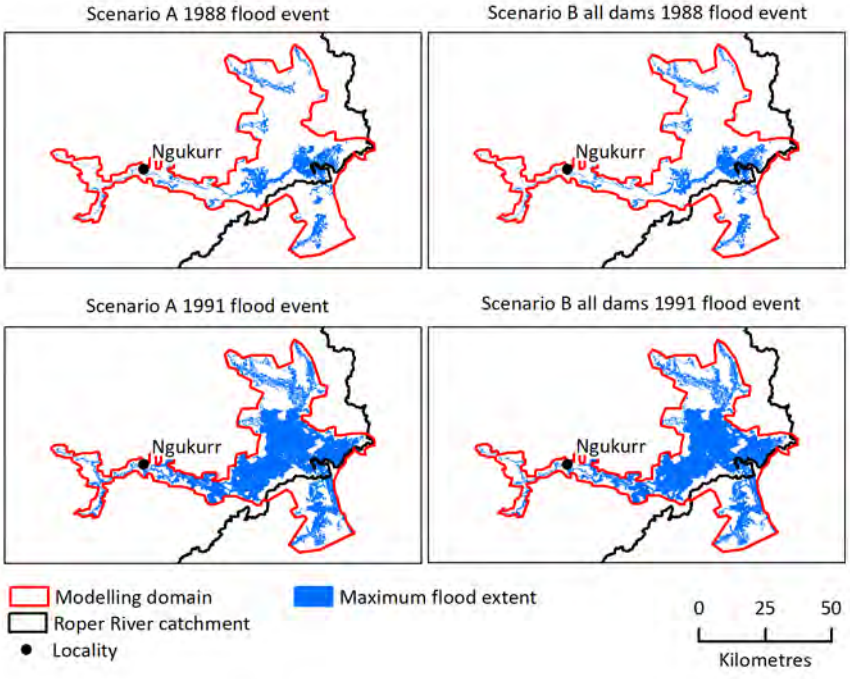

Figure 5-6 Maximum inundation extent in the Zone 2 model domain under scenarios A (Baseline) and B (all dams)

The 1988 flood event had an AEP of 1 in 2 and the 1991 flood event had an AEP of 1 in 13.

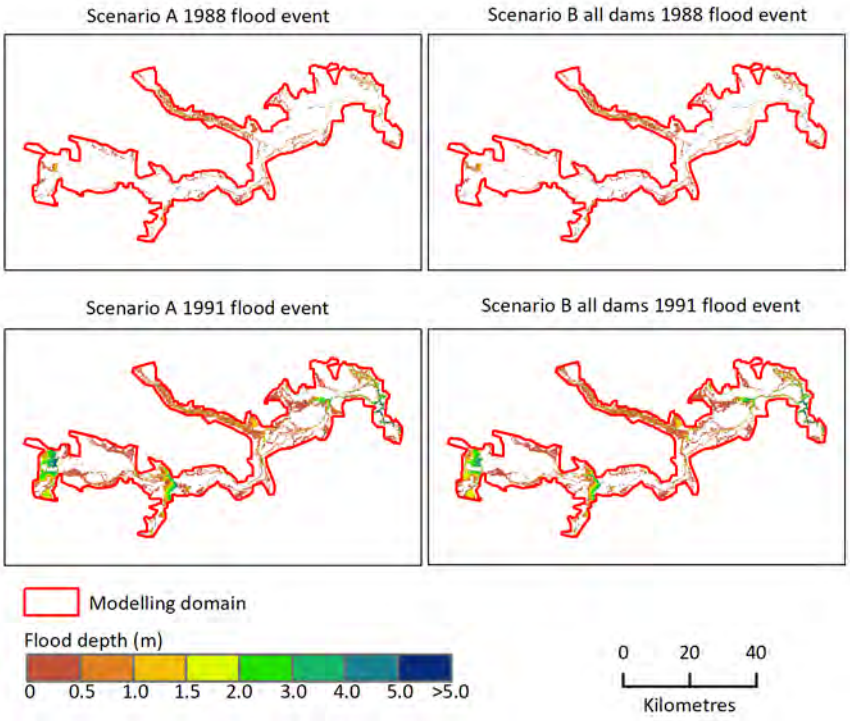

Figure 5-7 Depth at maximum inundation extent in the Zone 1 model domain under scenarios A (Baseline) and B (all dams)

The 1988 flood event had an AEP of 1 in 2 and the 1991 flood event had an AEP of 1 in 13.

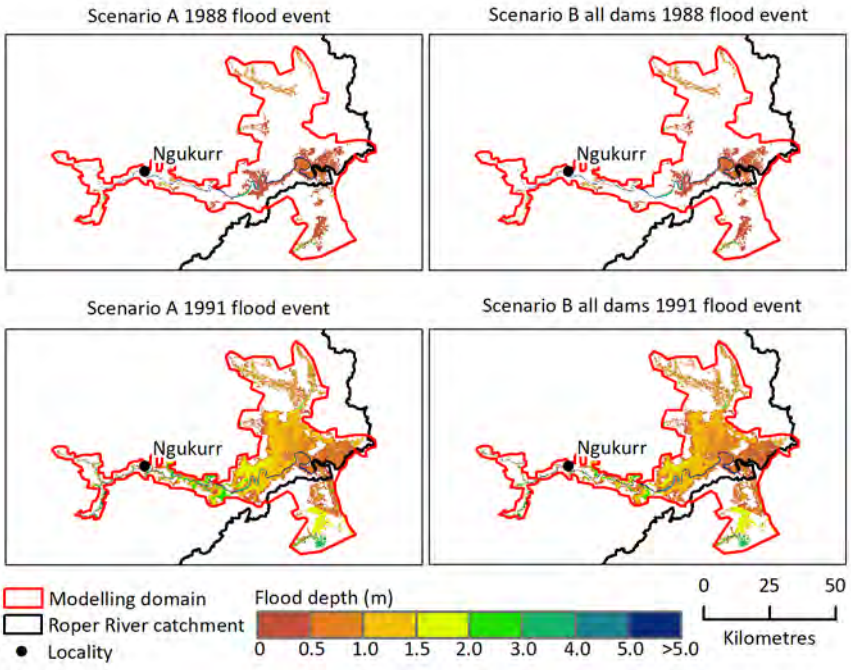

Figure 5-8 Depth at maximum inundation extent in the Zone 2 model domain under scenarios A (Baseline) and B (all dams)

The 1988 flood event had an AEP of 1 in 2 and the 1991 flood event had an AEP of 1 in 13.

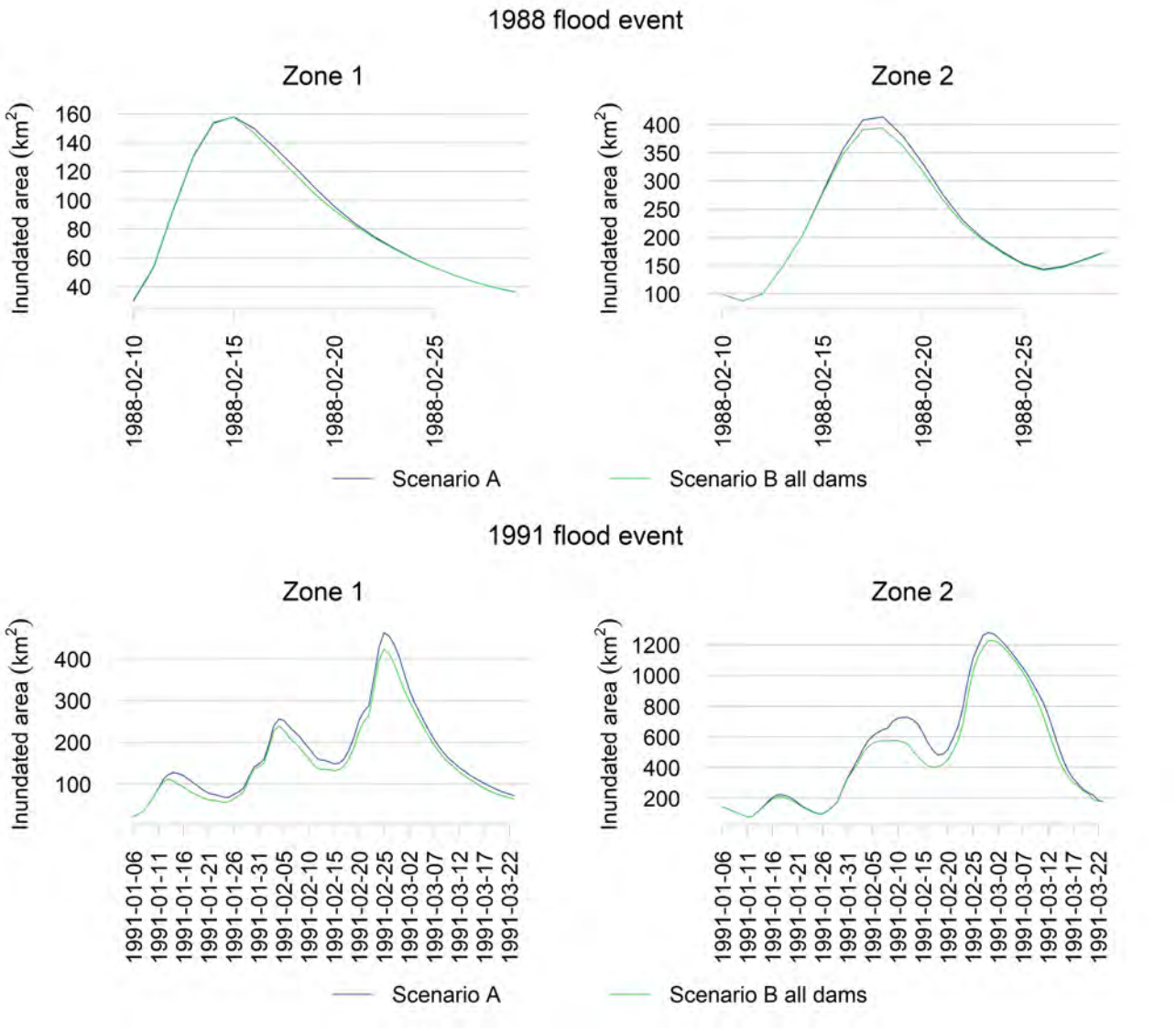

Figure 5-9 Comparison of inundated area in square kilometres over Zone 1 (left) and 2 (right) under scenarios A (Baseline) and B (all dams)

The 1988 flood event had an AEP of 1 in 2 and the 1991 flood event had an AEP of 1 in 13.

5.4.2 SCENARIO B CURRENT CLIMATE AND WATERHOUSE RIVER DAM SITE

Maps displaying the frequency of inundation as a percentage of the total days during the event (Figure 5-10 and Figure 5-11), maximum extent of inundation (Figure 5-12 and Figure 5-13), and the depth at the peak inundation (Figure 5-14 and Figure 5-15) reveal that both the 1988 flood event (with an AEP of 1 in 2) and the 1991 flood event (with an AEP of 1 in 13) experienced reduced inundation (in terms of frequency, extent, and depth) downstream of the Waterhouse dam site. However, it's important to note that these effects were found to be relatively minor.

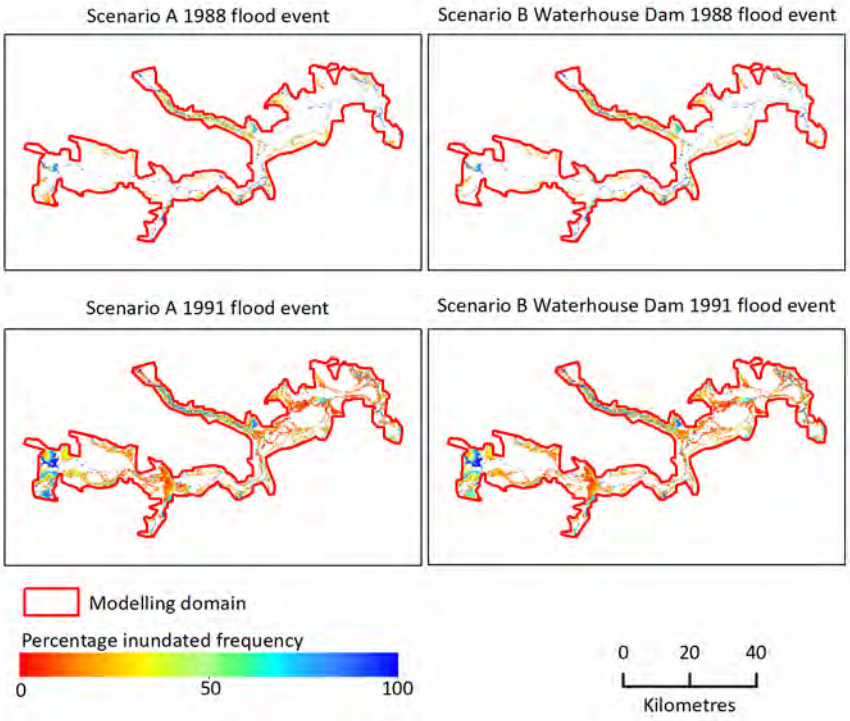

Figure 5-10 Percentage inundation frequency in the Zone 1 model domain under Scenario A (Baseline) and B (Waterhouse River dam)

The 1988 flood event had an AEP of 1 in 2 and the 1991 flood event had an AEP of 1 in 13.

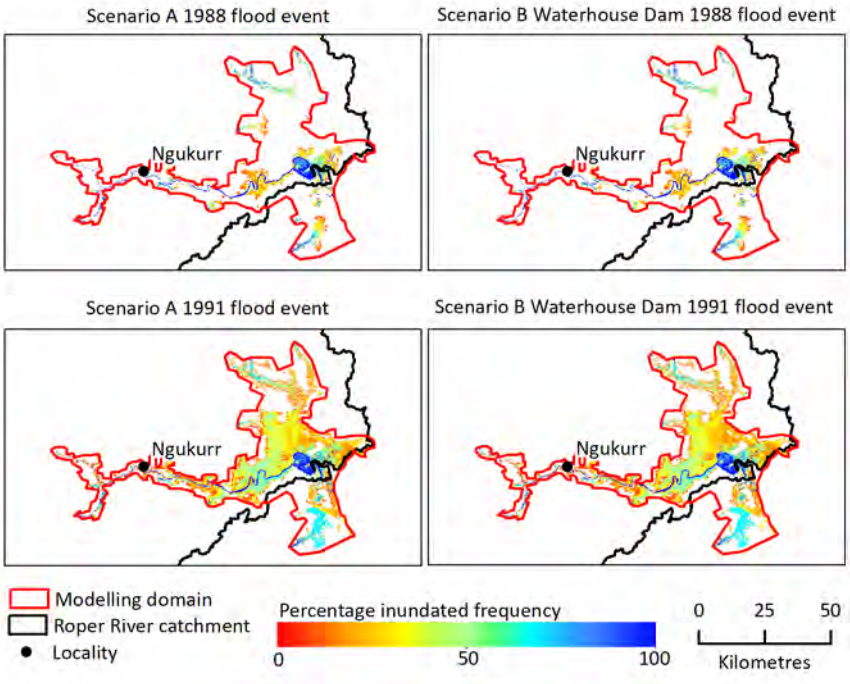

Figure 5-11 Percentage inundation frequency in the Zone 2 model domain under Scenario A (Baseline) and B (Waterhouse River dam)

The 1988 flood event had an AEP of 1 in 2 and the 1991 flood event had an AEP of 1 in 13.

The impacts of the Waterhouse Dam on flood characteristics over the hydrodynamic model domain are small (Figure 5-16). The maximum inundated area under scenarios A and B (Waterhouse dam) for the 1988 event (1 in 2 AEP) is 545 km^2 and 540 km^2 respectively. This represents a decrease in inundated area of about 1%. The maximum inundated area under scenarios A and B (Waterhouse dam) for the 1991 event is 1697 km^2 and 1658 km^2 respectively, representing a decrease of about 2%. As per Scenario B (all dams), the larger relative impact was found for the 1 in 13 AEP event was due to the different antecedent storage levels at the beginning of each event.

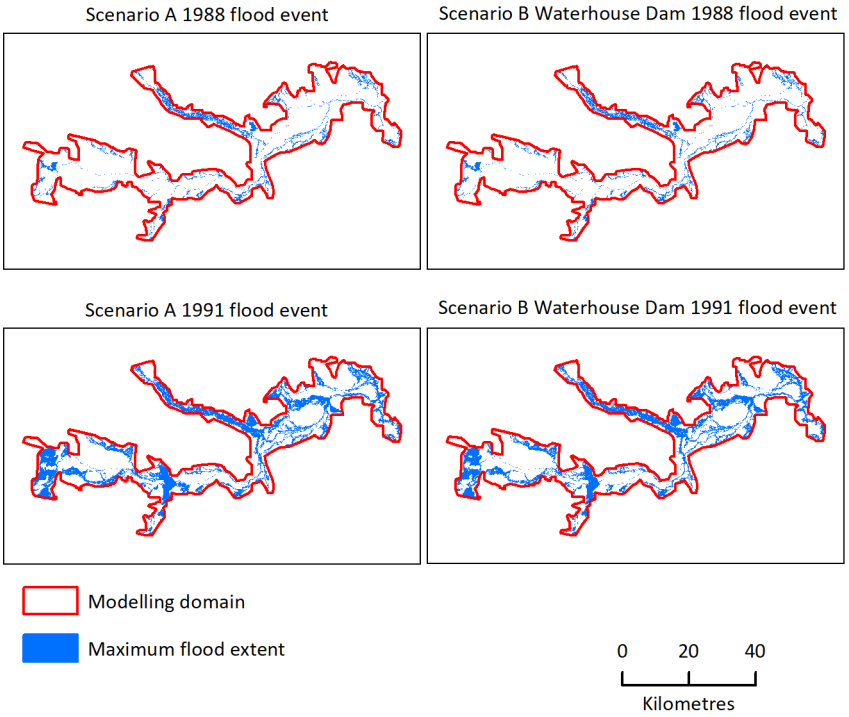

Figure 5-12 Maximum inundation extent in the Zone 1 model domain under scenarios A (Baseline) and B (Waterhouse River dam)

The 1988 flood event had an AEP of 1 in 2 and the 1991 flood event had an AEP of 1 in 13.

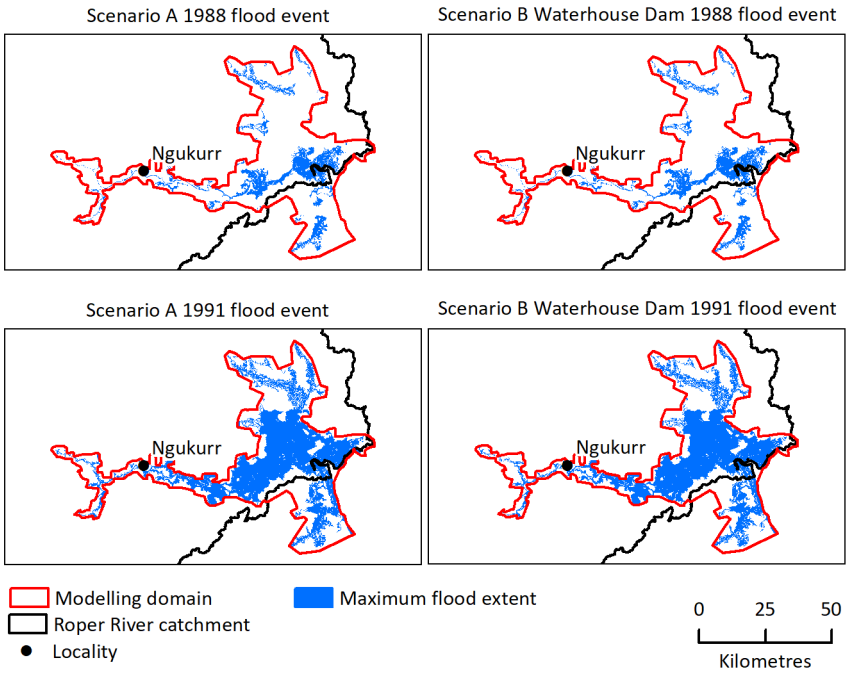

Figure 5-13 Maximum inundation extent in the Zone 2 model domain under scenarios A (Baseline) and B (Waterhouse River dam)

The 1988 flood event had an AEP of 1 in 2 and the 1991 flood event had an AEP of 1 in 13.

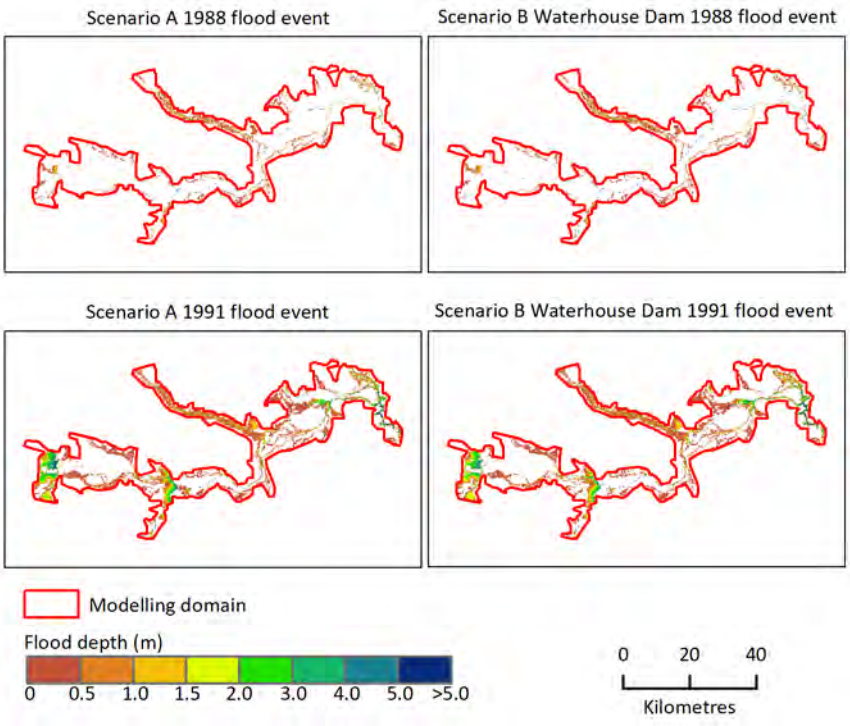

Figure 5-14 Depth at maximum inundation extent in the Zone 1 model domain under scenarios A (Baseline) and B (Waterhouse River dam)

The 1988 flood event had an AEP of 1 in 2 and the 1991 flood event had an AEP of 1 in 13.

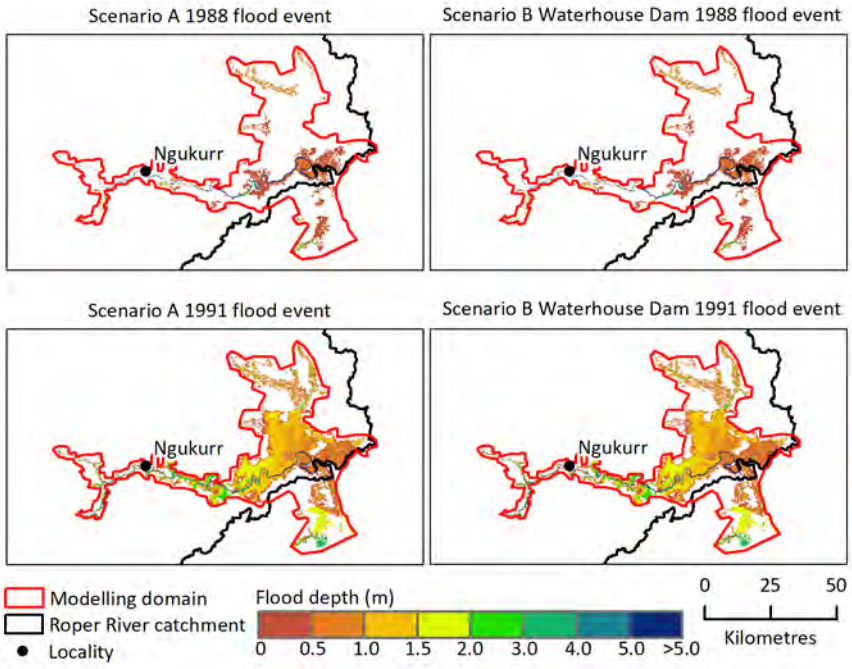

Figure 5-15 Depth at maximum inundation extent in the Zone 2 model domain under scenarios A (Baseline) and B (Waterhouse River dam)

The 1988 flood event had an AEP of 1 in 2 and the 1991 flood event had an AEP of 1 in 13.

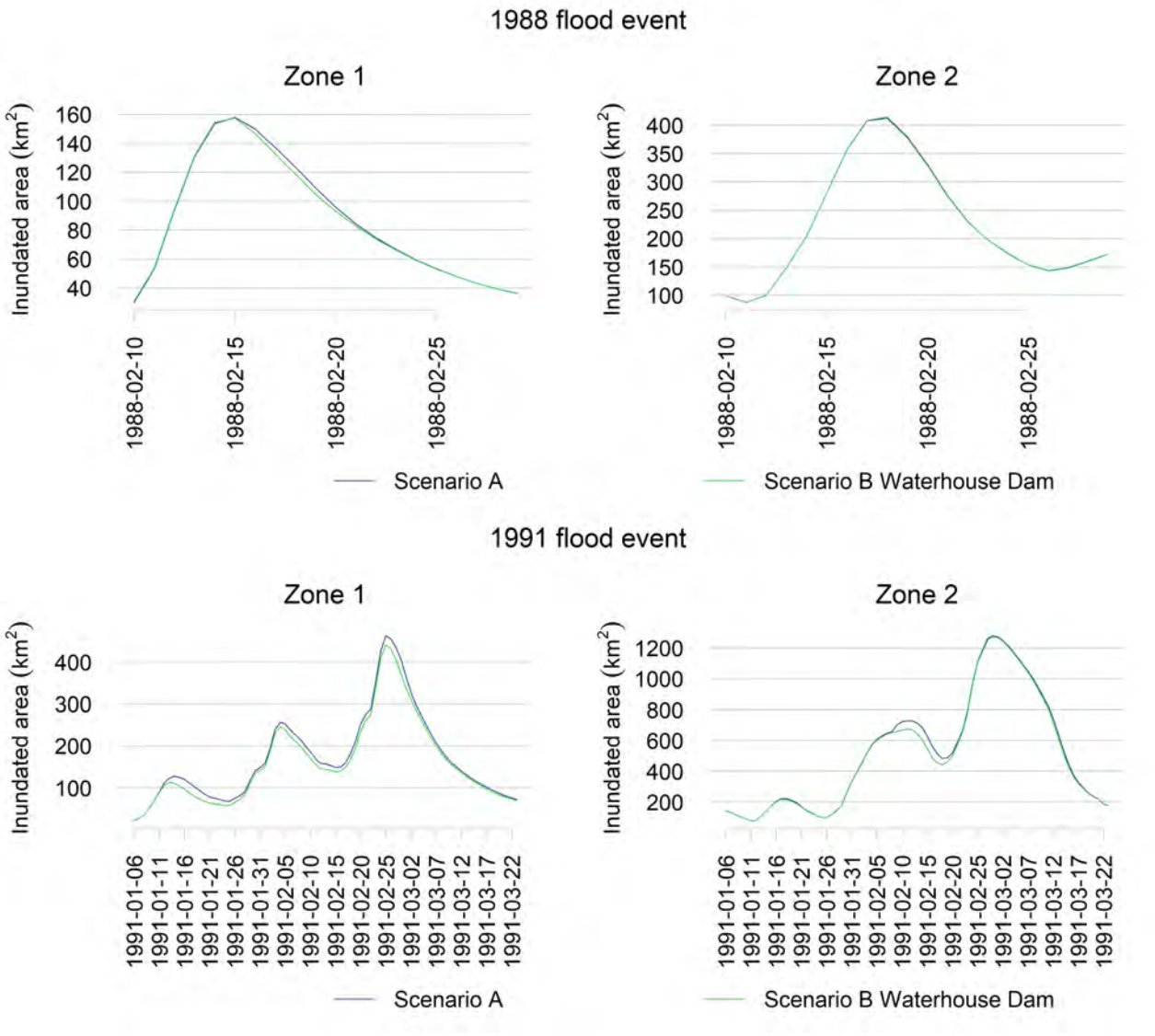

Figure 5-16 Comparison of inundated area in square kilometres over Zone 1 (left) and 2 (right) under scenarios A (Baseline) and B (Waterhouse River dam)

The 1988 flood event had an AEP of 1 in 2 and the 1991 flood event had an AEP of 1 in 13.

5.4.3 SCENARIO B CURRENT CLIMATE AND FLYING FOX CREEK DAM SITE

Maps of percentage inundated frequency (Figure 5-17 and Figure 5-18), maximum inundation extent (Figure 5-19 and Figure 5-20) and depth at maximum inundation (Figure 5-21 and Figure 5-22) show that for both the 1988 (AEP of 1 in 2) and 1991 (AEP of 1 in 13) flood events, the dams decrease inundation (frequency, extent and depth) downstream of the Flying Fox dam site however the effects are minor.

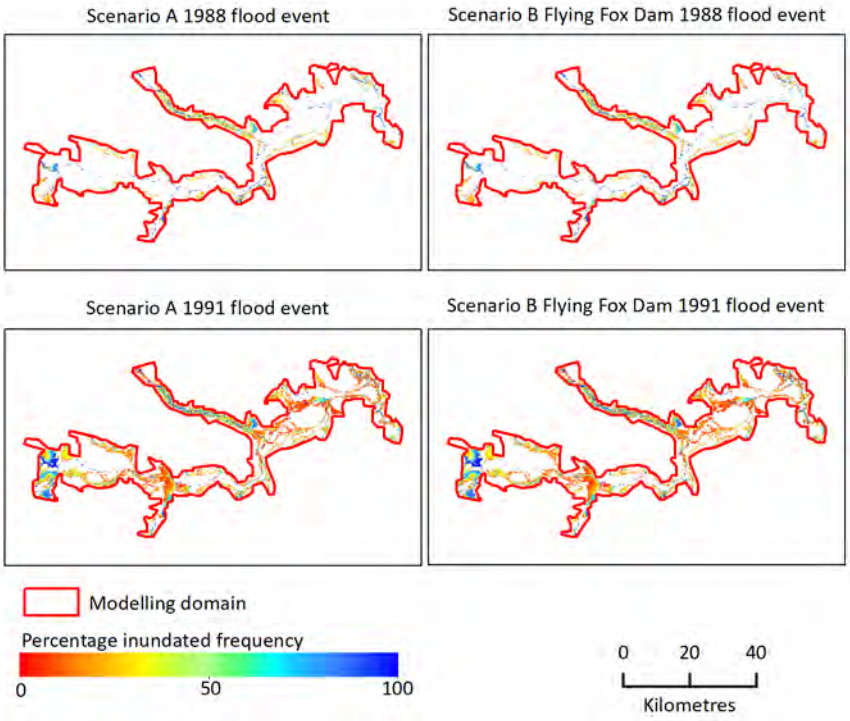

Figure 5-17 Percentage inundation frequency in the Zone 1 model domain under Scenario A (Baseline) and B (Flying Fox Creek dam)

The 1988 flood event had an AEP of 1 in 2 and the 1991 flood event had an AEP of 1 in 13.

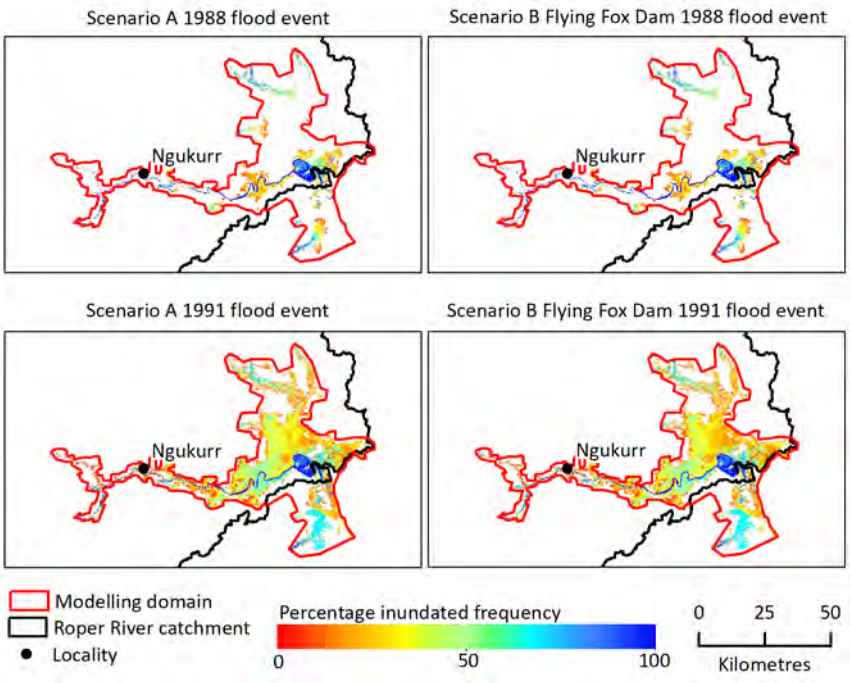

Figure 5-18 Percentage inundation frequency in the Zone 2 model domain under Scenario A (Baseline) and B (Flying Fox Creek dam)

The 1988 flood event had an AEP of 1 in 2 and the 1991 flood event had an AEP of 1 in 13.

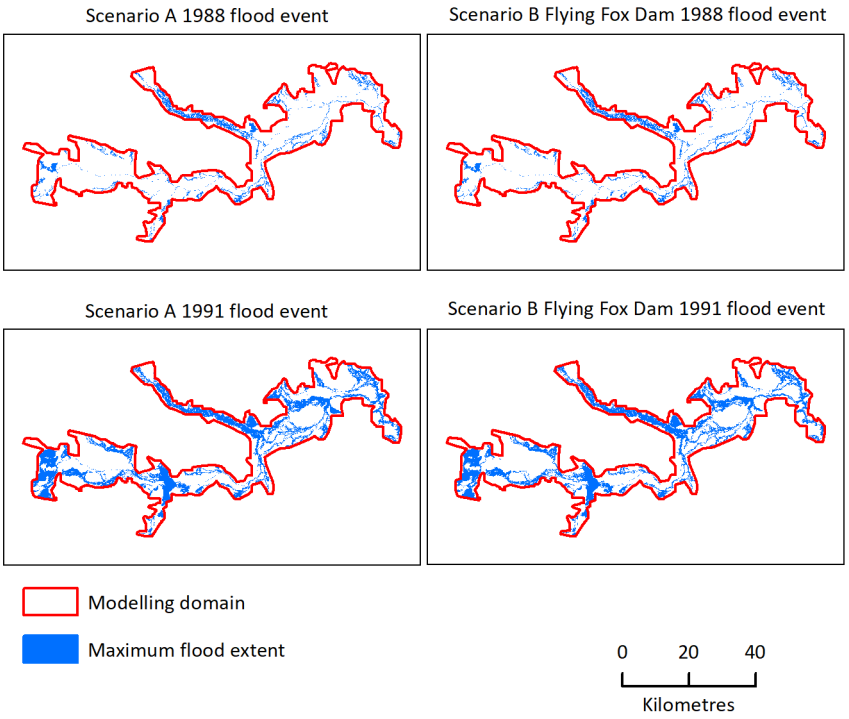

Figure 5-19 Maximum inundation extent in the Zone 1 model domain under scenarios A (Baseline) and B (Flying Fox Creek dam)

The 1988 flood event had an AEP of 1 in 2 and the 1991 flood event had an AEP of 1 in 13.

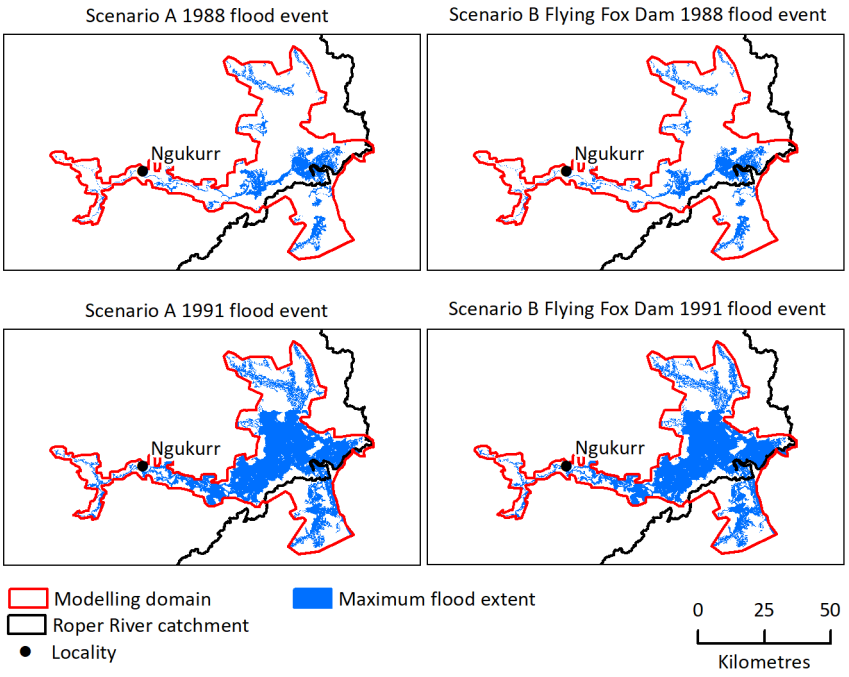

Figure 5-20 Maximum inundation extent in the Zone 2 model domain under scenarios A (Baseline) and B (Flying Fox Creek dam)

The 1988 flood event had an AEP of 1 in 2 and the 1991 flood event had an AEP of 1 in 13.

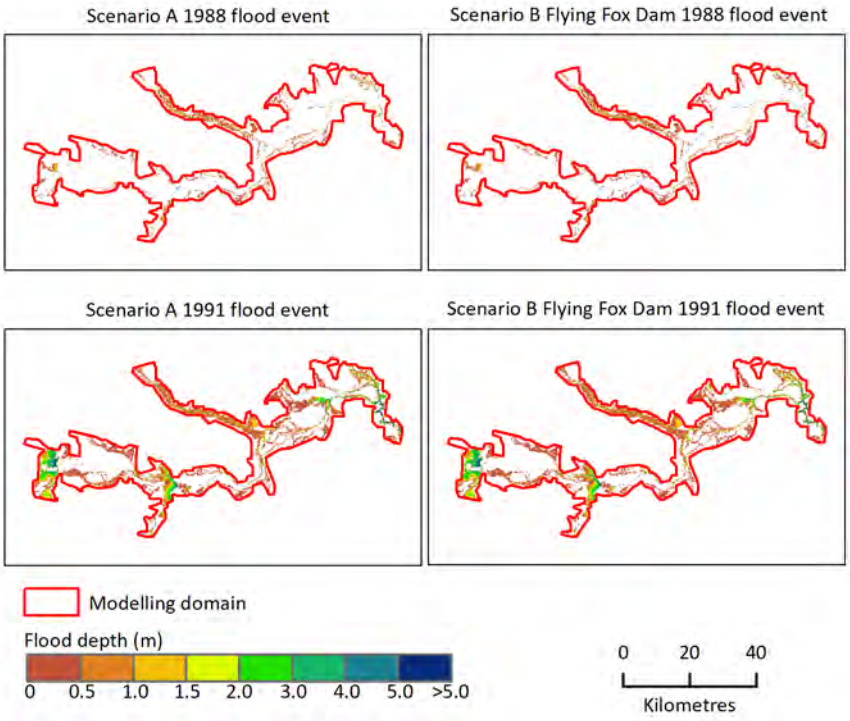

Figure 5-21 Depth at maximum inundation extent in the Zone 1 model domain under scenarios A (Baseline) and B (Flying Fox Creek dam)

The 1988 flood event had an AEP of 1 in 2 and the 1991 flood event had an AEP of 1 in 13.

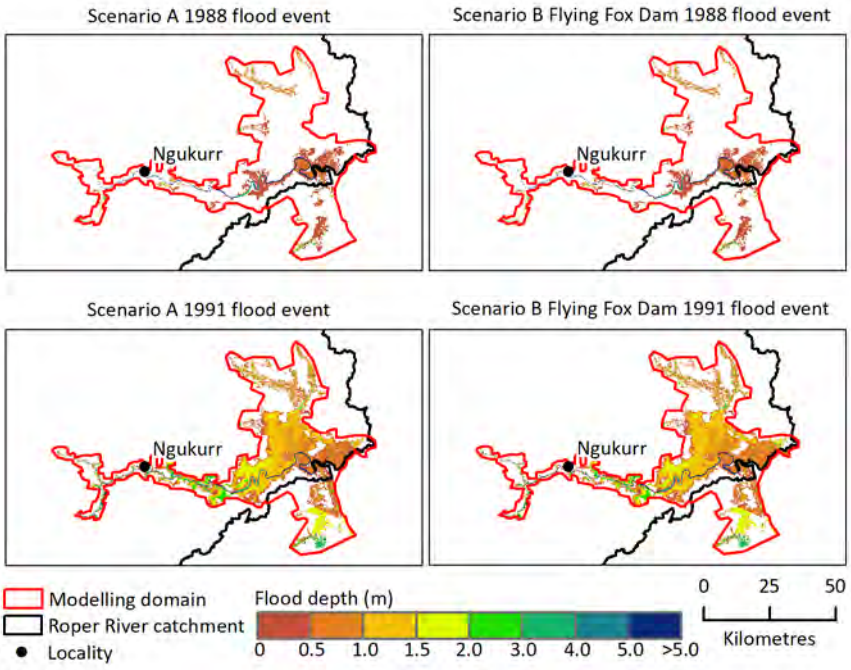

Figure 5-22 Depth at maximum inundation extent in the Zone 2 model domain under scenarios A (Baseline) and B (Flying Fox Creek dam)

The 1988 flood event had an AEP of 1 in 2 and the 1991 flood event had an AEP of 1 in 13.

The impacts of the potential Flying Fox dam on flood characteristics over the hydrodynamic model domain are small (Figure 5-23). The maximum inundated area under scenarios A and B (Flying Fox dam) for the 1988 event is 545 km^2 and 539 km^2 respectively. This represents a decrease in inundated area of about 1%. The maximum inundated area under scenarios A and B (Flying Fox dam) for the 1991 event is 1697 km^2 and 1675 km^2 respectively, again representing a decrease of about 1%.

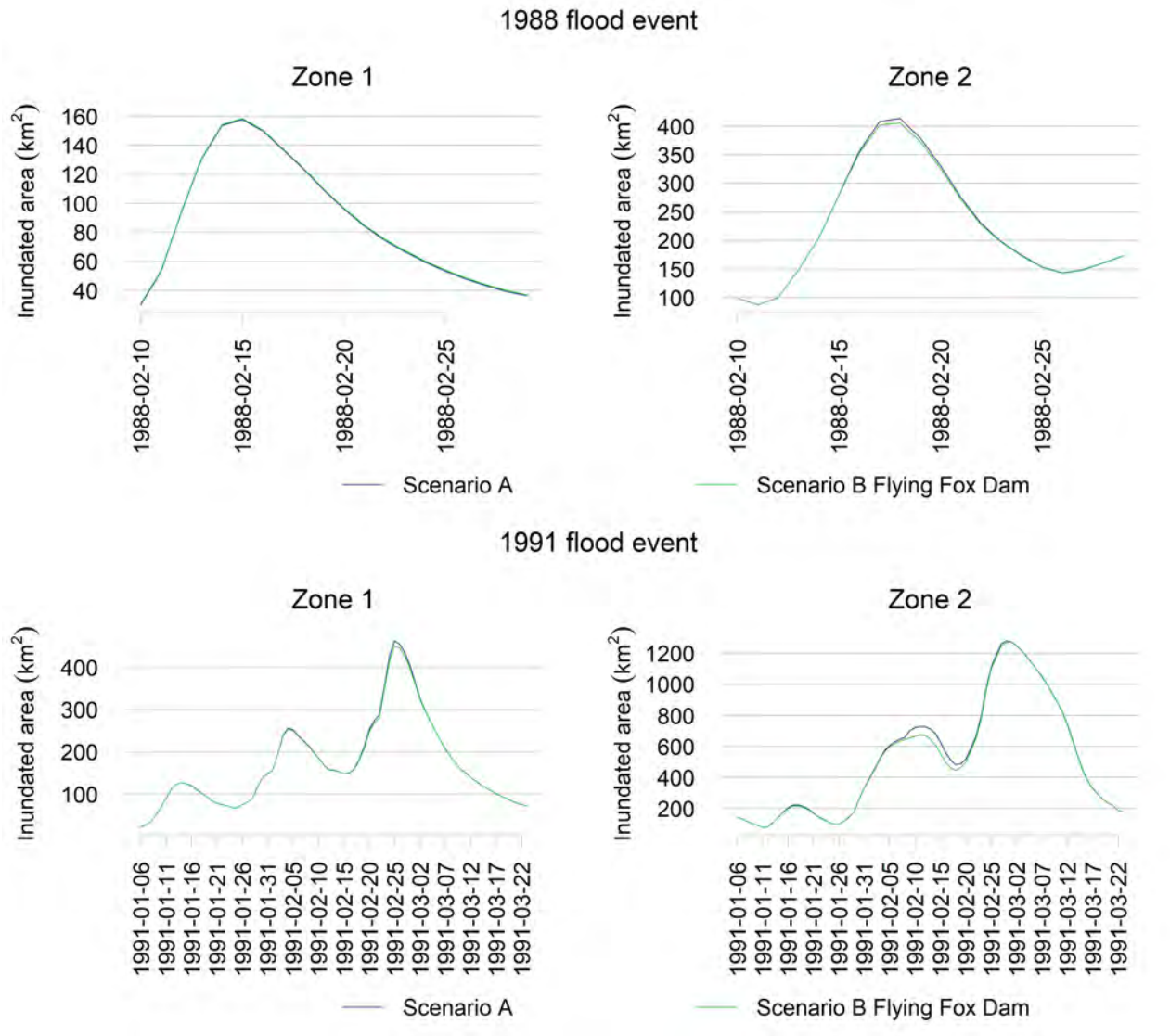

Figure 5-23 Comparison of inundated area in square kilometres over Zone 1 (left) and 2 (right) under scenarios A (Baseline) and B (Flying Fox Creek dam)

The 1988 flood event had an AEP of 1 in 2 and the 1991 flood event had an AEP of 1 in 13.

5.4.4 SCENARIO B CURRENT CLIMATE AND WATER HARVESTING

Maps of percentage inundated frequency (Figure 5-24 and Figure 5-25), maximum inundation extent (Figure 5-26 and Figure 5-27) and depth at maximum inundation (Figure 5-28 and Figure 5-29) show that water harvesting of an annual volume of 660 GL decreases inundation extent by a small to moderate amount for the 1988 (AEP of 1 in 2) event, but the relative decrease is far less for the 1991 (AEP of 1 in 13) event.

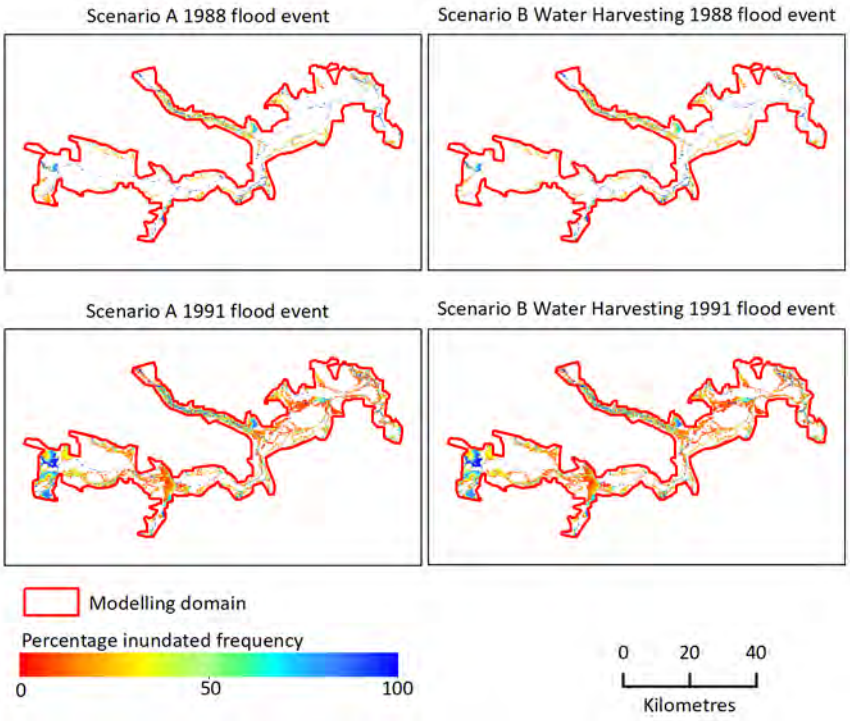

Figure 5-24 Percentage inundation frequency in the Zone 1 model domain under Scenario A (Baseline) and B (Water Harvesting)

The 1988 flood event had an AEP of 1 in 2 and the 1991 flood event had an AEP of 1 in 13.

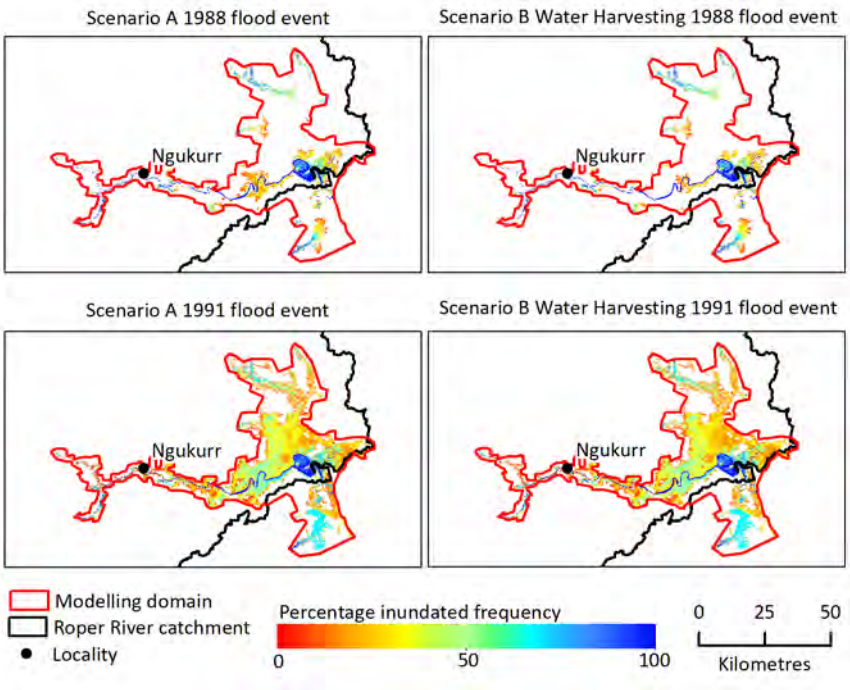

Figure 5-25 Percentage inundation frequency in the Zone 2 model domain under Scenario A (Baseline) and B (Water Harvesting)

The 1988 flood event had an AEP of 1 in 2 and the 1991 flood event had an AEP of 1 in 13.

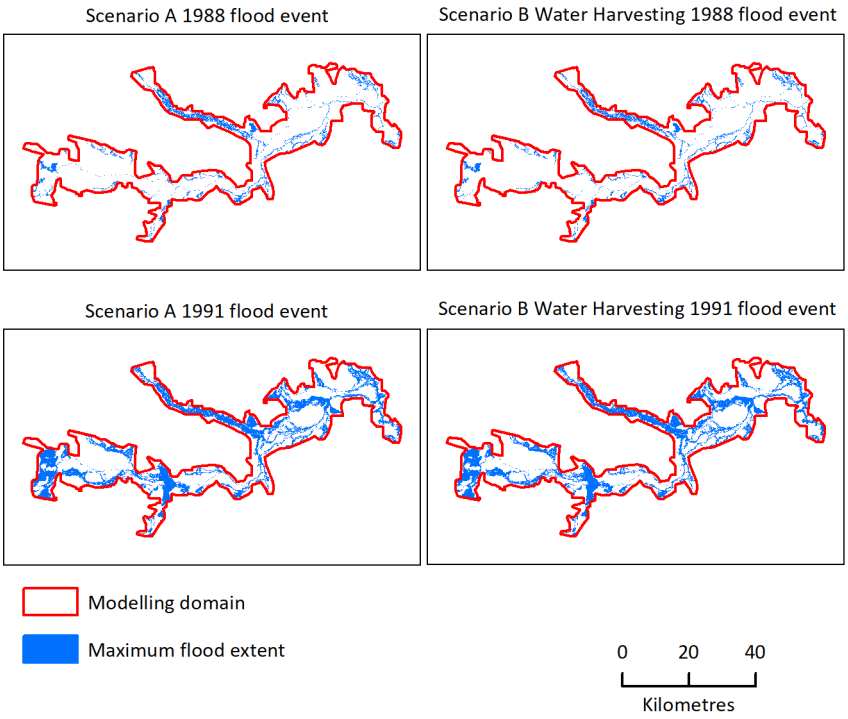

Figure 5-26 Maximum inundation extent in the Zone 1 model domain under scenarios A (Baseline) and B (Water Harvesting)

The 1988 flood event had an AEP of 1 in 2 and the 1991 flood event had an AEP of 1 in 13.

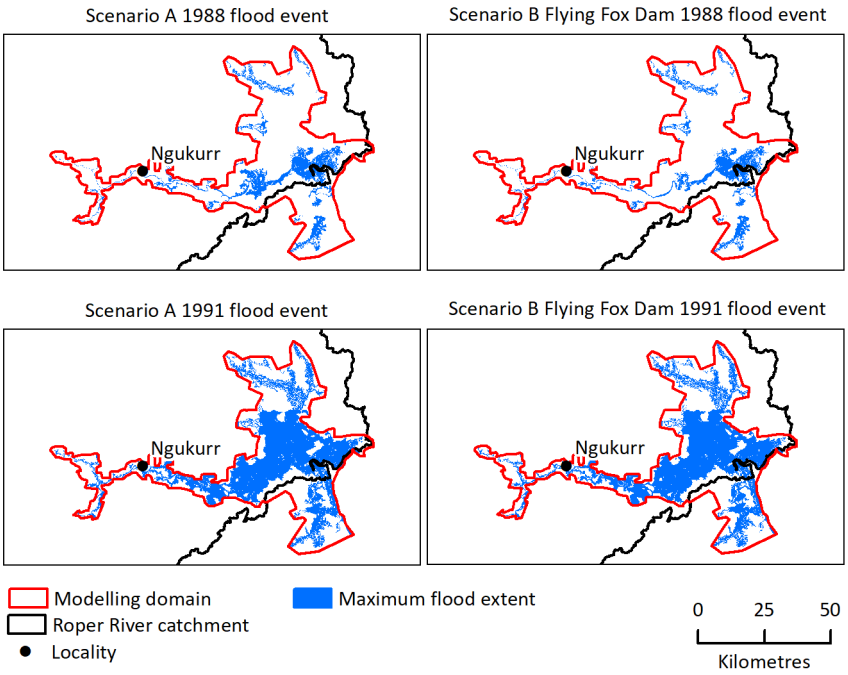

Figure 5-27 Maximum inundation extent in the Zone 2 model domain under scenarios A (Baseline) and B (Water Harvesting)

The 1988 flood event had an AEP of 1 in 2 and the 1991 flood event had an AEP of 1 in 13.

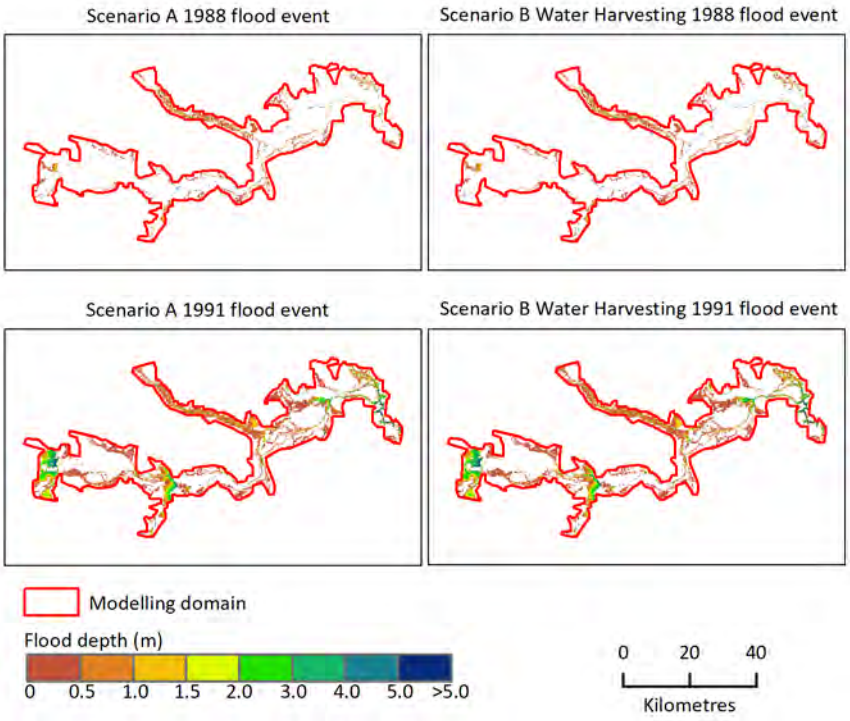

Figure 5-28 Depth at maximum inundation extent in the Zone 1 model domain under scenarios A (Baseline) and B (Water Harvesting)

The 1988 flood event had an AEP of 1 in 2 and the 1991 flood event had an AEP of 1 in 13.

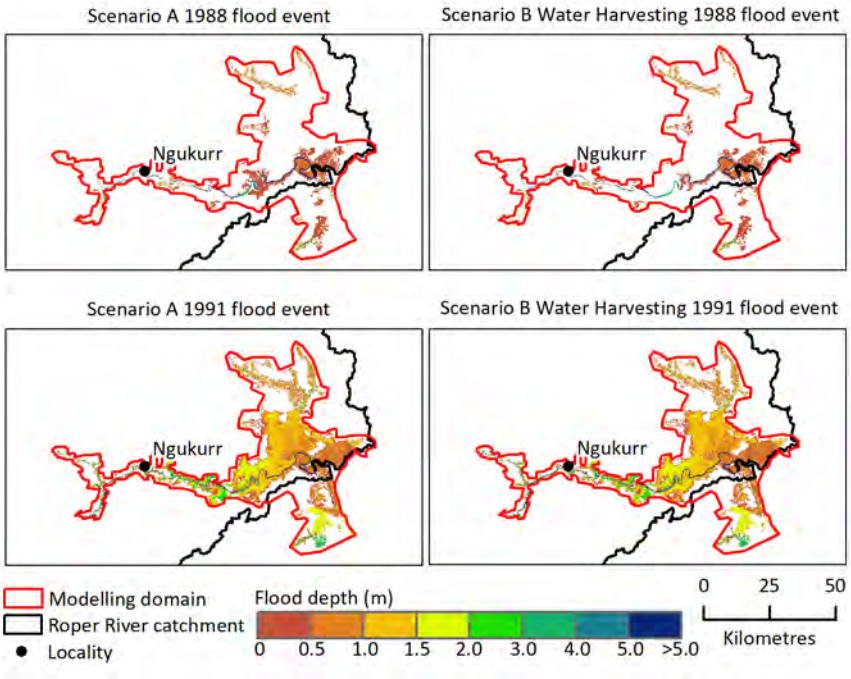

Figure 5-29 Depth at maximum inundation extent in the Zone 2 model domain under scenarios A (Baseline) and B (Water Harvesting)

The 1988 flood event had an AEP of 1 in 2 and the 1991 flood event had an AEP of 1 in 13.

The impacts of water harvesting on flood characteristics over the hydrodynamic model domain are larger for the smaller event relative to the size of the events (Figure 5-30). The maximum inundated area under scenarios A and B (water harvesting of 660 GL)for the 1988 event is 545 km^2 and 485 km^2 respectively. This represents a decrease in inundated area of about 11%. The maximum inundated area under Scenario A for the 1991 event is 1697 km^2. Under Scenario B (water harvesting of 660 GL), there was very little modelled change in maximum inundated area (decrease of about 0.02%).

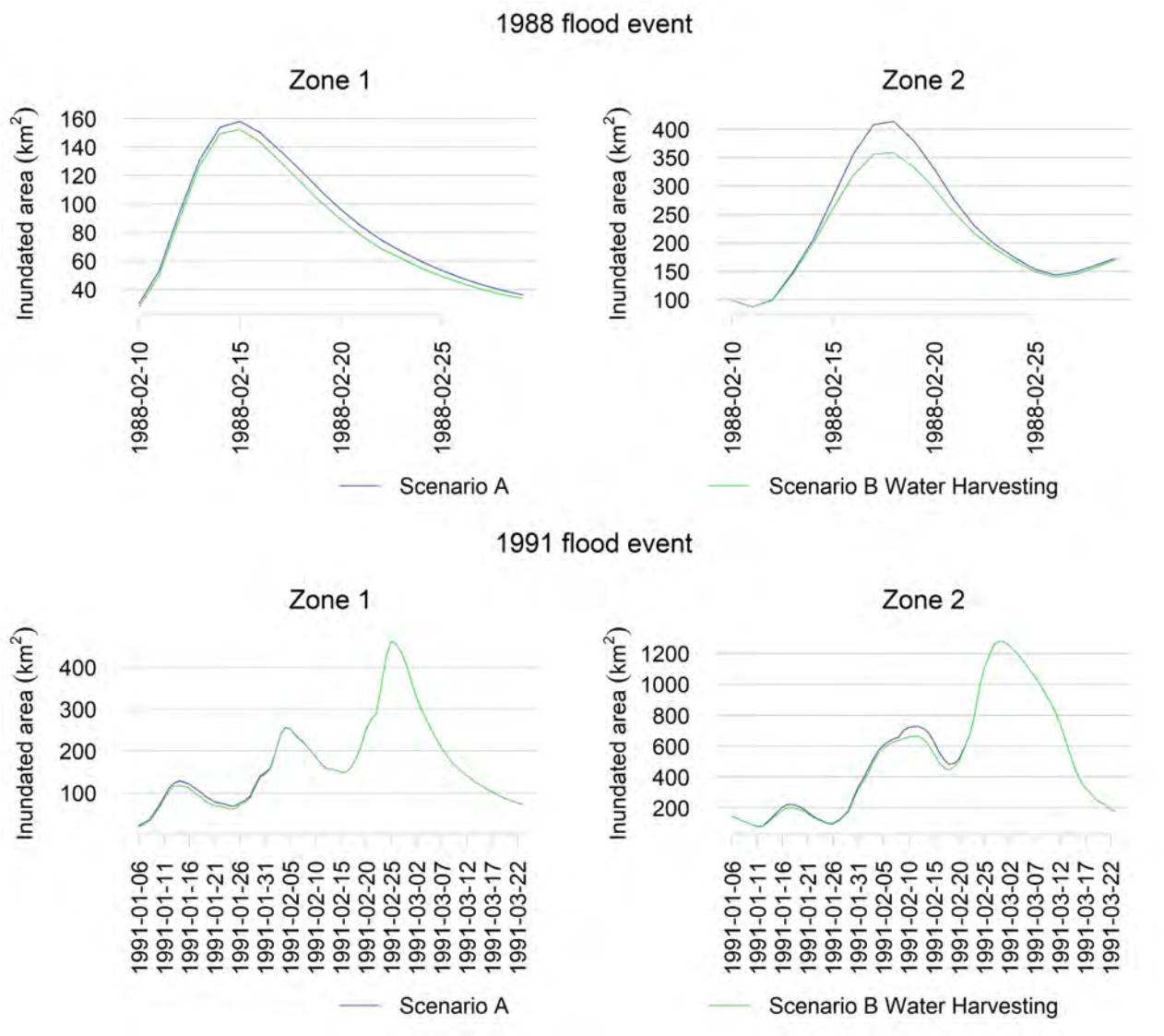

Figure 5-30 Comparison of inundated area in square kilometres over Zone 1 (left) and 2 (right) under scenarios A (Baseline) and B (Water Harvesting)

The 1988 flood event had an AEP of 1 in 2 and the 1991 flood event had an AEP of 1 in 13.

5.4.5 SCENARIO C SIMULATIONS

Figure 5-31 to Figure 5-36 show the difference between scenarios A, Cdry and Cwet in terms of percentage inundated frequency, maximum inundation extent and depth at maximum extent for the two events. The Zone 1 Roper River floodplains show marked decreases from baseline conditions in terms of inundated frequency, maximum inundated area and flood depth for Scenario Cdry. Conversely, a significant increase can be seen in Scenario Cwet compared to

Scenario A. Zone 2 displays similar responses to dry and wet conditions, however, under Scenario A more area is inundated in the south of the model domain than under Scenario Cwet. This flooding is driven by a boundary water source from the Towns River. Floodplains from Towns River connects to Roper floodplains during large floods, however, Towns River lies outside the Roper River system model domain. Consequently, this runoff source was erroneously mapped from the river system model and underestimated local flooding in the future climate scenarios. Towns River flooding is not likely to be impacted on potential water resource development in the Roper Catchment since it is external to the Roper River system and Towns River flooding appears to be largely driven by local runoff. Thus, this area will be largely ignored in this climate impacts analysis. It is recommended that the runoff of Towns River should be corrected in future work so the full effects of projected climate change could be assessed. The maximum inundated area for Zone 2 climate scenarios should be corrected by an additional 140 km^2.

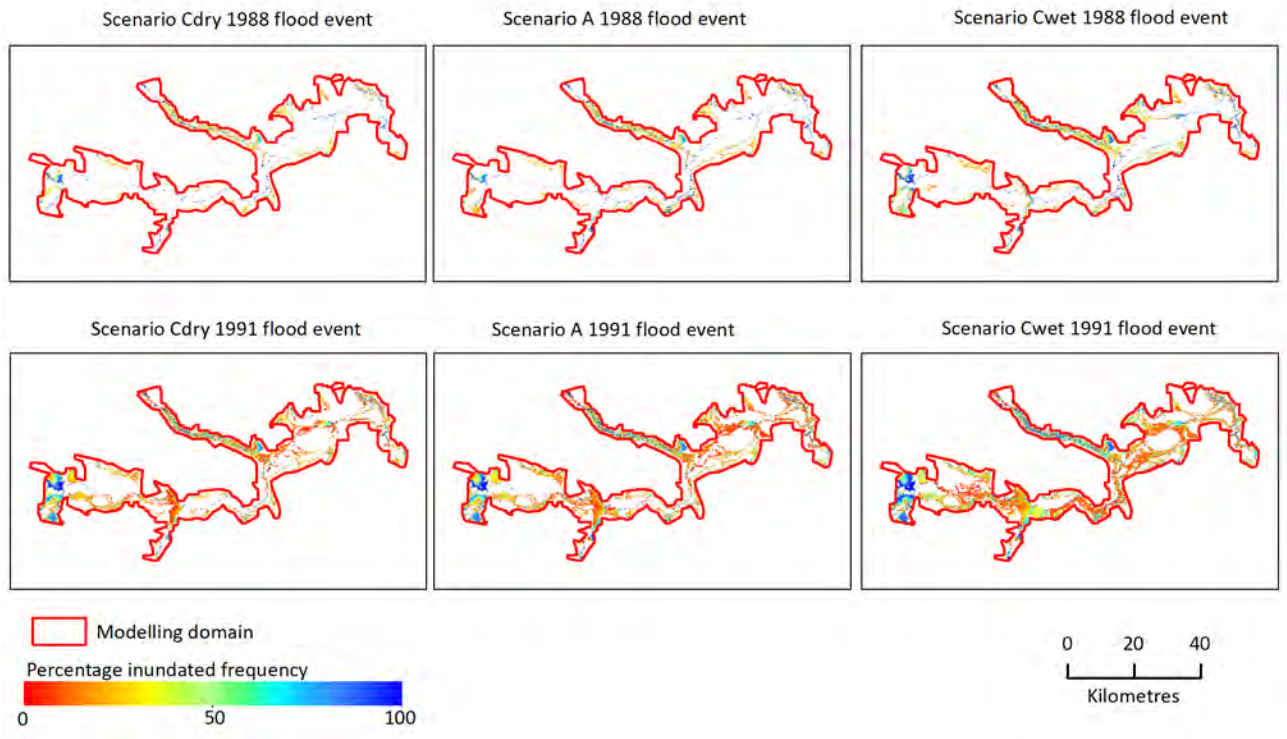

Figure 5-31 Percentage inundated frequency in the Zone 1 model domain under scenarios A and C

The 1988 flood event had an AEP of 1 in 2 and the 1991 flood event had an AEP of 1 in 13.

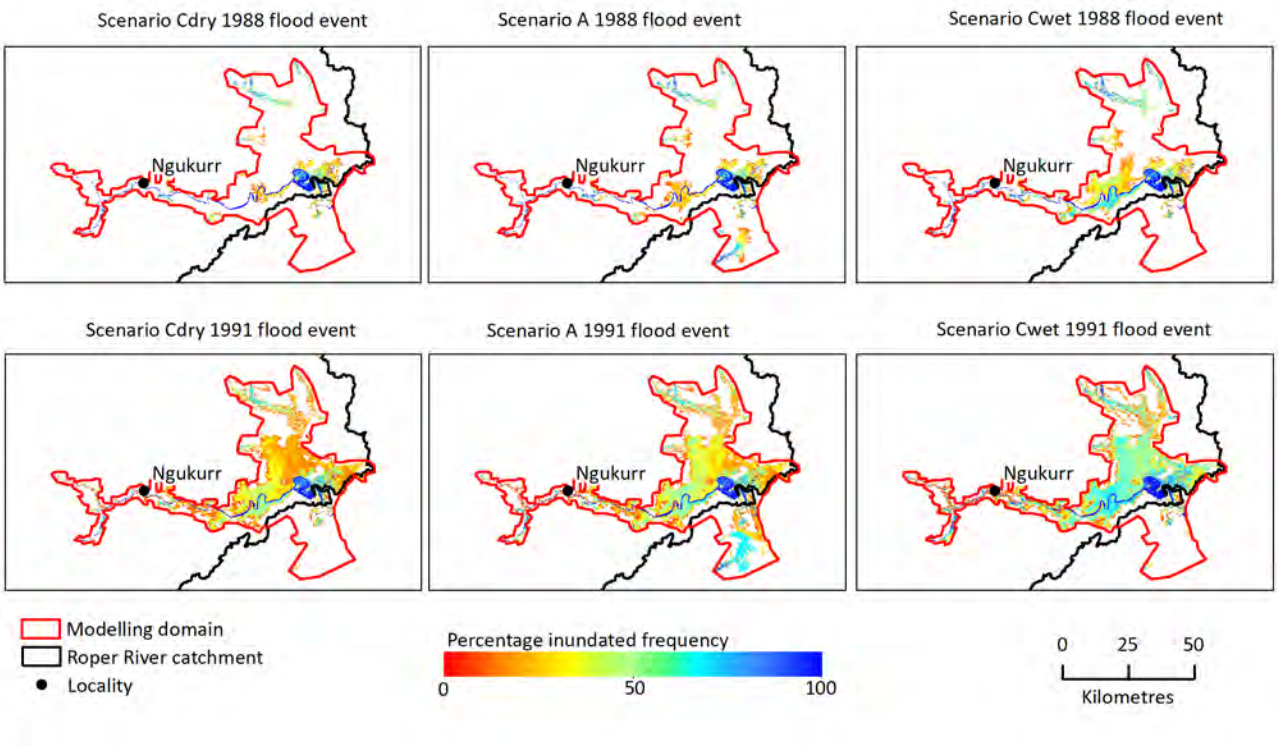

Figure 5-32 Percentage inundated frequency in the Zone 2 model domain under scenarios A and C

The 1988 flood event had an AEP of 1 in 2 and the 1991 flood event had an AEP of 1 in 13.

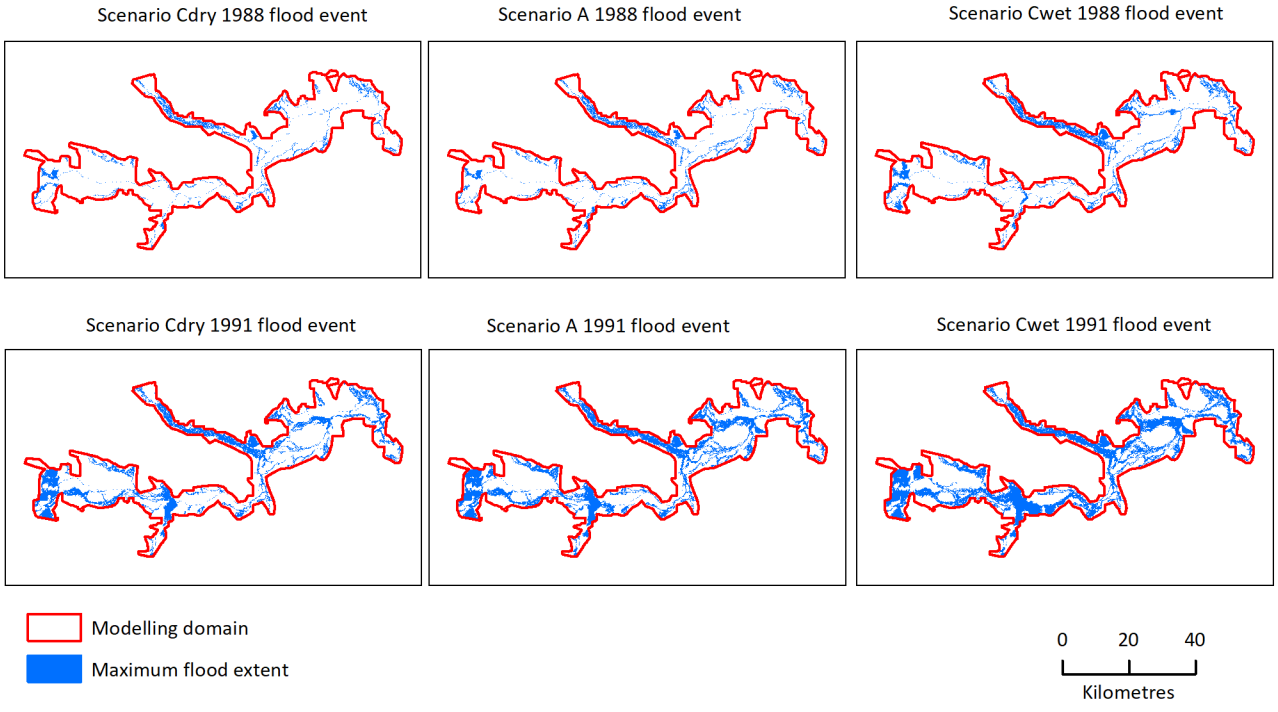

Figure 5-33 Maximum inundation extent in the Zone 1 model domain under scenarios A and C

The 1988 flood event had an AEP of 1 in 2 and the 1991 flood event had an AEP of 1 in 13.

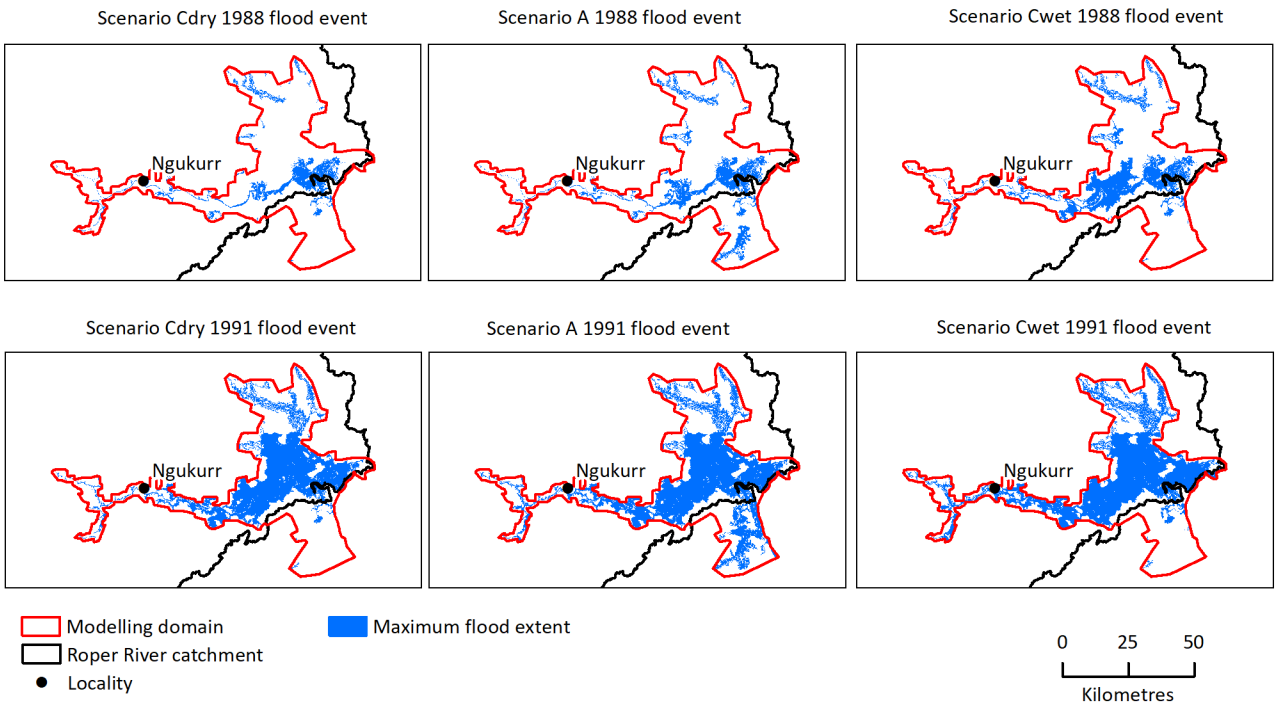

Figure 5-34 Maximum inundation extent in the Zone 2 model domain under scenarios A and C

The 1988 flood event had an AEP of 1 in 2 and the 1991 flood event had an AEP of 1 in 13.

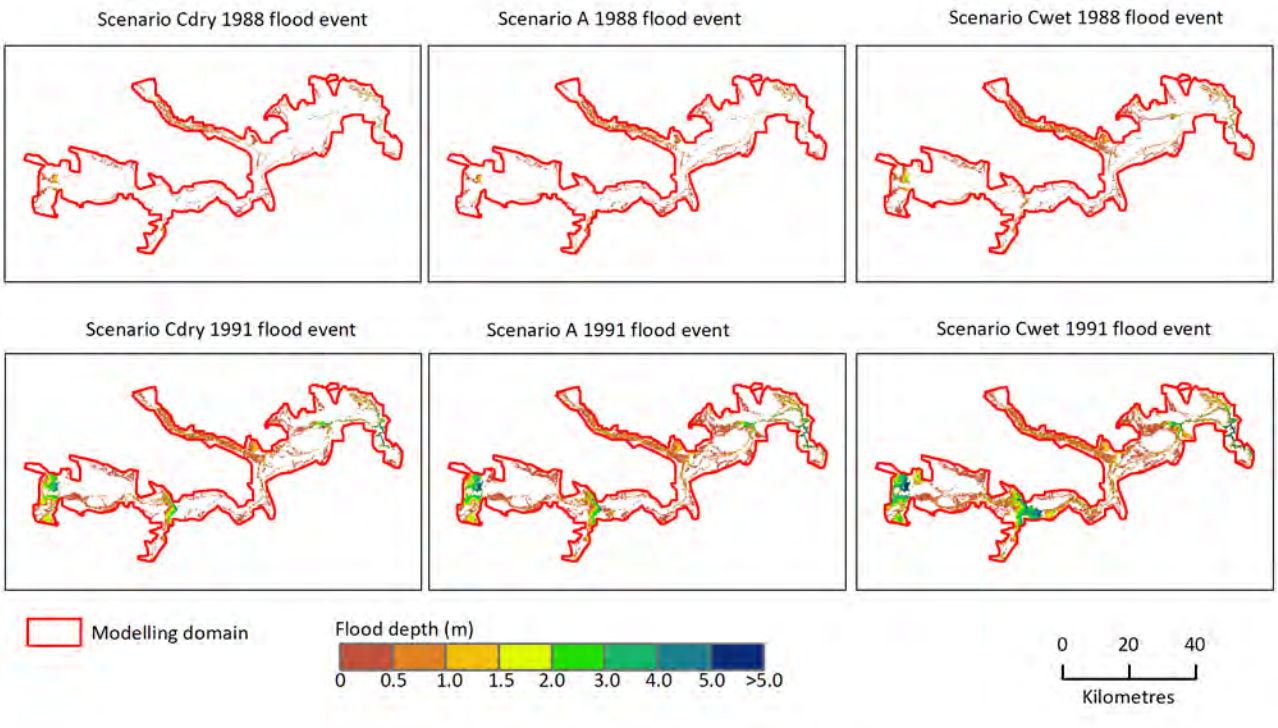

Figure 5-35 Depth at maximum inundation extent in the Zone 1 model domain under scenarios A and C

The 1988 flood event had an AEP of 1 in 2 and the 1991 flood event had an AEP of 1 in 13.

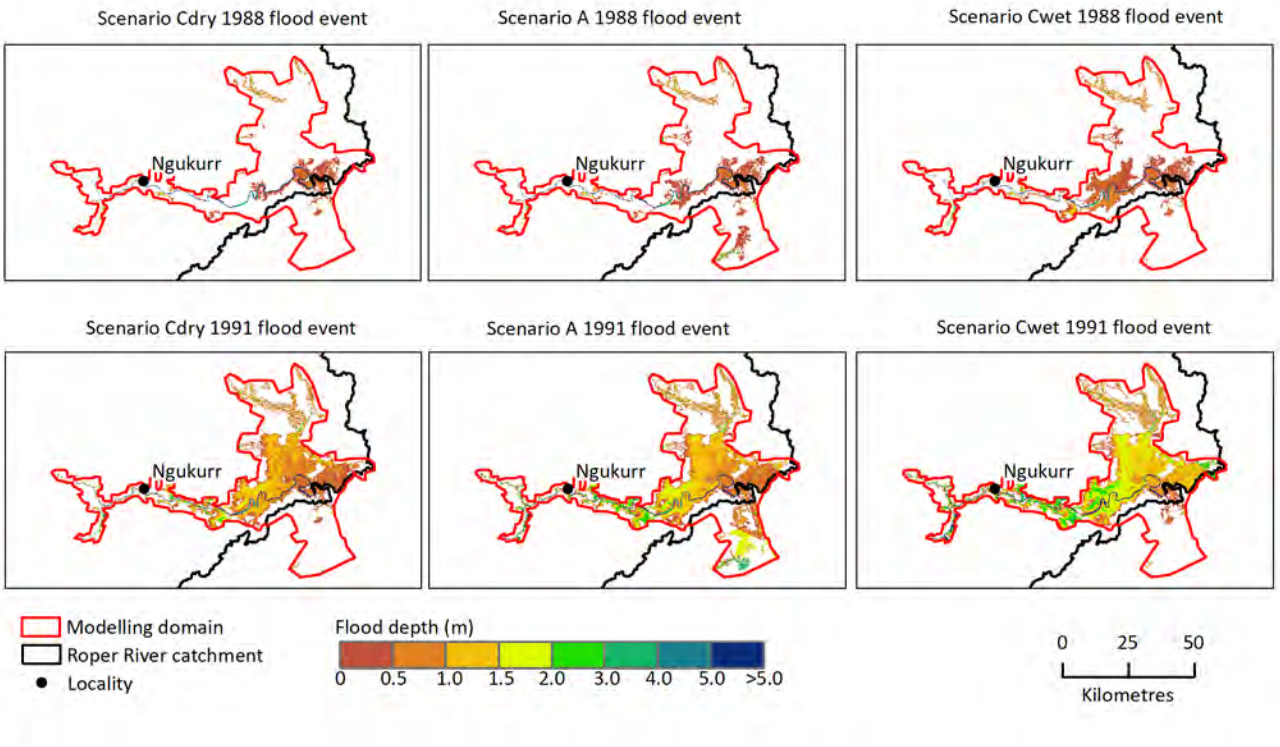

Figure 5-36 Depth at maximum inundation extent in the Zone 2 model domain under scenarios A and C

The 1988 flood event had an AEP of 1 in 2 and the 1991 flood event had an AEP of 1 in 13.

The time series in Figure 5-37 shows large differences between climate scenarios in inundated area occurred under scenarios Cdry and Cwet when compared to under Scenario A for both events. The differences are largest at times of peak inundation particularly during Scenario Cwet. This shows that the hydrodynamic models are able to simulate higher intensity flood events based on different climate inputs. As mentioned, the peak inundation areas under scenarios Cwet and Cdry are underestimated by about 140 km^2 around Towns River in Zone 2.

Under Scenario Cdry, the peak in inundated area decreased by about 25% and 22% for the 1988 and 1991 flood events, respectively. Under Scenario Cwet, the peak in inundated area increased by about 30 and 8% for each flood event, respectively. Figure 5-37 summarises inundated area under Scenario C and associated changes compared to Scenario A for the selected flood events. When adjusting for the underestimation around Towns River, inundated areas for the Scenario Cwet for Zone 2 1991 flood event (green line in lower right plot of Figure 5-37) would be higher than that for Scenario A (blue line in lower right of Figure 5-37).

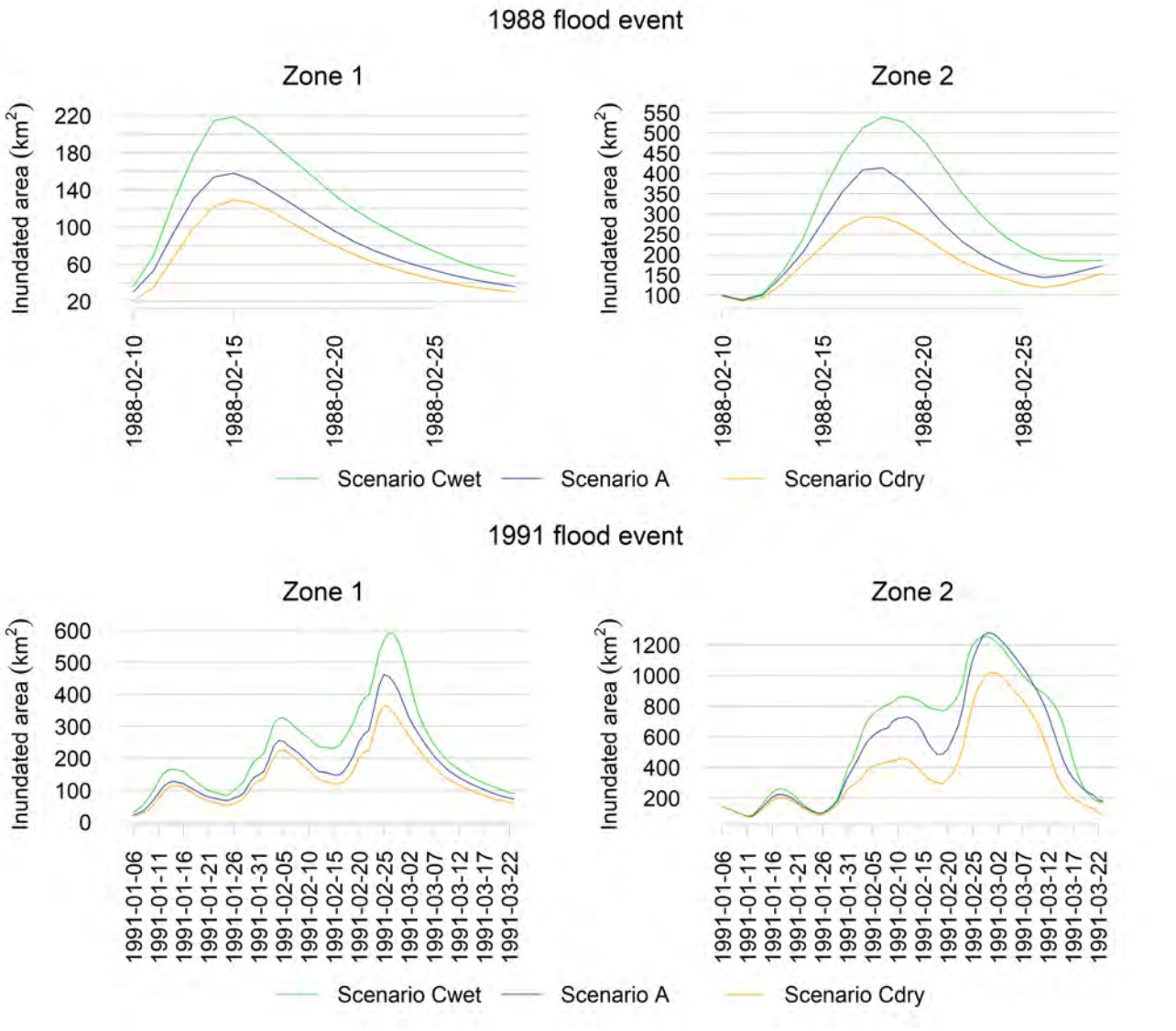

Figure 5-37 Comparison of inundated area in square kilometres (left) and mean depth in metres (right) over the Zone 1 and 2 domains under Scenario C

The 1988 flood event had an AEP of 1 in 2 and the 1991 flood event had an AEP of 1 in 13.

Table 5-2 Summary of inundated area under Scenario C and associated changes compared to Scenario A

The 1988 flood event had an AEP of 1 in 2 and the 1991 flood event had an AEP of 1 in 13.

* underestimation due to underpredictions for Towns River floodplain

	1988 FLOOD ZONE 1 Cdry	1988 FLOOD ZONE 2 Cdry	1991 FLOOD ZONE 1 Cdry	1991 FLOOD ZONE 2 Cdry	1988 FLOOD ZONE 1 Cwet	1988 FLOOD ZONE 2 Cwet	1991 FLOOD ZONE 1 Cwet	1991 FLOOD ZONE 2 Cwet
Maximum inundated area (km²)	129.2	292.1*	364.3	1019.5*	218.6	539.2*	593.0	1255.5*
% change in maximum inundated area	-18.2	-29.3*	-21.3	-20.3*	38.5	30.4*	28.2	-1.9*
Mean inundated area (km²)	70.2	176.2*	141.2	376.8*	119.7	290.8*	226.1	590.3*
% change in mean inundated area	-19.3	-21.0*	-17.3	-27.6*	37.6	30.4*	32.4	13.3*

5.4.6 SCENARIO D DRY (ALL DAMS) SIMULATIONS

Maps of percentage inundated frequency (Figure 5-38 and Figure 5-39), maximum inundation extent (Figure 5-40 and Figure 5-41) and depth at maximum inundation (Figure 5-42 and Figure 5-43) show that for both the 1988 (AEP of 1 in 2) and 1991 (AEP of 1 in 13) flood events, the dams combined with future dry climate decrease inundation (frequency, extent and depth) particularly for the 1991 event.

The impacts of the dams and future dry climate on flood characteristics over the hydrodynamic model domain are significant although the climate appears to be the main driver of the differences (Figure 5-44). The maximum inundated area under scenarios A and B (all dams) for the 1988 event is 545 km^2 and 401 km^2 respectively. This represents a decrease in inundated area of about 26%. The maximum inundated area under scenarios A and B (all dams) for the 1991 event is 1697 km^2 and 1204 km^2 respectively, representing a decrease of about 29%.

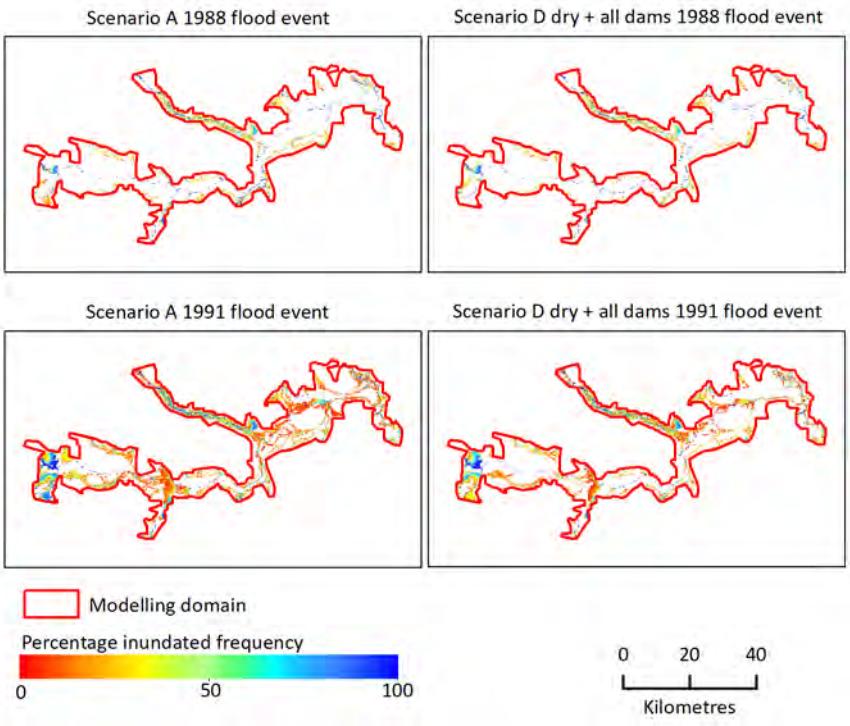

Figure 5-38 Percentage inundation frequency in the Zone 1 model domain under Scenario A (Baseline) and Ddry (all dams)

The 1988 flood event had an AEP of 1 in 2 and the 1991 flood event had an AEP of 1 in 13.

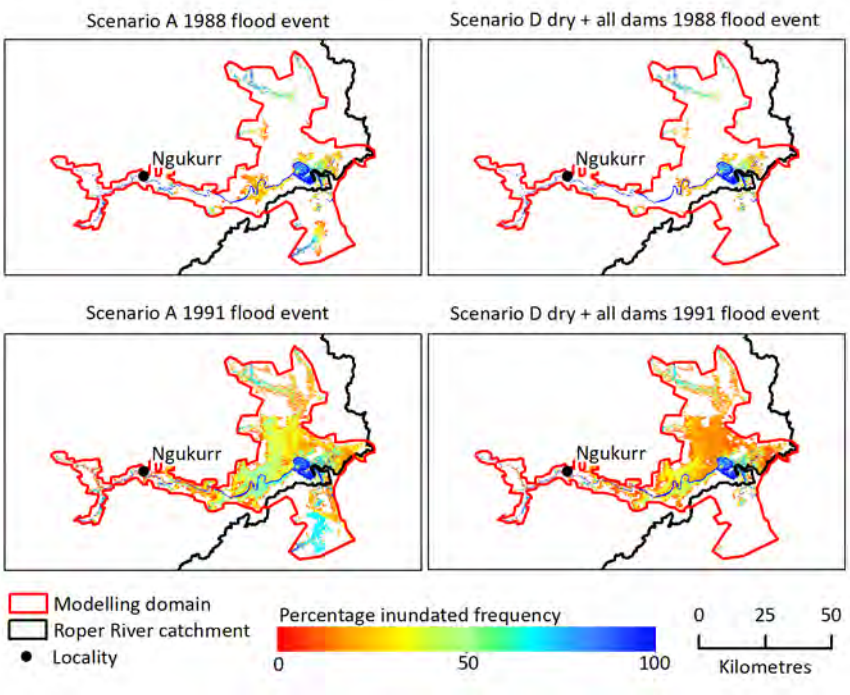

Figure 5-39 Percentage inundation frequency in the Zone 2 model domain under Scenario A (Baseline) and Ddry (all dams)

The 1988 flood event had an AEP of 1 in 2 and the 1991 flood event had an AEP of 1 in 13.

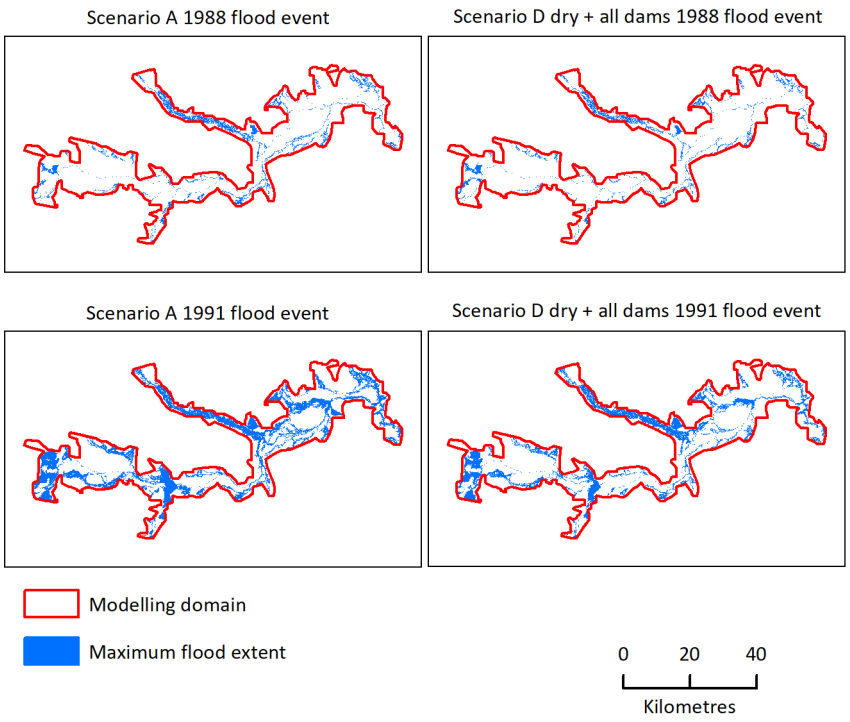

Figure 5-40 Maximum inundation extent in the Zone 1 model domain under scenarios A (Baseline) and Ddry (all dams)

The 1988 flood event had an AEP of 1 in 2 and the 1991 flood event had an AEP of 1 in 13.

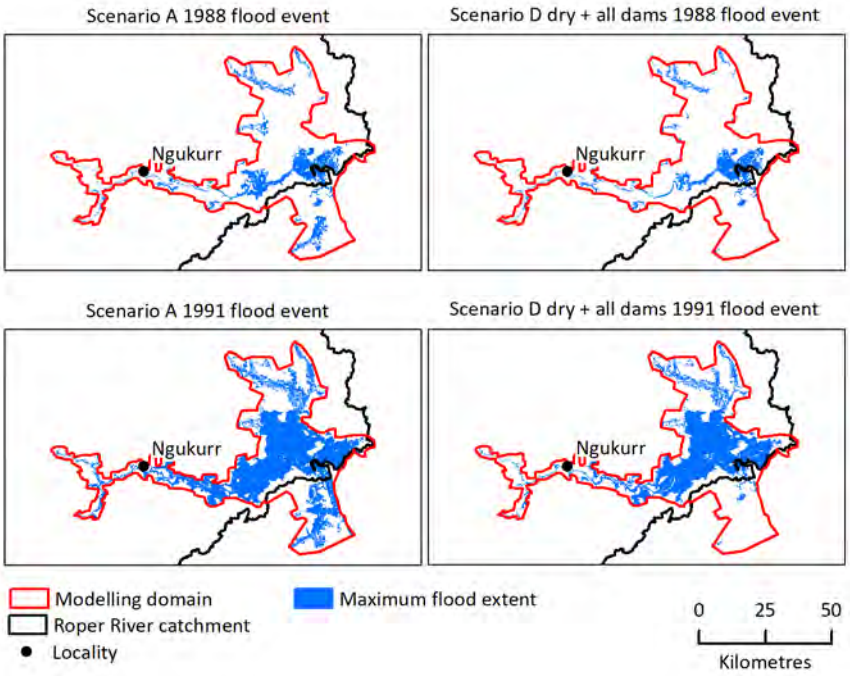

Figure 5-41 Maximum inundation extent in the Zone 2 model domain under scenarios A (Baseline) and Ddry (all dams)

The 1988 flood event had an AEP of 1 in 2 and the 1991 flood event had an AEP of 1 in 13.

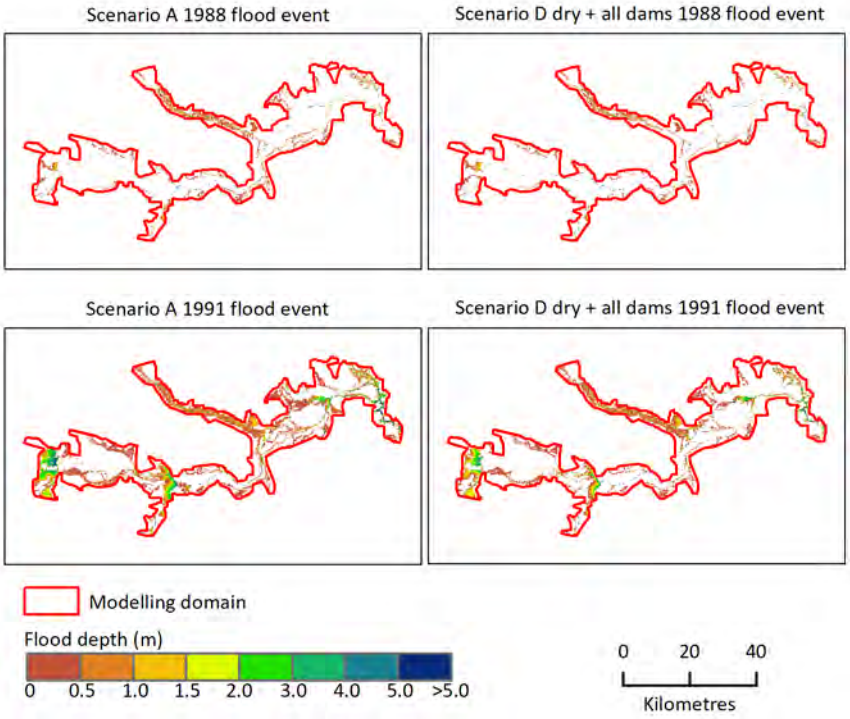

Figure 5-42 Depth at maximum inundation extent in the Zone 1 model domain under scenarios A (Baseline) and Ddry (all dams)

The 1988 flood event had an AEP of 1 in 2 and the 1991 flood event had an AEP of 1 in 13.

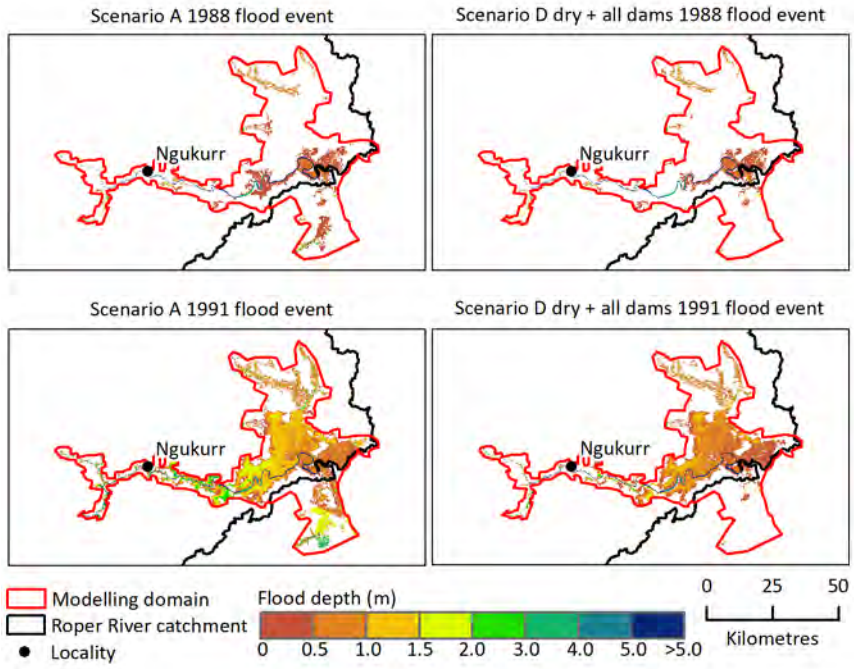

Figure 5-43 Depth at maximum inundation extent in the Zone 2 model domain under scenarios A (Baseline) and Ddry (all dams)

The 1988 flood event had an AEP of 1 in 2 and the 1991 flood event had an AEP of 1 in 13.

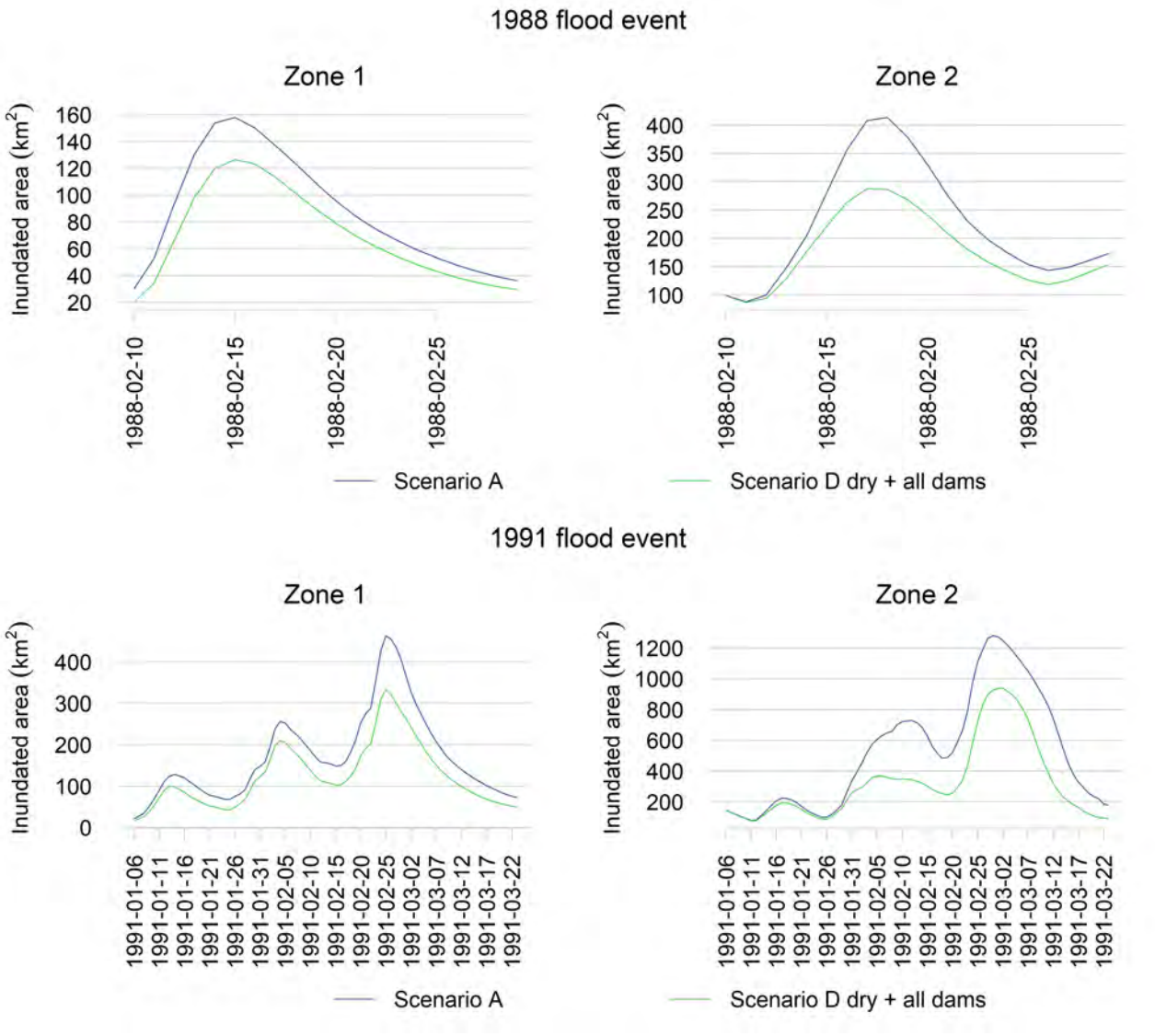

Figure 5-44 Comparison of inundated area in square kilometres over Zone 1 (left) and 2 (right) under scenarios A (Baseline) and Ddry (all dams)

The 1988 flood event had an AEP of 1 in 2 and the 1991 flood event had an AEP of 1 in 13.

5.4.7 SCENARIO D DRY (WATER HARVESTING) SIMULATIONS

Maps of percentage inundated frequency (Figure 5-45 and Figure 5-46), maximum inundation extent (Figure 5-47 and Figure 5-48) and depth at maximum inundation (Figure 5-49 and Figure 5-50) show that water harvesting under future dry climate substantially decreases inundation for the 1988 (AEP of 1 in 2) event, but there is relatively less of a decrease for the 1991 (AEP of 1 in 13) event.

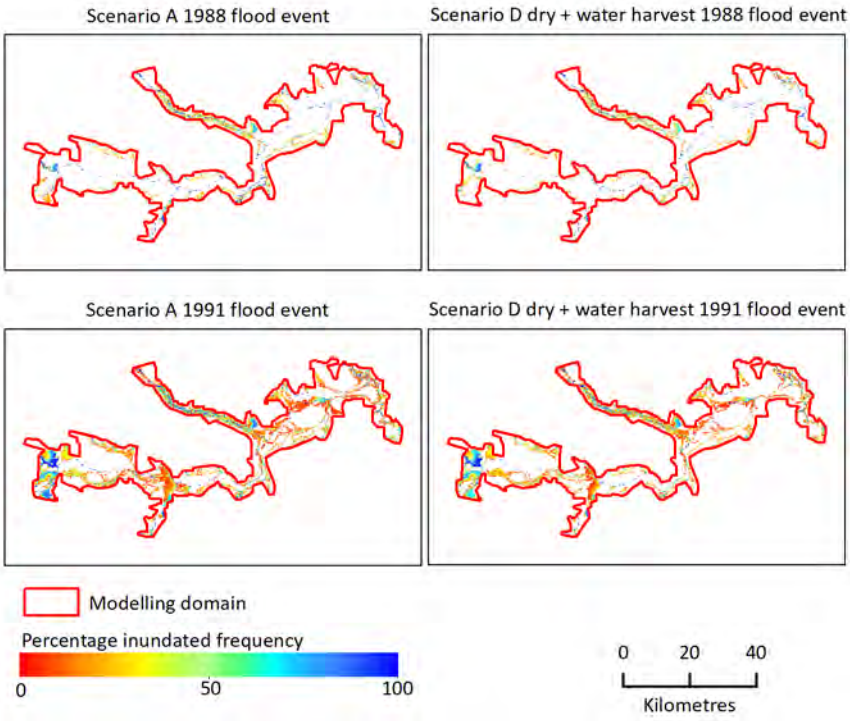

Figure 5-45 Percentage inundation frequency in the Zone 1 model domain under Scenario A (Baseline) and Ddry (water harvesting)

The 1988 flood event had an AEP of 1 in 2 and the 1991 flood event had an AEP of 1 in 13.

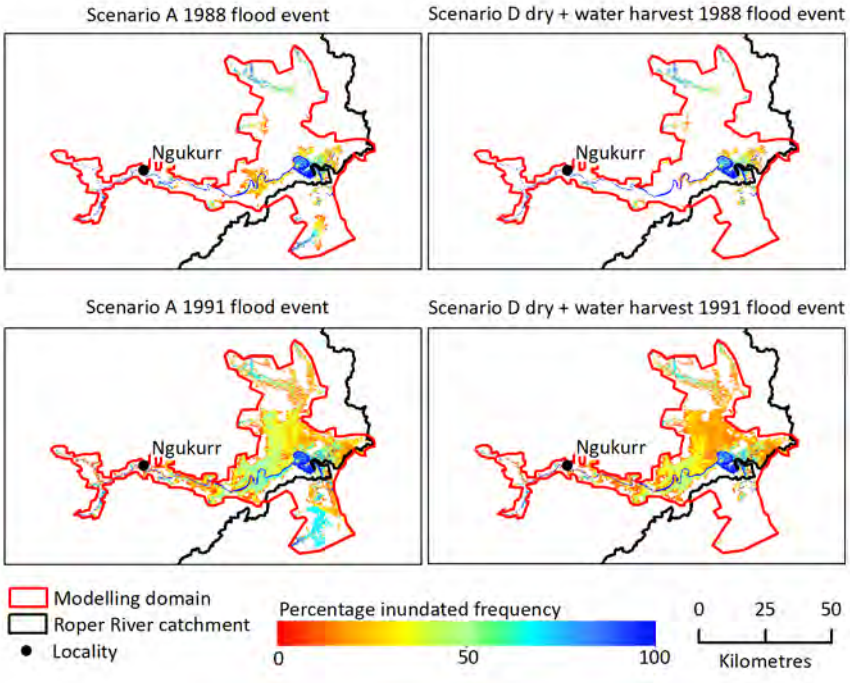

Figure 5-46 Percentage inundation frequency in the Zone 2 model domain under Scenario A (Baseline) and Ddry (water harvesting)

The 1988 flood event had an AEP of 1 in 2 and the 1991 flood event had an AEP of 1 in 13.

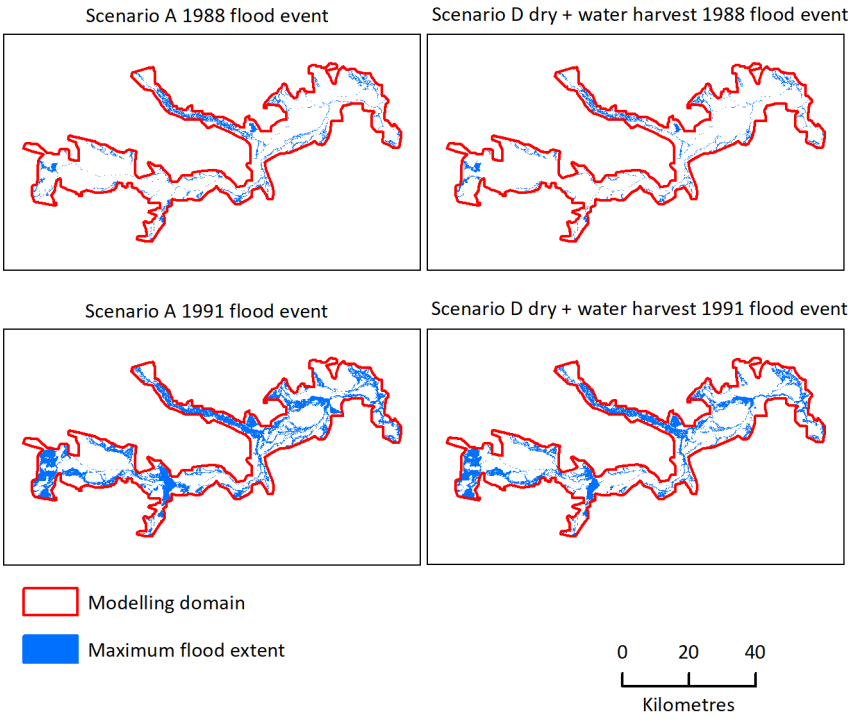

Figure 5-47 Maximum inundation extent in the Zone 1 model domain under scenarios A (Baseline) and Ddry (water harvesting)

The 1988 flood event had an AEP of 1 in 2 and the 1991 flood event had an AEP of 1 in 13.

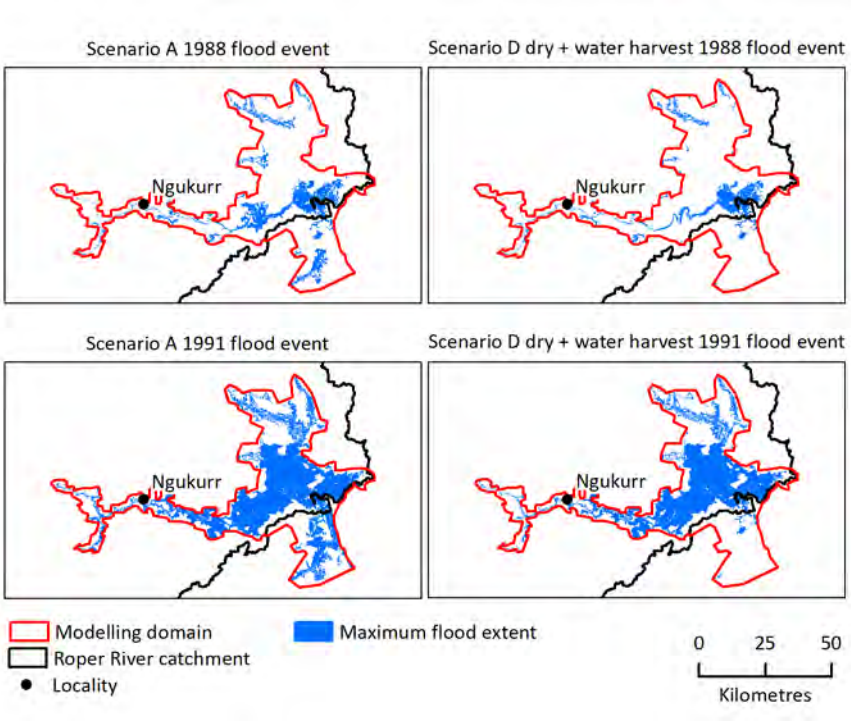

Figure 5-48 Maximum inundation extent in the Zone 2 model domain under scenarios A (Baseline) and Ddry (water harvesting)

The 1988 flood event had an AEP of 1 in 2 and the 1991 flood event had an AEP of 1 in 13.

The impacts of water harvesting under future dry climate on flood characteristics over the hydrodynamic model domain are relatively larger for the smaller event (Figure 5-51). The maximum inundated area under scenarios A and Ddry (waterharvesting) for the 1988 event is 545 km^2 and 374 km^2 respectively. This represents a decrease in inundated area of about 31%. The maximum inundated area under Scenario A for the 1991 event is 1697 km^2, and under Scenario D dry with water harvesting, it was 1330 km^2 (decrease of about 22%).

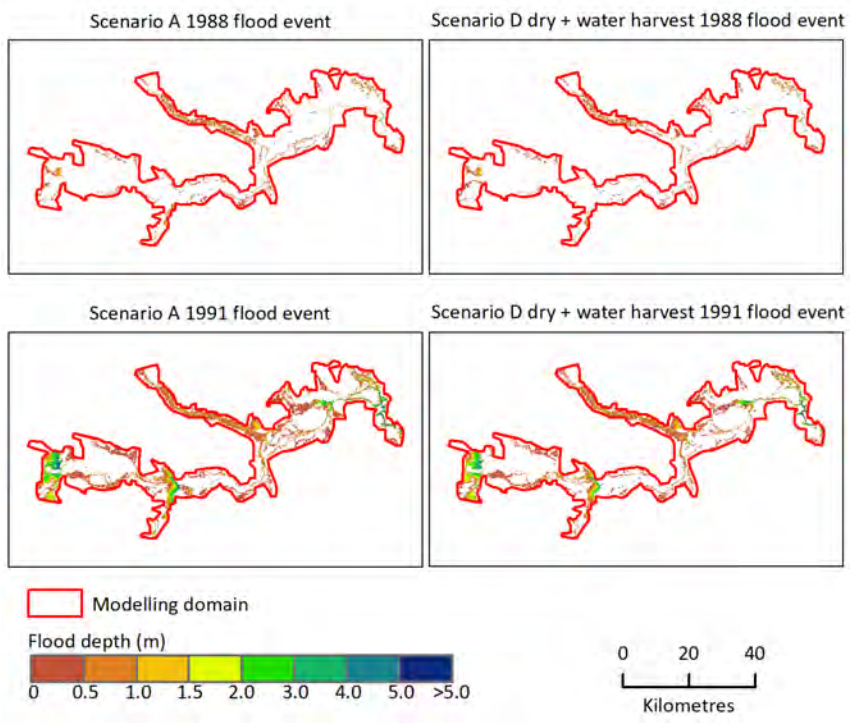

Figure 5-49 Depth at maximum inundation extent in the Zone 1 model domain under scenarios A (Baseline) and Ddry (water harvesting)

The 1988 flood event had an AEP of 1 in 2 and the 1991 flood event had an AEP of 1 in 13.

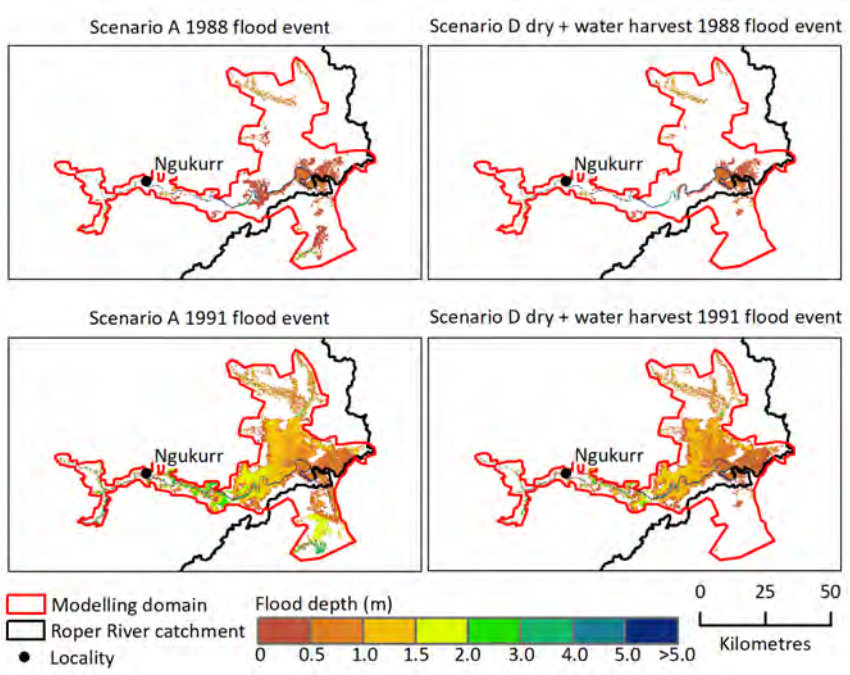

Figure 5-50 Depth at maximum inundation extent in the Zone 2 model domain under scenarios A (Baseline) and Ddry (water harvesting)

The 1988 flood event had an AEP of 1 in 2 and the 1991 flood event had an AEP of 1 in 13.

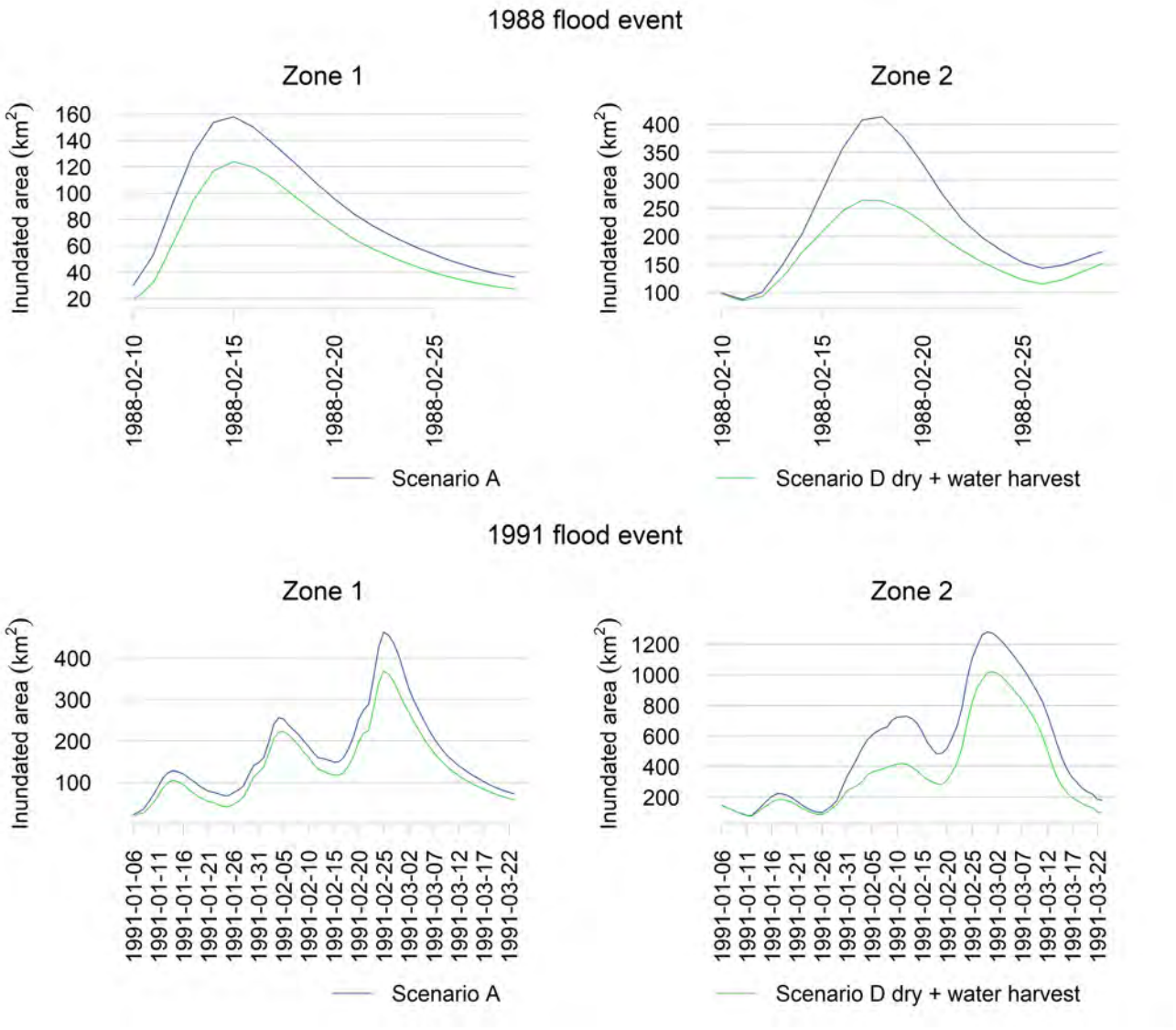

Figure 5-51 Comparison of inundated area in square kilometres over Zone 1 (left) and 2 (right) under scenarios A (Baseline) and Ddry (water harvesting)

The 1988 flood event had an AEP of 1 in 2 and the 1991 flood event had an AEP of 1 in 13.

6 Wetland connectivity assessment

6.1 Hydrological connectivity

Hydrological connectivity is defined as the water-mediated transfer of sediments, nutrients and organisms within and between water bodies (Pringle, 2003). It is a crucial determinant of ecosystem structure and functioning in freshwater habitats (Ward, 1989; Pringle, 2001; Hughes et al., 2009) and drives linkages among ecosystem elements in space and time (Fullerton et al., 2010). Habitat quality and the ecological integrity of floodplain wetlands depends on many factors, but a key determinant is how the wetland is hydrologically connected to the main river channel over time (Bunn and Arthington, 2002). In a wet tropical region, permanent flows often provide continuous instream connectivity; however, offstream wetlands may be isolated for significant periods when low flows are constrained to the main river channels. Flood pulses provide the opportunities for these offstream wetlands to be connected with the main river channels. During floods there is an exchange of water, sediments, chemicals and biota between the main channels and floodplain wetlands (Thoms, 2003). The importance of overbank flow connection for the productivity and exchanges of major aquatic biota in river–floodplain systems has been emphasised in many studies (e.g. Junk et al., 1989; Welcomme et al., 2006). The single most important factor for the persistence of the fish assemblage in an isolated wetland is the flow connection between the wetland and a river (Lasne et al., 2007). A high connectivity level is needed to conserve native fish diversity because the number of protected and native species increases with connectivity and the number of alien species and individuals can increase with isolation (Bunn and Arthington, 2002; Lasne et al., 2007).

Floodplain wetlands in the wet–dry tropics are under increasing pressure from water resource development, and there is a need for methods to assess the biophysical dynamics of these extensive and often remote ecosystems (Ward et al., 2013). These systems are characterised by strong seasonality in rainfall, with high river flows and extensive floodplain inundation occurring over an often brief wet season, followed by low to zero flows and water body contraction and isolation during the dry season (Cresswell et al., 2009; McDonald and McAlpine, 1991). The timing, extent, duration and inter-annual variability of inundation control the exchanges of water and biota between rivers and their floodplains and the degree of seasonal isolation and desiccation of water bodies determine the distribution of aquatic refugia that persist during the dry season (Junk et al., 1989). Wet–dry tropical savannas that are subject to seasonal inundation exhibit large differences in the length of the wet season and the amount of rainfall over the dry season (Warfe et al., 2011).

The river–floodplain systems in northern Australia are mostly unregulated and they support several offstream and instream wetlands of distinct ecology and environmental value (Close et al., 2012; Kennard, 2011). An important issue for the management of these wetlands under present and future climates, as well as future developments, is to know the extent, timing and duration of their connectivity within and between the waterbodies. This helps to drive ways of maintaining or even enhancing an optimal level of connection and biophysical exchanges between offstream wetlands and a river. This information is scarce for most of the Australian floodplains, since field-

based monitoring of connectivity for numerous individual wetlands is both difficult and time consuming. Several studies have used a combination of remotely sensed inundated area and concurrent river flow to predict how flooded area changes with river flow (Townsend and Walsh, 1998). The same approach has also been used to quantify how the number of inundated wetlands changes with river flow (Shaikh et al., 2001; Frazier et al., 2003). However, this approach is not dynamic and only gives information on potential wetland inundation when flow is not changing rapidly (due to the time difference between acquisition of the satellite images and the peak of inundation) and it is not possible to define the duration of wetland connectivity, which can have an important influence on wetland ecology. In the Assessment hydrodynamic modelling is used, which can quantify the time of floodplain inundation at a user-defined spatial and temporal resolution, and duration of hydrological connectivity between wetlands and rivers at a sub-daily time step.

6.2 Method of connectivity assessment

In the Assessment, connectivity of wetlands with rivers was considered through floodplain flows (i.e. overbank flooding). Connection and disconnection during overbank flooding were computed by identifying contiguous flow paths at every 6-hour time step. For this purpose, it was required to define a threshold water depth to ensure continuous water connection across minor topographic variations in the landscape. Following consideration of the low resolution of the floodplain topographic data and the high roughness of the floodplain landscape due to vegetation cover, a threshold water depth of 10 cm was used to distinguish between connected and disconnected flow paths. A wetland was considered hydrologically connected to other water bodies when it started receiving water from overbank flow and was considered disconnected when water receded below its bank level as shown in Figure 6-1.

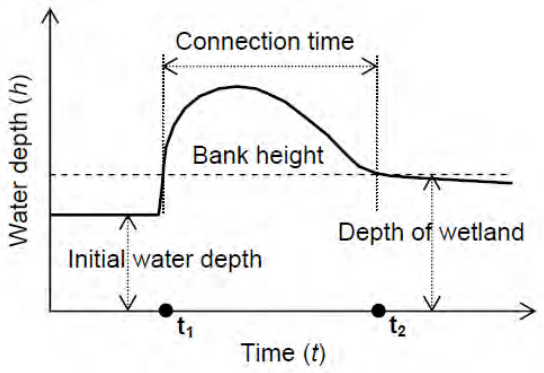

Figure 6-1 A schematic representation of wetland connectivity assessment

Connection to the flood waters and surrounding water bodies starts at time t1 and ends at t2 when the depth of inundation falls below the wetland bank height. The difference between t2 and t1 is the duration of the hydrological connection.

The connectivity analysis was undertaken in an ArcGIS 10 environment with geoprocessing scripted in Python to iterate through the flood extent raster for each 6-hour time step. The computational grid cells in the flood extent raster were classified as either a water cell or a dry cell, based on simulated water depth information. The spatial analyst 'pathdistance' function was used to calculate the least accumulative cost distance to the nearest source river line feature.

Point features representing the wetland locations were attributed with their connectivity distance for each time step with the 'extract multivalues to point' function. Points at a location which the flood extent did not reach for that time step, or did not connect with the source river network, returned a null connection for that time step. The same procedures were repeated for the entire simulation period and the results were accumulated to obtain the temporal sequence of connection and disconnection. Details of the connectivity analysis technique can be found in Karim et al. (2015).

6.3 Connectivity assessment for the Roper catchment

6.3.1 WATER ASSETS

The Roper floodplain supports several water assets including wetlands of national and international significance. The wetlands were identified using a combination of data sources. These included *A directory of important wetlands in Australia* (Environment Australia, 2001) and Google Earth imagery. Flood inundation layers of 50 days and 100 days were used to locate the wetlands. A total of 128 wetlands located within the hydrodynamic modelling domain were initially selected for connectivity assessment (Figure 6-2).

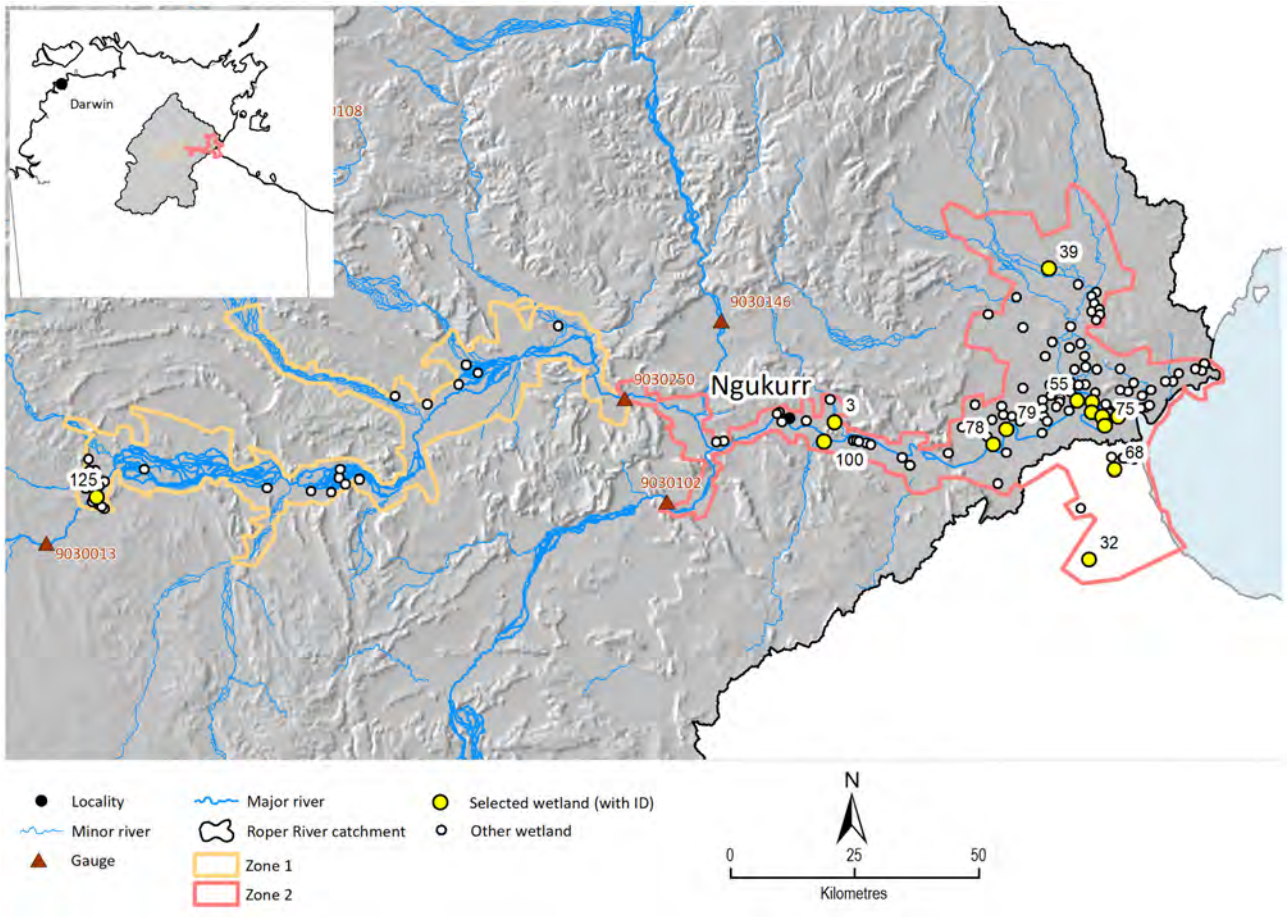

Figure 6-2 Wetlands and river network used for hydrological connectivity analysis in the Roper catchment

Given the very large number of wetlands on the Roper floodplain, initial connectivity results were investigated to select a subset of wetlands for further analysis. A total of 15 wetlands were selected based on spatial representation and inundation characteristics (Table 6-1). Refer to the companion technical report on ecology, Stratford et al. (2023), for further details on the physical and ecological characteristics of wetlands in the Roper catchment.

Table 6-1 List of selected wetlands in the Roper catchment

WETLAND ID	TYPE	LATITUDE (°)	LONGITUDE (°)
3	Walmaja	-14.738	134.815
32	Melaleuca open forest floodplain	-14.983	135.296
39	Waterbird colony	-14.458	135.217
42	Waterbird colony	-14.7	135.3
55	Mangrove	-14.697	135.272
60	Mangrove	-14.718	135.299
65	Mangrove	-14.725	135.349
68	Mangrove	-14.821	135.343
72	Mangrove	-14.726	135.319
75	Mangrove	-14.743	135.324
78	Mangrove	-14.777	135.115
79	Mangrove	-14.75	135.139
100	Waterbody	-14.773	134.796
125	Waterbody	-14.873	133.427
3	Walmaja	-14.738	134.815

6.3.2 WETLAND INUNDATION

The time series of simulated inundation depths from the hydrodynamic model, at a 24-hourly interval, were used to compute inundation duration. By analysing this information for the flooding periods, the total inundation duration at each computational grid was estimated. Figure 6-3 shows the maximum areal extent of inundation and spatial differences in inundation duration for the Roper hydrodynamic model domain for the flood event in 1991 (AEP 1 in 13). In general, duration of inundation is longer in the lower part of the floodplain. This is primarily due to the flat topography in this region compared to the upper floodplains. In addition to the Roper River, flooding along Maiwok Creek resulted in large areas of inundation along braided channels. Flooding adjacent to other rivers in the Roper catchment was limited in spatial extent. The results show some wetlands were located outside the overbank inundation zone. These wetlands, however, could be connected to the river through floodplain creeks (tributaries of the Roper River). Floodplains downstream of Ngukurr experienced more than 20 days of inundation. This was primarily due to the low relief of this area compared with Zone 1. Importantly it can be noted that inundation in Zone 1 is relatively short, typically 5 to 10 days, even during the large flood in 1991. As expected, areas close to the river experienced longer duration of inundation.

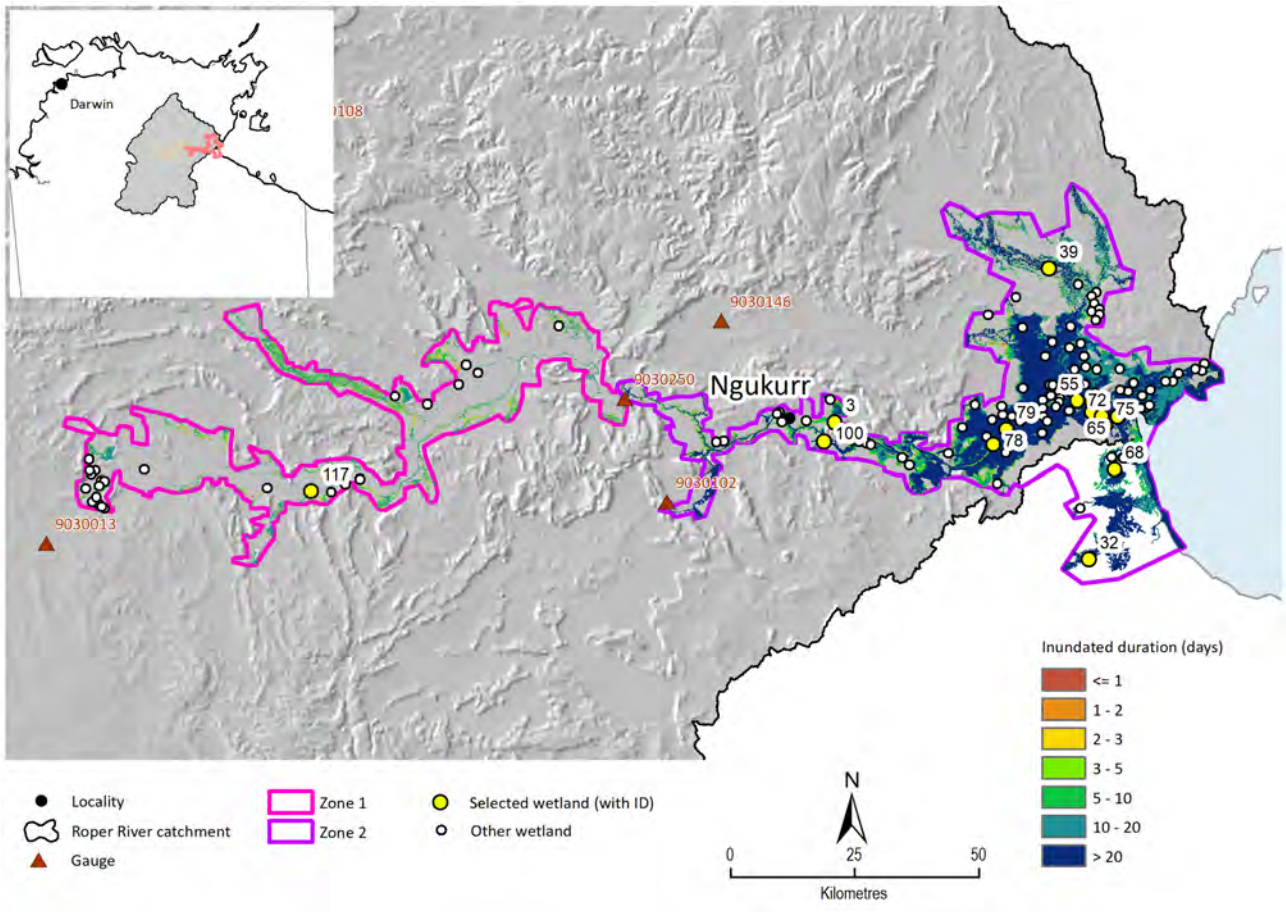

Figure 6-3 Typical example of spatial variation in inundation duration across floodplains of the Roper River for 1991 flood (AEP of 1 in 13)

6.3.3 CONNECTIVITY

Figure 6-4 shows a typical example of the timing and duration of the hydrological connection of wetlands to the major rivers in the Roper catchment during small, medium and large floods. The flood event of 2008 (AEP 1 in 5) produced the highest duration of connectivity. Large floods tend to inundate more of the floodplain, and also create longer duration of connectivity. However local variation in runoff and flood hydrographs (e.g. more than one peak) play an important role in connectivity duration. For example, the flood peak for the 1991 event is greater than that during 2008, however, the wetland connectivity is generally higher for the 2008 event. This is due to the persistence of relatively high volumes during the 2008 event compared to 1991. All wetlands were connected to the river during the 1991 (AEP of 1 in 13) and 2008 (AEP of 1 in 5) floods but one did not connect to the river during the 1988 flood (AEP of 1 in 2) and another in 2013. Some wetlands showed a pattern of connection and disconnection for all events, in particular 1991. This is due to the secondary peak in the flood hydrograph.

(a) 1988 flood

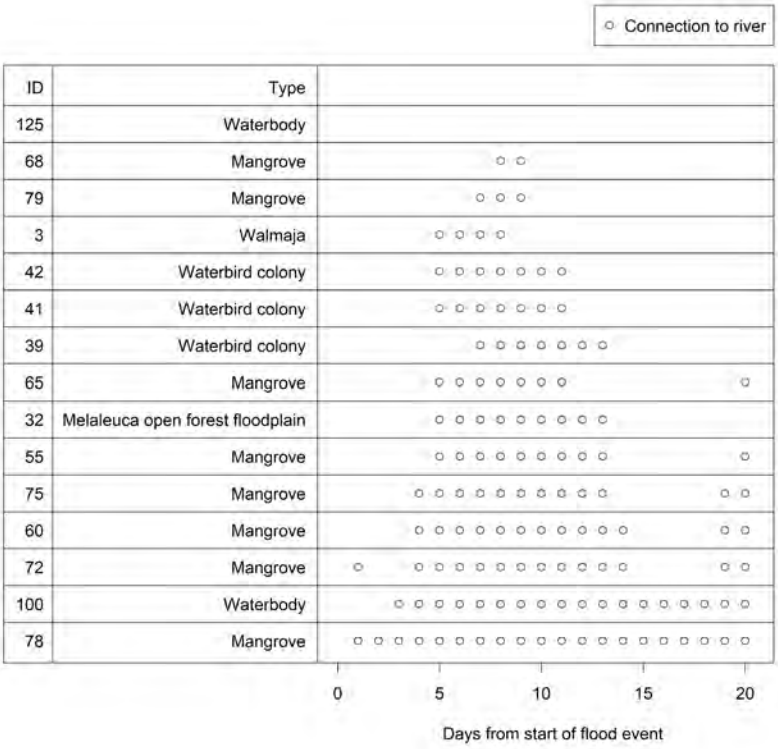

(b)

1991 flood

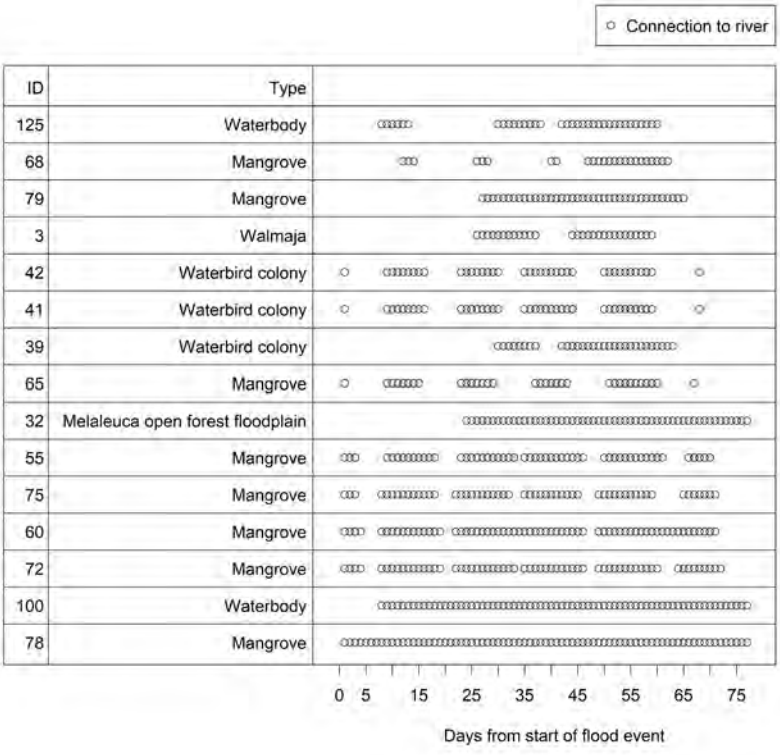

(c) 2008 flood

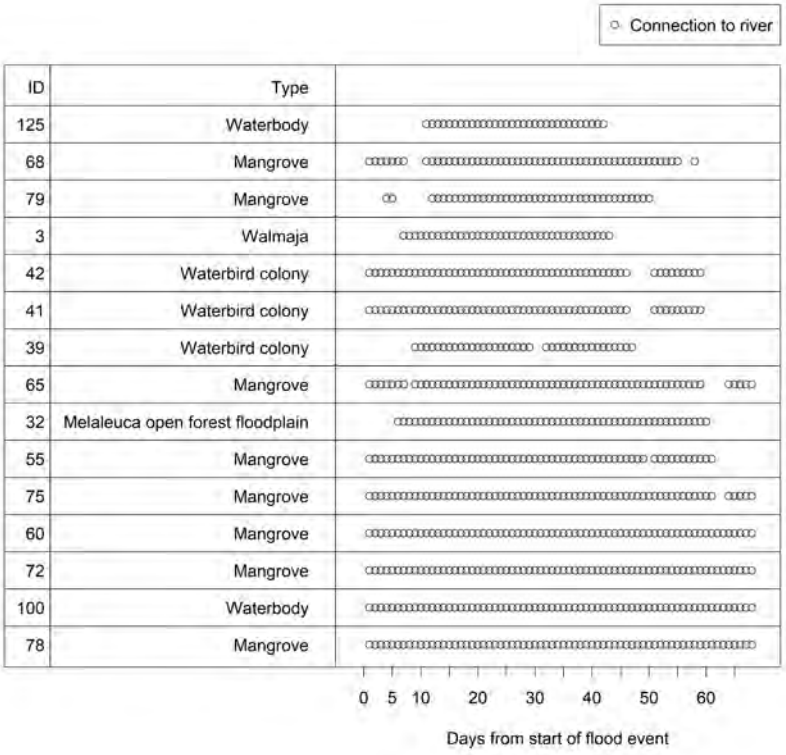

(d) 2013 flood

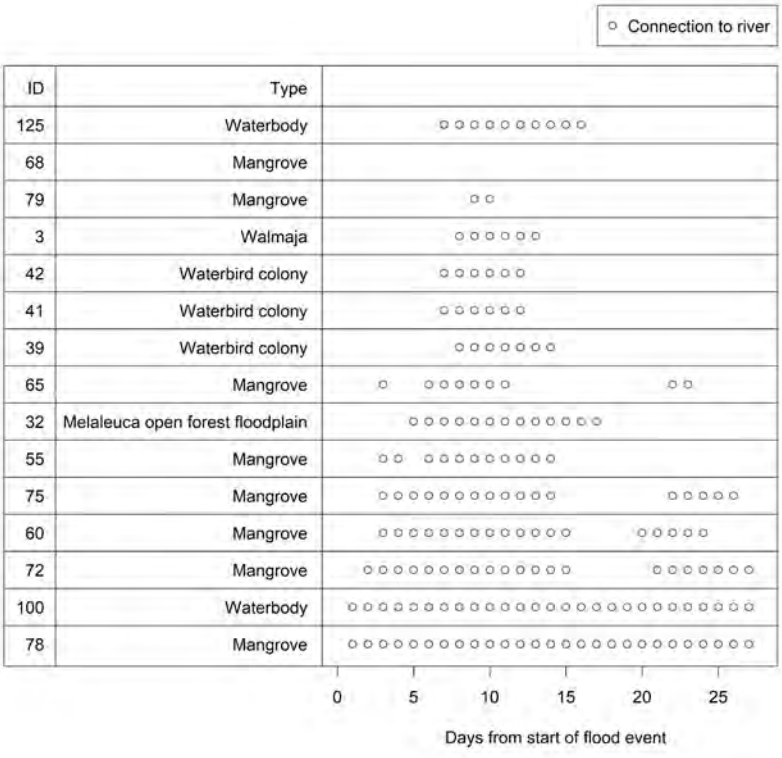

Figure 6-4 Timing and duration of connectivity of selected wetlands in the Roper catchment under Scenario A for the (a) 1988 flood (AEP of 1 in 2) (b) 1991 flood (AEP of 1 in 13) (c) 2008 flood (AEP of 1 in 5) and (d) 2013 flood (AEP 1 in 3) events

The effects of projected future climate and potential developments on hydrological connectivity were investigated. Table 6-2 presents a summary of predicted changes in connectivity for 128 wetlands in the Roper catchment under scenarios Cwet and Cdry and Scenario D for the flood events in 1988 and 1991 with annual exceedance probability (AEP) of 1 in 2, and 1 in 13 respectively. As expected, under Scenario Cwet the duration of connectivity increased and under Scenario Cdry the connectivity reduced. It is worth noting that the effect of changes in flow regimes under Scenario C is disproportionate between wetlands. For example, wetlands that are located far from rivers are more affected by changes in flow regimes compared to those that are close to rivers. The impacts to wetland connectivity under Scenario C also vary with flood magnitude. All scenario B runs saw decreases in connectivity but higher relative impacts were seen for the larger event and for climate change scenarios (Table 6-2).

Large changes in wetland connectivity were pronounced under projected future climate scenarios, particularly under Scenario Cwet. The impacts were generally more evident for the large flood (i.e. the 1991 event, AEP of 1 in 13) than the smaller flood event (i.e. the 1988 event. AEP of 1 in 2). A reduction in connectivity of approximately 28% was projected under Scenario Cdry. The changes in connectivity varies based on flood magnitude. As expected under Scenario B (all dams) the reduction in wetland connectivity (19%) was found to be higher than under scenario B (Waterhouse River dam) (9%) and B (Flying Fox Creek dam) (6%). Under Scenario B (water harvest of 660 GL) the wetland connectivity was modelled to reduce by up to 8%. The greatest reductions in wetland connectivity were found under Scenario D. Under Scenario Ddry (all dams) wetland connectivity reduced by 41% and under Scenario D (water harvesting) wetland connectivity reduced by 30%. Antecedent effects and flood timing relative to the start of the wet season are important to acknowledge here. In particular, the larger of the two events (1991) is earlier in the wet season and follows a reasonably dry period. It is likely that any dams in this situation are not full or at least have substantial free airspace. Additionally, water harvest operations are more likely to be active at the start of the wet season or following the first substantial flow of the wet season. In the late wet season water harvest licence volumes may have been already pumped, and therefore, pumping will have ceased or partly ceased.

Changes in wetland connectivity follow the same pattern as changes in maximum inundation extents for both development and future climate scenarios. However, the magnitude of the changes to wetland connectivity are particularly pronounced showing that wetland connectivity is more sensitive to changes in flow regime than maximum inundation extent.

Table 6-2 Summary of mean changes in wetland connectivity for 171 wetlands under Scenario D for the flood events of 2001 (AEP of 1 in 16), 2006 (AEP of 1 in 2) and 2009 (AEP of 1 in 5)

'+' indicates increase and '–' indicates decrease in duration of connectivity. The number in parenthesis is the change in % with respect to mean connectivity at historical climate.

FLOOD EVENT	AEP	MEAN CONNECTIVITY (DAYS)	CHANGE IN MEAN CONNECTIVITY, DAYS (%)							
			DRY CLIMATE	WET CLIMATE	ALL DAMS	WATER HARVEST	DRY WITH ALL DAMS	DRY WITH WATER HARVEST	WATER-HOUSE DAM	FLYING FOX DAM
1988	1/2	1.16	-0.03 (-2.2)	+0.55 (+47.1)	-0.02 (-2)	-0.05 (-4.7)	-0.03 (-2.2)	-0.06 (-4.7)	0 (0)	-0.02 (-1.3)
1991	1/13	17.4	-4.93 (-28.4)	+5.89 (+33.9)	-3.23 (-18.6)	-1.38 (-7.9)	-7.11 (-41)	-5.14 (-29.6)	-1.57 (-9)	-1.06 (-6.1)

6.4 Summary

Typical examples of the timing and duration of the hydrological connection of wetlands to the major rivers in the Roper catchment during small, medium and large floods showed that the flood event of 2008 (AEP 1 in 5) produced the highest duration of connectivity even though the flood peak for the 1991 event (AEP 1 in 13) is greater than that during 2008. This is due to the persistence of relatively high volumes during the 2008 event compared to 1991. The 1991 event displayed patterns of connections and disconnection due to the secondary peak in the flood hydrograph.

Large changes in wetland connectivity were pronounced under Scenario C, particularly under Scenario Cwet. Changes to wetland connectivity were generally highest for the large flood (e.g. the 1991 event, AEP of 1 in 13). As expected the changes to wetland connectivity under Scenario B (all dams) were found to be high compared to scenarios B (Waterhouse River dam) and B (Flying Fox Creek dam) highlighting the cumulative impact of multiple dams. The greatest reductions in wetland connectivity were found under Scenario D.

7 Summary

This part of the Assessment had two major components: calibration of one- and two-dimensional coupled floodplain hydrodynamic (MIKE FLOOD) models; followed by scenario modelling under projected future climates (Cdry and Cwet) and hypothetical developments (dams and water harvesting). The outputs from the hydrodynamic modelling were used to:

- identify areas susceptible to flooding under historical climate and current development
- estimate changes in inundation across the floodplains under projected future climate and hypothetical development scenarios
- quantify hydrological connectivity of floodplain wetlands in terms of extent, timing and duration of connection of offstream wetlands to main river channels
- quantify changes in hydrological connectivity due to changed flow regimes.

Observed daily discharge and stage height data were obtained from Northern Territory Government. A MIKE FLOOD model was configured for each study area (Zone 1 and Zone 2) and observed tidal data, Sacramento rainfall-runoff simulations and discharge data from AWRA-R simulations were used as input at the model boundaries. Flood inundation maps for individual flood events were produced using high-quality MODIS and Landsat imagery. Composite flood maps were also produced by combining all images to delineate maximum flooding extent. These were used to calibrate hydrodynamic models for each zone. A calibrated hydrodynamic model was used to simulate the impacts of future climate and developments on floodplain inundation and hydrological connectivity of wetlands.

The hydrodynamic model was calibrated for the 1988, 1991, 2008 and 2013 flood events using inundation maps derived from MODIS and Landsat imagery. The models were calibrated primarily by adjusting the infiltration rate. While a good match was attained for the flood peaks, there were differences in rising and falling limbs of the flood hydrograph. In general, model predictions were found to be better for large floods.

Compared to the Landsat and MODIS inundation maps, the hydrodynamic model captured overall inundation patterns. This includes the coastal flat areas and ephemeral waterways that become active during flood events.

Future climate scenario modelling showed marked changes in inundation areas in the Roper River floodplain compared Scenario A, with the major differences observed under scenarios Cdry and Cwet. For example, maximum inundation extents increased by 39 and 28% for the 1988 (AEP of 1 in 2) and 1991 (AEP of 1 in 13) events, respectively, for Zone 1 under Scenario Cwet. For the same zone but under Scenario Cdry, maximum inundation extents decreased by 18 and 21% for the 1988 and 1991 events, respectively.

The reduction in modelled maximum inundation extent under Scenario B was small relative to the reduction in Scenario Cdry. Under Scenario B (all dams) the reduction in maximum inundation extent was up to 7% for the 1991 event (AEP of 1 in 13). Reductions in maximum inundation extent under scenarios B (Waterhouse River dam) and B (Flying Fox Creek dam) were 2 and 1%

respectively, for the 1991 event (AEP of 1 in 13). Under Scenario B (water harvesting of 660 GL) the reduction in maximum inundation extent for the 1988 (AEP of 1 in 2) event was 11%. The development scenario modelling demonstrated that these reductions in maximum inundation extent are largely dependent on the timing of the events, i.e. dam volumes and thus their capturing capacities varies depending on the time of the wet season and how dry the catchment has been in years prior.

Under Scenario C large changes in wetland connectivity relative to Scenario A were observed. Increases in wetland connectivity (up to 47%) under Scenario Cwet were greater than the decrease (up to 28%) in connectivity under Scenario Cdry. This pattern is consistent with the changes in maximum inundation area, however wetland connectivity is shown to be more sensitive to changes to flow regime than maximum inundation extent. It is worth noting that the effect of changes in flow regimes under Scenario C is disproportionate between wetlands, with more impacts on wetlands that are located far from rivers. The impacts of future climate also vary with flood magnitude.

8 References

Arcement GJ and Schneider VR (1989) Guide for selecting Manning's roughness coefficients for natural channels and floodplain. Water Supply Paper 2339, US Geological Survey, Colorado.

Arthington AH, Godfrey PC, Pearson RG, Karim F and Wallace J (2014) Biodiversity values of remnant freshwater floodplain lagoons in agricultural catchments: evidence for fish of the Wet Tropics bioregion, northern Australia. Aquatic Conservation: Marine and Freshwater Ecosystems 25(3), 336–352.

Bayley PB (1991) The flood pulse advantage and the restoration of river-floodplain systems. Regulated Rivers: Research and Management 6, 75–86.

Bayley PB (1995) Understanding large river-floodplain ecosystems. BioScience 45, 153–158.

Beighley RE, Eggert K, Dunne T, He Y and Gummadi V (2009) Simulating hydrologic and hydraulic processes throughout the Amazon River Basin. Hydrological Processes 23(8), 1221–1235.

Bunn SE and Arthington AH (2002) Basic principles and ecological consequences of altered flow regimes for aquatic biodiversity. Environmental Management 30, 492–507.

Bunn SE, Thoms MC, Hamilton SK and Capon SJ (2006) Flow variability in dryland rivers: boom, bust and the bits in between. River Research and Applications 22, 179–186.

Charles S, Petheram C, Berthet A, Browning G, Hodgson G, Wheeler M, Yang A, Gallant S, Marshall A, Hendon H, Kuleshov Y, Dowdy A, Reid P, Read A, Feikema P, Hapuarachchi P, Smith T, Gregory P and Shi L (2016) Climate data and their characterisation for hydrological and agricultural scenario modelling across the Fitzroy, Darwin and Mitchell catchments. A technical report from the CSIRO Northern Australia Water Resource Assessment to the Government of Australia. CSIRO, Australia.

Chiew FHS, Teng J, Vaze J, Post DA, Perraud JM, Kirono DGC and Viney NR (2009) Estimating climate change impact on runoff across southeast Australia: method, results, and implications of the modeling method. Water Resources Research 45(10), W10414. DOI: 10.1029/2008WR007338.

Chormanski J, Swiatek DM and Michalowski R (2009) A hydrodynamic model coupled with GIS for flood characteristics analysis in the Biebrza riparian wetland. Oceanological and Hydrobiological Studies 38, 65–73.

Chow VT (1959) Open channel hydraulics. McGraw-Hill International Edition, Singapore.

Close P, Wallace J, Bayliss P, Bartolo R, Burrows D and Pusey B (2012) Assessment of the likely impacts of development and climate change on aquatic ecological assets in Northern Australia. A report for the National Water Commission, Australia. Charles Darwin University.

Connell Wagner Pty Ltd (2001) Flood investigation of the communities of Beswick, Mataranka, Djilkminggan and Elsey – study report. Department of Lands, Planning and Environment.

Cresswell R, Petheram C, Harrington G, Buettikofer H, Hodgen M and Davies PM (2009) Chapter 1: Water resources in northern Australia. In: Stone P (ed) Northern Australia Land and Water Science Review. Final Report to the Northern Australia Land and Water Taskforce. Canberra, Australia.

CSIRO (2009a) Water in the Timor Sea Drainage Division. A report to the Australian Government from the CSIRO Northern Australia Sustainable Yields Project. CSIRO Water for a Healthy Country Flagship, Australia.

CSIRO (2009b) Water in the Mitchell catchment. In: CSIRO (2009) Water in the Gulf of Carpentaria Drainage Division. A report to the Australian Government from the CSIRO Northern Australia Sustainable Yields Project. CSIRO Water for a Healthy Country Flagship, Australia.

CSIRO (2009c) Water in the Van Diemen region. In: CSIRO (2009) Water in the Timor Sea Drainage Division. A report to the Australian Government from the CSIRO Northern Australia Sustainable Yields Project. CSIRO Water for a Healthy Country Flagship, Australia.

DHI (2012) MIKE21 flow model, Hydrodynamic Module, scientific documentation. DHI Water and Environment Pty Ltd, Horsholm, Denmark.

DHI (2016) MIKE21 flow model FM, Hydrodynamic Module, user guide. DHI Water and Environment Pty Ltd, Horsholm, Denmark.

DHI (2021) MIKE 11 A modelling System for Rivers and Channels, reference manual. DHI Water and Environment Pty Ltd, Horsholm, Denmark.

Dhu T, Dunn B, Lewis B, Lymburner L, Mueller N, Telfer E, Lewis A, McIntyre A, Minchin S and Phillips C (2017) Digital earth Australia – unlocking new value from earth observation data. Big Earth Data 1:1-2: 64–74.

Doble RC, Crosbie RS, Smerdon BD, Peeters L and Cook FJ (2012) Groundwater recharge from overbank floods. Water Resource Research 48, W09522.

Ebert EE, Janowiak JE and Kidd C (2007) Comparison of near-real-time precipitation estimates from satellite observations and numerical models. Bulletin of the American Meteorological Society 88, 1–47.

Ebert EE (2009) Methods for verifying spatial forecasts. 4th International Verification Methods Workshop, Helsinki, 4–6 June 2009.

Environment Australia (2001) A directory of important wetlands in Australia, third edition. Environment Australia, Canberra.

Faulks JJ (2001) Roper River catchment: an assessment of the physical and ecological condition of the Roper River and its major tributaries. Department of Lands, Planning and Environment, Northern Territory.

Frazier P, Page K, Louis J, Briggs S and Robertson A (2003) Relating wetland inundation to river flow using Landsat TM data. International Journal of Remote Sensing 24, 1–16.

Fullerton AH, Burnett KM, Steel EA, Flitcroft RL, Pess GR, Feist BE, Torgersen CE, Miller DJ and Sanderson BL (2010) Hydrological connectivity for riverine fish: measurement challenges and research opportunities. Freshwater Biology 55, 2215–2237.

Gallant JC, Dowling TI, Read AM, Wilson N, Tickle PK and Inskeep C (2011) 1 second SRTM-derived digital elevation models version 1.0. Geoscience Australia, Canberra.

Gallardo B, Gascon S, Gonzalez-Sanchis M, Cabezas A and Comın FA (2009) Modelling the response of floodplain aquatic assemblages across the lateral hydrological connectivity gradient. Marine and Freshwater Research 60, 924–935.

Ganf GG, White SD and Oliver RL (2010) Allocating water to the wetlands of the Murray Valley to maximise aquatic plant species diversity. In: Saintilan N and Overton IC (eds) Ecosystem response modelling in the Murray–Darling Basin. CSIRO Publishing, Canberra, Australia.

Geoscience Australia (2011) The national dynamic land cover dataset. Geoscience Australia Record 2011/31, Canberra.

Guerschman JP, Warren G, Byrne G, Lymburner L, Mueller N and Van-Dijk A (2011) MODIS-based standing water detection for flood and large reservoir mapping: algorithm development and applications for the Australian continent. CSIRO Water for a Healthy Country National Research Flagship Report, Canberra.

Guinot V (2003) Godunov-type schemes: an introduction for engineers. Elsevier.

Heiler G, Hein T, Schiemer F and Bornette G (1995) Hydrological connectivity and flood pulses as the central aspects for the integrity of a river-floodplain system. Regulated Rivers: Research and Management 11, 351–361.

Hess LL, Melack JM, Novo EM, Barbosa C and Gastil M (2003) Dual-season mapping of wetland inundation and vegetation for the central Amazon basin. Remote Sensing of Environment 87, 404–428.

Horritt MS and Bates PD (2002) Evaluation of 1D and 2D numerical models for predicting river flood inundation. Journal of Hydrology 268, 87–99.

Hughes JM, Schmidt DJ and Finn DS (2009) Genes in streams: using DNA to understand the movement of freshwater fauna and their riverine habitat. BioScience 59, 573–585.

Hughes JD, Yang A, Marvanek S, Wang B, Petheram C and Philip S (2023) River model calibration and scenario analysis for the Roper catchment. A technical report from the CSIRO Roper River Water Resource Assessment to the Government of Australia. CSIRO, Australia.

Jeffrey SJ, Carter JO, Moodie KB and Beswick AR (2001) Using spatial interpolation to construct a comprehensive archive of Australian climate data. Environmental Modelling and Software 16/4, 309–330. DOI: 10.1016/S1364-8152(01)00008-1.

Junk WJ, Bayley PB and Sparks RE (1989) The flood pulse concept in river-floodplain systems. Canadian Special Publication of Fisheries and Aquatic Sciences 106, 110–127.

Karim F, Petheram C, Marvanek S, Ticehurst C, Wallace J and Gouweleeuw B (2011) The use of hydrodynamic modelling and remote sensing to estimate floodplain inundation and flood discharge in a large tropical catchment. In: Chan F, Marinova D and Andersson RS (eds) MODSIM 2011. Modelling and Simulation Society of Australia and New Zealand, 3796–3802.

Karim F, Kinsey-Henderson A, Wallace J, Arthington A and Pearson R (2012) Modelling wetland connectivity during overbank flooding in a tropical floodplain in north Queensland, Australia. Hydrological Processes 26(18), 2710–2723.

Karim F, Dutta D, Marvanek S, Petheram C, Ticehurst C, Lerat J, Shaun K and Ang Y (2015) Assessing the impacts of climate change and dams on floodplain inundation and wetland connectivity in the Australian wet-dry tropics of northern Australia. Journal of Hydrology 522, 80–94.

Kennard MJ (2011) Priorities for identification and sustainable management of high conservation value aquatic ecosystems in northern Australia. In: TRaCK Final Report. Department of Sustainability, Environment, Water, Population and Communities, Darwin.

Knapton A (2009) Gulf water study: an integrated surface – groundwater model of the Roper River catchment, Northern Territory. E-Publications Collection. https://hdl.handle.net/10070/580682.

Kvocka D, Falconer RA and Bray M (2015) Appropriate model use for predicting elevations and inundation extent for extreme flood events. Natural Hazards 79, 1791–1808.

Lasne E, Lek S and Laffaillea P (2007) Patterns in fish assemblages in the Loire floodplain: the role of hydrological connectivity and implications for conservation. Biological Conservation 139, 258–268.

LWA (2009) An Australian handbook of stream roughness coefficients. Land and Water Australia, Canberra.

McDonald NS and McAlpine JM (1991) Floods and droughts: the northern climate. In: Haynes CD, Ridpath MG and Williams MAJ (eds) Monsoonal Australia – landscape, ecology and man in the Northern Lowland. Blakema Publishers, Rotterdam.

McJannet D, Yang A and Seo L (2023) Climate data characterisation for hydrological and agricultural scenario modelling across the Victoria, Roper and Southern Gulf catchments. A technical report from the CSIRO Victoria, Roper and Southern Gulf Water Resource Assessments for the National Water Grid. CSIRO, Australia.

Middleton BA (2002) The flood pulse concept in wetland restoration. In: Middleton BA (ed) Flood pulsing in wetlands: restoring the natural hydrological balance. John Wiley and Sons, New York.

Neal J, Villanueva I, Wright N, Willis T, Fewtrell T and Bates P (2012) How much physical complexity is needed to model flood inundation? Hydrological Processes 26, 2264–2282.

Neelz S and Pender G (2013) Benchmarking the latest generation of 2D hydraulic modelling packages. Report –SC120002. Environment Agency, United Kingdom, Bristol.

Nicholas AP and Mitchell CA (2003) Numerical simulation of overbank processes in topographically complex floodplain environments. Hydrological Processes, 17, 727–746.

Ogden, R and Thoms M (2002) The importance of inundation to floodplain soil fertility in a large semi-arid river. International Society of Limnology Proceedings 28(2), 1922–2010.

Opperman JJ, Luster R, McKenney BA, Roberts M and Meadows AW (2010) Ecologically functional floodplains: connectivity, flow regime, and scale. Journal of the American Water Resources Association 46(2), 211–226.

Overton IC (2005) Modelling floodplain inundation on a regulated river: integrating GIS, remote sensing and hydrological models. River Research and Applications 21, 991–1001.

Peake P, Fitzsimons J, Frood D, Mitchell M, Withers N, White M and Webster R (2011) A new approach to determining environmental flow requirements: sustaining the natural values of floodplains of the southern Murray–Darling Basin. Ecological Management and Restoration 12, 128–137.

Petheram C, Rustomji P, McVicar TR, Cai W, Chiew FHS, Vleeshouwer J, Van Niel TG, Li L, Cresswell RG, Donohue RJ, Teng J and Perraud J-M (2012) Estimating the impact of projected climate change on runoff across the tropical savannas and semiarid rangelands of Northern Australia. Journal of Hydrometeorology 13(2), 483–503.

Petheram C and Yang A (2013a) Climate data and their characterisation for hydrological and agricultural scenario modelling across the Flinders and Gilbert catchments. A technical report to the Australian Government from the CSIRO Flinders and Gilbert Agricultural Resource Assessment, part of the North Queensland Irrigated Agriculture Strategy. CSIRO Water for a Healthy Country and Sustainable Agriculture flagships, Australia.

Petheram C, Rogers L, Eades G, Marvanek S, Gallant J, Read A, Sherman B, Yang A, Waltham N, McIntyre-Tamwoy S, Burrows D, Kim S, Tomkins K, Poulton P, Bird M, Atkinson F, Gallant S and Lerat J (2013b) Assessment of water storage options in the Flinders and Gilbert catchments. A technical report to the Australian Government from the CSIRO Flinders and Gilbert Agricultural Resource Assessment, part of the North Queensland Irrigated Agriculture Strategy. CSIRO Water for a Healthy Country and Sustainable Agriculture flagships, Australia.

Petheram C, Yang A, Seo L, Rogers L, Baynes F, Marvanek S, Hughes J, Ponce Reyes R, Wilson P, Stratford D, Philip S (2022) Assessment of surface water storage options and reticulation infrastructure in the Roper River catchment. A report from the CSIRO Roper River Water Resource Assessment to the Government of Australia. CSIRO, Australia.

Phelps QE, Tripp SJ, Herzog DP and Garvey JE (2015) Temporary connectivity: the relative benefits of large river floodplain inundation in the lower Mississippi River. Restoration Ecology 23, 53–56.

Pollino CA, Barber E, Buckworth R, Deng A, Ebner B, Kenyon R, Liedloff A, Merrin LE, Moeseneder C, Nielsen DL, O'Sullivan J, Ponce Reyes R, Robson BJ, Stratford DS, Stewart-Koster B and Turschwell M (2018) Synthesis of knowledge to support the assessment of impacts of water resource development to ecological assets in northern Australia: asset descriptions. A technical report to the Australian Government from the CSIRO Northern Australia Water Resource Assessment, part of the National Water Infrastructure Development Fund: Water Resource Assessments. CSIRO, Australia.

Pringle CM (2001) Hydrologic connectivity and the management of biological reserves: a global perspective. Ecological Applications 11, 981–998.

Pringle C (2003) What is hydrologic connectivity and why is it ecologically important? Hydrological Processes 17, 2685–2689.

Lester RE, Webster IT, Fairweather PG and Young WJ (2011) Linking water-resource models to ecosystem-response models to guide water-resource planning – an example from the Murray–Darling Basin, Australia. Marine and Freshwater Research 62, 279–289.

Schumann G, Bates PD, Horritt MS, Matgen P and Pappenberger F (2009) Progress in integration of remote sensing–derived flood extent and stage data and hydraulic models. Reviews of Geophysics 47, RG4001.

Shaikh M, Green D and Cross H (2001) A remote sensing approach to determine environmental flows for wetlands of the Lower Darling River, New South Wales, Australia. International Journal of Remote Sensing 22, 1737–1751.

Sims NC, Warren G, Overton IC, Austin J, Gallant J, King DJ, Merrin LE, Donohue R, McVicar TR, Hodgen MJ, Penton DJ, Chen Y, Huang C and Cuddy S (2014) RiM-FIM floodplain inundation modelling for the Edward-Wakool, Lower Murrumbidgee and Lower Darling River systems. Report prepared for the Murray-Darling Basin Authority. CSIRO Water for a Healthy Country Flagship, Canberra.

Sims NC, Anstee A, Barron O, Botha E, Lingtao L, Lehmann E, McVicar T, Paget M, Ticehurst C, Van Niel T and Warren G (2016) Earth observation remote sensing. A technical report from the CSIRO Northern Australia Water Resource Assessment to the Government of Australia, Australia.

Sparks RE (1995) Need for ecosystem management of large rivers and their floodplains. BioScience 45, 168–182.

Stelling GS and Verwey A (2005) Numerical flood simulation. In: Anderson MG (ed) Chapter 16, Encyclopedia of Hydrological Sciences, 1–14.

Stratford D, Merrin L, Linke S, Kenyon R, Ponce Reyes R, Buckworth R, Deng R, McGinness H, Pritchard J, Seo L and Waltham N (2023) Assessment of the potential ecological outcomes of water resource development in the Roper catchment. A technical report from the CSIRO Roper River Water Resource Assessment for the National Water Grid. CSIRO, Australia.

Thomas M, Philip S, Stockman U, Wilson PR, Searle, R, Hill J, Bui E, Gregory, L, Watson, I, Wilson PL and Gallant G (2022) Soils and land suitability for the Roper catchment, Northern Territory. A technical report from the CSIRO Roper River Water Resource Assessment for the National Water Grid. CSIRO, Australia.

Thoms MC (2003) Floodplain–river ecosystems: lateral connections and the implications of human interference. Geomorphology 56, 335–349.

Ticehurst CJ, Chen Y, Karim F, Dutta D and Gouweleeuw B (2013) Using MODIS for mapping flood events for use in hydrological and hydrodynamic models: experiences so far. Proceedings of MODSIM2013, 20th International Congress on Modelling and Simulation, Adelaide.

Ticehurst C, Dutta D, Karim F, Petheram C and Guerschman JP (2015) Improving the accuracy of daily MODIS OWL flood inundation mapping using hydrodynamic modelling. Natural Hazards. DOI: 10.1007/s11069-015-1743-5.

Tockner K, Bunn SE, Gordon C, Naiman RJ, Quinn GP and Stanford JA (2008) Floodplains: Critically threatened ecosystems. In: Polunin N (ed) Aquatic Ecosystems, 45–61. Cambridge University Press.

Tockner KA, Lorang MS and Stanford JA (2010) River flood plains are model ecosystems to test general hydrogeomorphic and ecological concepts. River Research and Applications 26, 76–86.

Townsend PA and Walsh SJ (1998) Modeling floodplain inundation using an integrated GIS with radar and optical remote sensing. Geomorphology 21, 295–312.

Tuteja NK and Shaikh M (2009) Hydraulic modelling of the spatio-temporal flood inundation patterns of the Koondrook Perricoota forest wetlands- the living Murray. Proc. 18th World IMACS, MODSIM Congress, Cairns.

Ward DP, Hamilton SK, Jardine TD, Pettit NE, Tews EK, Olley JM and Bunn SE (2013) Assessing the seasonal dynamics of inundation, turbidity, and aquatic vegetation in the Australian wet-dry tropics using optical remote sensing. Ecohydrology 6(2), 312–323.

Ward JV (1989) The four-dimensional nature of lotic ecosystems. Journal of the North American Benthological Society 8, 2–8.

Warfe DM, Pettit NE, Davies PM, Pusey BJ, Hamilton SK, Kennard MJ, Townsend SA, Bayliss P, Ward DP, Douglas MM, Burford MA, Finn M, Bunn SE and Halliday IA (2011) The 'wet-dry' in the wet-dry tropics drives river ecosystem structure and processes in northern Australia. Freshwater Biology 56, 2169–2195.

Watson I, Petheram C, Bruce C and Chilcott C (eds) (2023) Water resource assessment for the Roper catchment. A report from the CSIRO Roper River Water Resource Assessment for the National Water Grid. CSIRO, Australia.

Welcomme RL, Bene C, Brown CA, Arthington A, Dugan P, King JM and Sugunan V (2006) Predicting the water requirements of river fisheries. In: Verhoeven JTA, Beltman B, Bobbink R and Whigham DF (eds) Wetlands and Natural Resource Management. Springer-Verlag: Berlin.

Xu H (2006) Modification of normalised difference water index (NDWI) to enhance open water features in remotely sensed imagery. International Journal of Remote Sensing 27(14), 3025–3033.

As Australia's national science agency and innovation catalyst, CSIRO is solving the greatest challenges through innovative science and technology.

CSIRO. Unlocking a better future for everyone.

Contact us

1300 363 400
+61 3 9545 2176
csiroenquiries@csiro.au
csiro.au

For further information

Environment
Dr Chris Chilcott
+61 8 8944 8422
chris.chilcott@csiro.au

Environment
Dr Cuan Petheram
+61 467 816 558
cuan.petheram@csiro.au

Agriculture and Food
Dr Ian Watson
+61 7 4753 8606
Ian.watson@csiro.au